

LONG ACOUSTIC CLADDED BUFFER RODS

by

**Amir Masoud Miri, B.Sc. Tehran University
Tehran, Iran**

**Department of Electrical Engineering
McGill University
Montreal, Quebec
September, 1991**

**A thesis submitted to the Faculty of Graduate Studies and Research
in partial fulfillment of the requirements for the degree of
Master of Engineering**

**(c) Amir Masoud Miri
1991**

ABSTRACT

Experimental investigations and theoretical considerations of long acoustic cladde buffer rods are presented and their superiority over uncladde rods is shown. These rods consist of a core and a cladding which are so designed to confine acoustic energy in the core, giving rise to a perfect guidance. Different rods with different core dopant material, concentration and profile were designed and their acoustic performance was studied by ultrasonic pulse-echo experiment. Tapered rods are also introduced. A cladde silica rod of a large diameter is tapered gradually to a rod of a small diameter and gives it the ability to be used where tiny features or openings are dealt with. Novel metallic acoustic rods both cladde and uncladde are presented and a comparison is made between these rods and conventional metal rods. Acoustic lenses are fabricated at the end of a few rods including cladde silica tapered silica and cladde metallic rods and ultrasonic focus and unfocus measurements carried out at 5 and 10MHz are presented for all the rods.

Finally, the application of our unique rods at elevated temperatures is discussed. Ultrasonic measurements are performed at medium temperatures (up to 270°C) on a high viscosity liquid and at high temperatures (around 750°C) on molten aluminum. It is shown that our cladde acoustic rods are proper candidates for use at high temperatures to monitor the properties of molten metals specially good for molten aluminum or low melting point temperature (below 1000°C) metals.

RESUME

Une étude expérimentale et théorique des longues tiges acoustiques avec gaine est présentée et leur supériorité sur les tiges sans gaine est démontré. Ces tiges ont un coeur et une gaine et elles sont conçues de telle sorte que l'énergie acoustique y soit guidée. Plusieurs tiges avec différents matériaux de doping, différentes concentrations et différents profils acoustiques pour le coeur ont été fabriquées et les rendements acoustiques ont été étudiés avec des mesures de pulse-echo. Des tiges avec des extrémités effilées ont aussi été étudiées. Une tige avec une gaine de silica d'un grand diamètre est effilée graduellement. Ainsi des tiges de petit diamètres peuvent être fabriquées, rendant l'accès des tiges à des cavités avec une petite ouverture, possible. Des tiges de métal d'un nouveau type, avec et sans gaine sont étudiées pour la première fois, et une comparaison avec les tiges de métal conventionnelles y est présentée. Des lentilles acoustiques sont fabriquées sur les bouts de certaines tiges et des mesures ultrasoniques (avec et sans focus) sont réalisées à des fréquences de 5 et 10MHz.

Les applications de nos tiges à des températures élevées sont discutées. Des mesures ultrasoniques sont réalisées à des températures moyennes (jusqu' à 270°C) pour des liquides avec une grande viscosité, et à des températures élevées (750°C pour l'aluminium en fonte. Nous démontrons ainsi la supériorité de nos tiges acoustiques avec gaine, comme moniteur des propriétés des métaux en fonte à températures élevées, tout spécialement comme moniteur des propriétés de l'aluminium en fonte et des métaux avec une basse température de fonte (en-dessous de 1000°C).

ACKNOWLEDGEMENTS

I wish to express my sincere gratitude to my thesis supervisor, Dr. C.K. Jen, for his guidance, kindness and support which has made this study possible. He has inspired me with and taught me philosophies which are crucial for successful research. I will always be grateful to him for what I have learned from him, not only concerning science and research but also in regards to dedication and perseverance.

I would also like to thank Prof. Z. Wang for his kind help on molten metal experiments. I also wish to express my thanks to Profs. E.L. Adler and I. Shih for their always welcome and useful suggestions regarding my studies.

Special thanks are given to Christian Néron for his scanning acoustic microscope measurements and helpful discussions with respect to instrumentation.

The cladded glass rods were supplied by Mr. L. Bonnell and Dr. K. Abe at National Optics Institute in Sainte-Foy, Quebec. Mr. H. Soda, Professors A. Ohno and A. McLean at University of Toronto supplied us with metallic rods.

I would like to express my heartfelt thanks to my dear parents and my brother whom without their support throughout my life, I would never be where I am today. I will forever be indebted to them for their giving me the best lesson in my life, "*how to be a man*".

Finally, I would like to thank my so dear wife, Nazi, for her love, patience, sacrifice and encouragement throughout this study. My everything is of no worth in return to her love. And so, I dedicate this thesis and all my other academic achievements to my wife and our little daughter, Leyla.

This research was partially supported by the Natural Sciences and Engineering Research Council of Canada (NSERC) and Northern Telecom. Special appreciation is given to Industrial Materials Institute, National Research Council of Canada where the entire thesis research has been carried out.

TABLE OF CONTENTS

Abstract	i
Resume	ii
Acknowledgements	iii
Table of Contents	iv
List of Figures	vi
List of Tables	xi
CHAPTER 1: Introduction	1
CHAPTER 2: Long Acoustic Cladded Buffer Rods	4
2.1 Experimental System and Isotropic Buffer Rods	4
2.2 Cladded Rods Under Weak Guidance conditions	8
2.3 Cladded Glass Rods With Radially Graded Acoustic Velocity profiles	11
2.4 Waveguide Materials	13
2.5 Buffer Rod Profile Measurements	14
2.5.1 Sample Fabrication	14
2.5.2 Acoustic Velocity Profile Measurements	15
2.6 Ultrasonic Pulse-Echo Measurements	22
2.6.1 Longitudinal Waves	22
2.6.2 Shear Waves	31
2.7 Visualizing the Acoustic Field	35
2.7.1 Methods of Visualizing an Acoustic Field	35
2.7.2 Experimental Setup	36
2.8 The Effect of the Center Dip on the Acoustic Performance of the Cladded Rods	40
2.9 Spherical Concave Lens	42
2.9.1 The Lens Fabrication Process	42
2.9.2 Acoustic Measurements	43
CHAPTER 3: Tapered Rods	48
3.1 Characterization of Tapered Rods	49
3.1.1 Ultrasonic Measurements	49
3.1.2 Scanning Electron Microscopy Measurement	50

CHAPTER 4: Metallic Long Acoustic Buffer Rods	56
4.1 Experimental Aspects	57
4.1.1 OCC Method	63
4.2 Cladded Metallic Buffer Rod	63
4.2.1 Spherical Concave Lens	72
CHAPTER 5: Application of Long Cladded Acoustic Buffer Rods at Elevated Temperatures	75
5.1 Introduction	75
5.2 Ultrasonic Pulse-Echo Measurement at Elevated Temperatures	77
5.3 Ultrasonic Pulse-Echo Measurement Performed on Molten Aluminum	82
5.3.1 Corrosion	83
5.3.2 Wetting	84
5.4 Discussion	87
CHAPTER 6: Conclusions	88
References	90

LIST OF FIGURES

- Figure 2.1 (a) A common ultrasonic pulse-echo measurement with an ultrasonic transducer, a liquid couplant and a sample. (b) A typical measurement result of (a) (c) The zoomed picture of (b). 6
- Figure 2.2 (a) The reflected 5MHz longitudinal echoes through a 250mm long, 10mm diameter pyrex glass rod. (b) The zoomed picture of (a.) 7
- Figure 2.3 (a) The reflected 10MHz longitudinal echoes through a 250mm long, 10mm diameter pyrex glass rod. (b) The zoomed picture of (a). 7
- Figure 2.4 A cladded acoustic rod, consisting of a core and a cladding. 10
- Figure 2.5 The dominant particle displacement components of the lowest order of (a) Torsional, (b) Radial-Axial, (c) Flexural and (d) Longitudinal modes. 11
- Figure 2.6 Two long cladded buffer rods fabricated by the MCVD method at National Optics Institute. 17
- Figure 2.7 Some of the samples used in the LFB SAM measurement of the acoustic velocity profiles. 17
- Figure 2.8 Acoustic velocity profiles of the 6.1% GeO₂ doped step index glass rod. 18
- Figure 2.9 Acoustic velocity profiles of the 8% GeO₂ doped GRIN glass rod. 19
- Figure 2.10 Acoustic velocity profiles of the 3.5% TiO₂ doped step index glass rod. 20
- Figure 2.11 Acoustic velocity profiles of the 9.8% P₂O₅ doped step index glass rod. 21
- Figure 2.12 (a) The reflected 5MHz longitudinal echoes through a 182mm long cladded glass rod (No. 2). (b) The zoomed picture of (a). 25
- Figure 2.13 (a) The reflected 10MHz longitudinal echoes through a 182mm long cladded glass rod (No. 2). (b) The zoomed picture of (a). 25
- Figure 2.14 (a) The reflected 5MHz longitudinal echoes through a 392mm long cladded glass rod (No. 3). (b) The zoomed picture of (a). 26

Figure 2.15	<i>(a) The reflected 10MHz longitudinal echoes through a 392mm long cladded glass rod (No. 3). (b) The zoomed picture of (a).</i>	26
Figure 2.16	<i>(a) The reflected 5MHz longitudinal echoes through a 395mm long cladded glass rod (No. 4). (b) The zoomed picture of (a).</i>	27
Figure 2.17	<i>(a) The reflected 10MHz longitudinal echoes through a 395mm long cladded glass rod (No. 4). (b) The zoomed picture of (a).</i>	27
Figure 2.18	<i>(a) The reflected 5MHz longitudinal echoes through a 260mm long cladded glass rod (No. 5) (b) The zoomed picture of (a).</i>	28
Figure 2.19	<i>(a) The reflected 10MHz longitudinal echoes through a 260mm long cladded glass rod (No. 5) (b) The zoomed picture of (a).</i>	28
Figure 2.20	<i>(a) The reflected 5MHz longitudinal echoes through a 400mm long cladded glass rod (No. 6). (b) The zoomed picture of (a).</i>	29
Figure 2.21	<i>(a) The reflected 10MHz longitudinal echoes through a 400mm long cladded glass rod (No. 6). (b) The zoomed picture of (a).</i>	29
Figure 2.22	<i>(a) The reflected 30MHz longitudinal echoes through a 392mm long cladded glass rod (No. 3). (b) The zoomed picture of (a).</i>	30
Figure 2.23	<i>(a) The reflected 5MHz shear echoes through a 250mm long pyrex glass rod (No. 1). (b) The zoomed picture of (a).</i>	32
Figure 2.24	<i>(a) The reflected 5MHz shear echoes through a 182mm long cladded glass rod (No. 2). (b) The zoomed picture of (a).</i>	32
Figure 2.25	<i>(a) The reflected 5MHz shear echoes through a 392mm long cladded glass rod (No. 3). (b) The zoomed picture of (a).</i>	33
Figure 2.26	<i>(a) The reflected 5MHz shear echoes through a 395mm long cladded glass rod (No. 4). (b) The zoomed picture of (a).</i>	33
Figure 2.27	<i>(a) The reflected 5MHz shear echoes through a 260mm long cladded glass rod (No. 5). (b) The zoomed picture of (a).</i>	34
Figure 2.28	<i>(a) The reflected 5MHz shear echoes through a 400mm long cladded glass rod (No. 6). (b) The zoomed picture of (a).</i>	34
Figure 2.29	<i>Schematic of a Schlieren visualization system.</i>	37
Figure 2.30	<i>Photographs of the experimental set-up for the visualization of ultrasound, (a) He-Ne laser and transducer, (b) ultrasonic frequency generator, CCD camera and monitor. (c) A complete view.</i>	38
Figure 2.31	<i>Image of acoustic waves coming out of a 290mm long 8.6% GeO₂ doped step index rod. Arrow indicates the rod-water interface.</i>	39

Figure 2.32	<i>Image of acoustic waves coming out of a 392mm long 8% GeO₂ doped GRIN rod. Arrow indicates the rod-water interface</i>	39
Figure 2.33	<i>The first reflected shear echo from the end of a 65mm long cladded rod with a center index dip, (a) at 5MHz and (b) at 10MHz</i>	41
Figure 2.34	<i>The first reflected shear echo from the end of a 66mm long cladded rod without a center index dip, (a) at 5MHz and (b) at 10MHz.</i>	41
Figure 2.35	<i>The setup for spherical concave lens fabrication at the end of glass rods.</i>	42
Figure 2.36	<i>Schematic for the focussing measurement setup.</i>	44
Figure 2.37	<i>(a) Photograph of the experimental setup for focusing measurement (b) Shows the pulser, detector and receiver units, from left to right respectively.</i>	45
Figure 2.38	<i>The axial amplitude variation for the received signal near the focal point.</i>	46
Figure 2.39	<i>(a) The received echoes when a flat sample is located at the focal point (b) is the higher magnification near B_0^0.</i>	46
Figure 2.40	<i>Setup for acoustic scanning of a grid.</i>	47
Figure 2.41	<i>A line scan of a grid scanned at the focus of a long buffer rod with a spherical concave lens at it's end surface.</i>	47
Figure 3.1	<i>Tapered acoustic buffer rods.</i>	51
Figure 3.2	<i>The measured (a) V_{LSAW} and (b) V_{LSSCW} profiles for the cladded rods shown in Fig. 3.1.</i>	52
Figure 3.3	<i>The reflected 30MHz longitudinal echoes through a 225mm long tapered rod. (a) in air, (b) in water without a reflector (c) in water with a reflector. The lower trace is a zoomed picture near B_0^0.</i>	53
Figure 3.4	<i>The reflected 5MHz longitudinal echoes through a 225mm long tapered rod in air. The lower trace is a zoomed picture.</i>	54
Figure 3.5	<i>A scanning electronic micrograph of a concave surface fabricated at the thin end of the tapered rod.</i>	54
Figure 3.6	<i>The measured surface profile of the lens fabricated at the thin end of the tapered rod in two perpendicular directions.</i>	55
Figure 3.7	<i>The axial amplitude variation for the received signal near the focus.</i>	55

Figure 4.1	<i>(a) The reflected 5MHz longitudinal echoes through the 290mm long conventional aluminum rod. (b) A higher magnification picture near B_0^0.</i>	59
Figure 4.2	<i>(a) The reflected 5MHz longitudinal echoes through the 285mm long OCC aluminum rod. (b) A higher magnification picture near B_0^0.</i>	59
Figure 4.3	<i>(a) The reflected 10MHz longitudinal echoes through the 290mm long conventional aluminum rod. (b) A higher magnification picture near B_0^0.</i>	60
Figure 4.4	<i>(a) The reflected 10MHz longitudinal echoes through the 290mm long OCC aluminum rod. (b) A higher magnification picture near B_0^0.</i>	60
Figure 4.5	<i>(a) The reflected 5MHz longitudinal echoes through the 73mm long conventional tin rod. (b) A higher magnification picture near B_0^0.</i>	61
Figure 4.6	<i>(a) The reflected 5MHz longitudinal echoes through the 98mm long OCC tin rod. (b) A higher magnification picture near B_0^0.</i>	61
Figure 4.7	<i>The reflected 10MHz longitudinal echoes through the 73mm long conventional tin rod.</i>	62
Figure 4.8	<i>(a) The reflected 10MHz longitudinal echoes through the 98mm long OCC tin rod. (b) A higher magnification picture near B_0^0.</i>	62
Figure 4.9	<i>A cross section view of a cladded metallic buffer rod.</i>	66
Figure 4.10	<i>(a) An optical and (b) an SEM image of the tin/lead alloy core - tin cladding interface.</i>	67
Figure 4.11	<i>(a) The reflected 1MHz longitudinal echoes through the 80mm long cladded metallic rod shown in Fig.4.9. (b) is a higher magnification near B_0^0.</i>	68
Figure 4.12	<i>(a) The reflected 2MHz longitudinal echoes through the 80mm long cladded metallic rod shown in Fig.4.9. (b) is a higher magnification near B_0^0.</i>	68
Figure 4.13	<i>(a) The reflected 5MHz longitudinal echoes through the 80mm long cladded metallic rod shown in Fig.4.9. (b) is a higher magnification near B_0^0.</i>	69
Figure 4.14	<i>(a) The reflected 10MHz longitudinal echoes through the 80mm long clad metallic rod shown in Fig.4.9. (b) is a higher magnification near B_0^0.</i>	69
Figure 4.15	<i>Image of an acoustic beam from the 80mm long cladded buffer rod shown in Fig.4.9. Arrow indicates the rod-water interface.</i>	70

Figure 4.16	<i>The measured V_{LSSCW} profiles for two orthogonal scans across the center of the cladded metallic rod shown in Fig.4.9.</i>	70
Figure 4.17	<i>(a) A 10MHz ultrasonic pulse-echo measurement with the cladded buffer rod shown in Fig.4.9, a liquid couplant and a sample. (b) A typical measurement result of (a) near B_0^0.</i>	71
Figure 4.18	<i>The axial amplitude variation for the received signal near the focal point, at 5MHz.</i>	73
Figure 4.19	<i>The axial amplitude variation for the received signal near the focal point, at 10MHz.</i>	73
Figure 4.20	<i>The received 5MHz longitudinal echoes when a flat sample is located at the focal point. (b) is the higher magnification near B_0^0.</i>	74
Figure 4.21	<i>The received 10MHz longitudinal echoes when a flat sample is located at the focal point. (b) is the higher magnification near B_0^0.</i>	74
Figure 5.1	<i>Setup for Ultrasonic pulse-echo measurement for high viscosity Dow Corning 200 Fluid.</i>	78
Figure 5.2	<i>An ultrasonic pulse-echo reflection measurement performed on hot liquid sample (Dow Corning 200 Fluid). The temperature was 160°C.</i>	79
Figure 5.3	<i>An ultrasonic pulse-echo reflection measurement performed on hot liquid sample (Dow Corning 200 Fluid). The temperature was 240°C.</i>	79
Figure 5.4	<i>An ultrasonic pulse-echo reflection measurement performed on hot liquid sample (Dow Corning 200 Fluid). The temperature was 270°C.</i>	80
Figure 5.5	<i>An ultrasonic pulse-echo reflection measurement performed on hot liquid sample (Dow Corning 200 Fluid). The temperature was (a) 50°C, (b) 100°C and (c) 150°C.</i>	81
Figure 5.6	<i>A small furnace for melting Aluminum. (a) The side view and (b) the bottom view of the furnace.</i>	82
Figure 5.7	<i>A cladded buffer rod whose working-tip is plasma sprayed by zirconia.</i>	83
Figure 5.8	<i>The 10MHz pulse-echo measurement performed at 750°C on molten aluminum without a reflector.</i>	86
Figure 5.9	<i>The 10MHz pulse-echo measurement performed at 750°C on molten aluminum with a reflector.</i>	86

LIST OF TABLES

Table 2.1	<i>Buffer Rod Material Considerations.</i>	14
Table 2.2	<i>Description of the glass rods used in our experiments.</i>	16

CHAPTER 1: Introduction

For the past several decades, ultrasonic inspection has been widely employed in the industry to nondestructively evaluate the quality of materials, characterize materials and detect subsurface defects, etc. For example, in metallurgical industry the unique ability of ultrasonic waves to "see through" liquid metal is exploited to detect anomalous behavior within the melt [1],[2]. Today ultrasonic pulse-echo techniques are in widespread use for the nondestructive evaluation of materials. Since these techniques are sometimes applied in adverse conditions such as elevated temperatures [1]-[4] and pressures [5], buffer rods are often necessary to avoid exposing the ultrasonic transducer to such conditions. In addition, long and small diameter buffer rods are sometimes required to probe materials inside a closure which has only tiny accessible openings.

In many ultrasonic measurements employing a buffer rod, a test sample is attached to one end, and the echoes coming from the sample are analyzed to obtain ultrasonic velocity and attenuation [1],[4], or to detect voids or inclusions in the test sample. However, some spurious echoes may be present due to the wave diffraction and the finite rod diameter. Such echoes are unwanted because they always arrive later than the directly transmitted or reflected longitudinal echoes and may interfere with the desired signals from the sample. These unwanted echoes are referred to as trailing echoes [6]. The ultrasonic signal strength

is also weakened because of the wave diffraction. Previously Jen et al reported isotropic buffer rods with a notched periphery and a tapered shape [7] and anisotropic single crystal buffer rods with a collimating or focussing mechanism for a particular mode [8] to eliminate these trailing echoes.

In this thesis theoretical considerations and experimental measurements of one additional type of long acoustic buffer rods with low trailing signals are presented. They are cladded rods with small velocity differences between core and cladding. Here, a novel type of metallic rods both uncladded and cladded with high acoustic performance are presented. Since in this work acoustic imaging through a liquid couplant, which does not support shear wave, onto the sample is of our main interest, mostly longitudinal acoustic waves are considered. However, to complete this study we performed a set of shear pulse-echo measurement on our buffer rods and also measured their shear acoustic velocity profiles. The applications of such cladded buffer rods for acoustic imaging at high temperatures and/or high frequencies, and our unique metallic acoustic probes are the main original contributions of this thesis.

Chapter 2 indicates the need for the improvement of the reported buffer rods. Theoretical considerations and some experimental measurements of the cladded buffer rods are also given. The performance of acoustic rods and cladded rods having radially graded velocity profiles are considered and discussed. Both longitudinal and shear ultrasonic pulse-echo measurements are presented and the superiority of cladded rods over uncladded rods is concluded from the excellent results of these experiments. A spherical concave lens is also fabricated at the end surface of these rods. The lens fabrication process and focus measurements are given and the focussing behavior is shown. At the end of chapter two the effect of a center dip appearing in the velocity profile along the radial direction, on the acoustic performance of the cladded rods is discussed.

In chapter 3 cladded rods with very small diameter, proper for working where tiny features are dealt with, are presented. The ultrasonic characterization and measurements are also given.

Metallic acoustic buffer rods are presented and discussed in chapter 4. For the first time a new kind of metallic rod fabricated by Ohno Continuous Casting (OCC) method is used as an acoustic buffer rod. A comparison between these rods and conventional metal rods is made. Through a set of pulse-echo measurements, It is shown that the OCC rods

have better acoustic performance over the conventional rods. The nice features of the OCC method are briefly discussed. A cladded type of OCC rods was also designed and its excellent acoustic behavior is shown. An acoustic lens is also fabricated at the end of this cladded rod, the focus measurements are presented and the focussing behavior is shown.

An additional original contribution of this work is presented in chapter 5 where the application of our long acoustic cladded buffer rods at elevated temperatures is presented. The cladded rod is used as an acoustic imaging probe at high temperatures. Ultrasonic pulse-echo measurements are performed at high temperatures on molten aluminum. The results show that our cladded buffer rod is an excellent candidate as an acoustic probe proper for use at elevated temperatures. Finally, an overall evaluation of the cladded buffer rods is given in chapter 6.

CHAPTER 2: Long Acoustic Cladded Buffer Rods

As mentioned earlier, one concern in ultrasonic measurements with long buffer rods is that the unwanted trailing echoes may overlap with the desired echoes from the sample. The ratio between the energy sum of all trailing echoes over that of the first arrived longitudinal echo may be used to evaluate the degree of diffraction in the rod. In order to reduce this ratio one obvious method is to increase the diameter or shorten the length of the rod. However, in this chapter a type of long buffer rod but with low spurious signals is presented and discussed. That is the *long acoustic cladded buffer rod*.

2.1 Experimental System and Isotropic Buffer Rods

In general, a typical ultrasonic imaging system used to image samples which are immersed in a liquid, is composed of a pulser and a broadband receiver operated in the pulse-echo mode, broadband longitudinal wave transducers and a mechanical raster scanner. Figure 2.1a shows a common ultrasonic pulse-echo measurement arrangement which consists of an ultrasonic transducer without a buffer rod, a liquid couplant of distance d and a flat and parallel sample of thickness h . In Figs. 2.1b and 2.1c the echo S_0 is the reflected longitudinal echo from the sample surface and echoes S_1, S_2, S_3, \dots are the echoes traversing

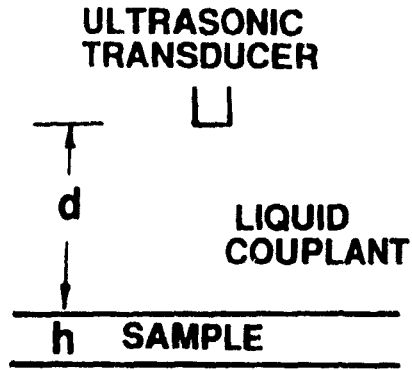
back and forth between the top and bottom surfaces of the sample. Figure 2.1c is a zoomed image of 2.1b. If h is known and acoustic travelling time t_h in the sample is measured, then the ultrasonic velocity v of the sample can be obtained from the relation $v = 2h/t_h$. A typical measurement is given in Fig. 2.1b where $t_{cl} = 2d/v_w$ is the acoustic delay time in the liquid couplant and v_w is the longitudinal velocity of the liquid couplant.

If a buffer rod is to be used in the above measurement to isolate the transducer from liquid couplant or sample it should not prevent the measurement of, for instance, v of the sample. However, this is not possible if a buffer rod is not chosen properly. Figures 2.2 and 2.3 show the 5 and 10MHz reflected echoes through a 250mm long Pyrex glass rod of 10mm diameter. The echo B_0^0 , is the first longitudinal arrival. Echoes $B_0^1, B_0^2, B_0^3, \dots$ are the so-called trailing echoes [6] which result from the wave diffraction and finite rod diameter. The arrival time delay difference between echoes B_0^0 , and B_0^1 , (or B_0^1 , and B_0^2 , etc.) defined as t_T was found to be [6]

$$t_T = \frac{2a/\cos\theta}{v_s} - \frac{2a \tan\theta}{v_L} \quad (1)$$

where a is the rod radius; θ is equal to $\sin^{-1}(v_s/v_L)$; v_s and v_L are the shear and longitudinal wave velocities in the isotropic rod.

It is obvious that this type of buffer rod cannot be efficiently used in ultrasonic measurement or evaluation of materials. Because there is always a possibility that the desired echoes from sample or from the material under inspection overlap with the trailing echoes. To eliminate the trailing echoes and to enhance the signal strength of the desired echo clad rods are introduced. Theoretical considerations and experimental results are presented and discussed in the next sections.



(a)

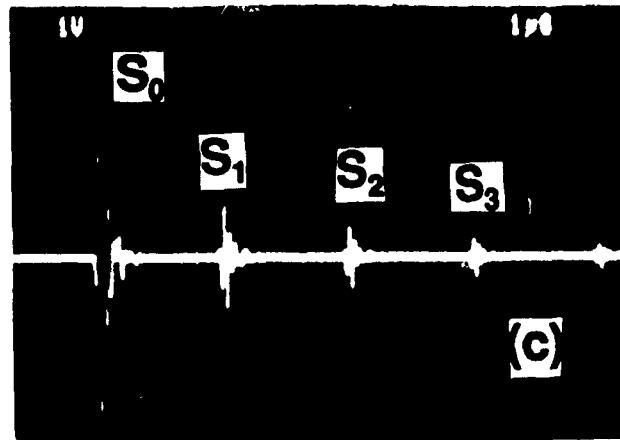
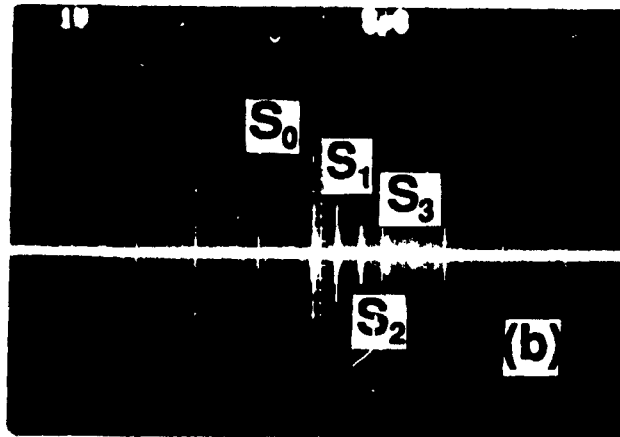


Figure 2.1 (a) A common ultrasonic pulse-echo measurement with an ultrasonic transducer, a liquid couplant and a sample. (b) A typical measurement result of (a). (c) The zoomed picture of (b).

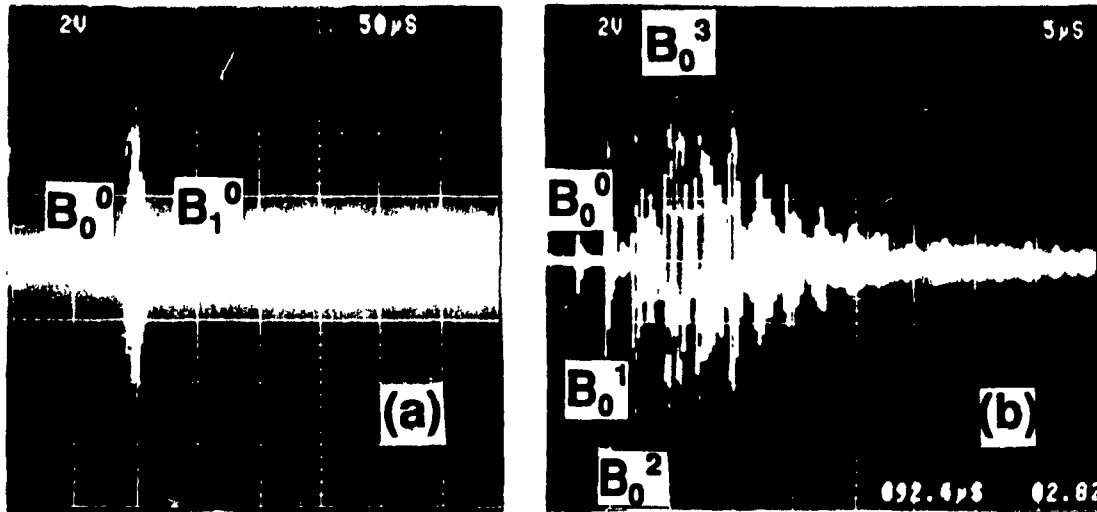


Figure 2.2 (a) The reflected 5MHz longitudinal echoes through a 250mm long, 10mm diameter pyrex glass rod. (b) The zoomed picture of (a).

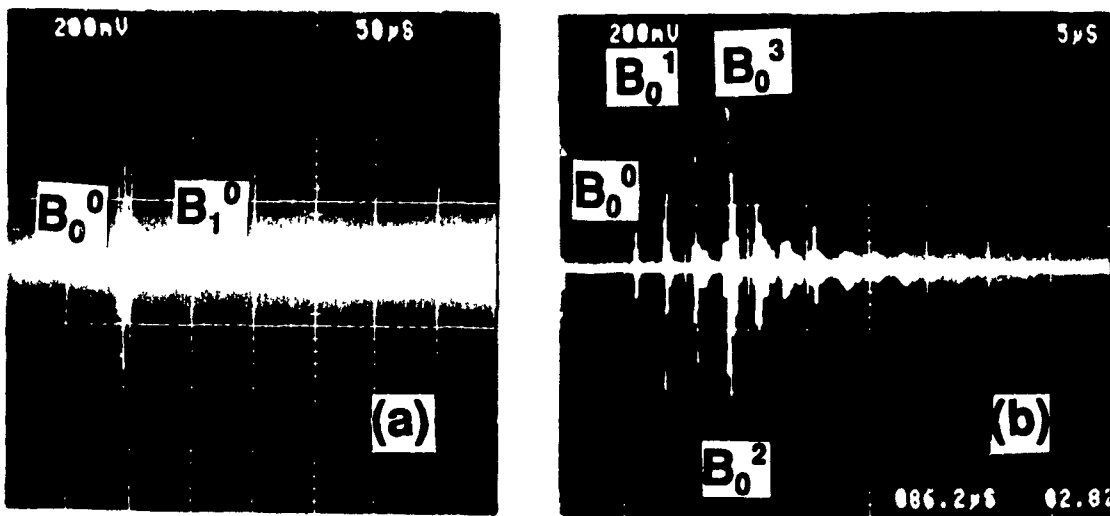


Figure 2.3 (a) The reflected 10MHz longitudinal echoes through a 250mm long, 10mm diameter pyrex glass rod. (b) The zoomed picture of (a).

2.2 Cladded Rods Under Weak Guidance Conditions

A cladded acoustic buffer rod consists of a core and a cladding as shown in Fig. 2.4. Under certain conditions it can support elastic waves propagating within the core area. An acoustic buffer rod is characterized by the material density, ρ , bulk longitudinal wave velocity, V_L , and bulk shear wave velocity, V_S . In general, the guidance of acoustic wave within the core area requires that the shear wave velocity of the core be smaller than that of the cladding, *i.e.*

$$V_{S, \text{CORE}} < V_{S, \text{CLAD}}$$

If this velocity difference is less than a few percent, the acoustic energy launched into the core is under weak guidance. Such acoustic rods are called weakly guiding acoustic rods which have the advantage of low acoustic dispersion. Under the weakly guiding conditions, according to the definition above, we have [9];

$$0 < \sigma_s \ll 1$$

or;

$$0 < \sigma_\rho \ll 1$$

where $\sigma_s = \frac{V_{s2} - V_{s1}}{V_{s2}}$ and $\sigma_\rho = \left| \frac{\rho_2 - \rho_1}{\rho_2} \right|$, In the expressions the subscripts 1 and 2 correspond to the core and cladding regions, respectively.

For guided acoustic waves the particle displacement vector \vec{u} can be expressed as [9];

$$\vec{u} = \nabla\phi + \nabla \times \vec{\Psi}$$

where ϕ and $\vec{\Psi}$ are the scalar and vector potential functions. They are governed by following equations [9];

$$\nabla^2 \vec{\Psi} - \left(\frac{1}{V_s} \right)^2 \frac{\partial^2 \vec{\Psi}}{\partial t^2} = 0 \quad (2)$$

and

$$\nabla^2\Phi - \left(\frac{1}{v_L}\right)^2\frac{\partial^2\Phi}{\partial t^2} = 0 \quad (3)$$

ϕ and $\bar{\Psi}$ are generally coupled each other to satisfy the boundary conditions between the rod core and the cladding. But under the weak guiding conditions the two equations are approximately uncoupled, *i.e.* the solution ϕ and solution $\bar{\Psi}$ can satisfy the boundary conditions independently.

Solving the equations gives four types of guided acoustic modes existing in such rods. They are Flexural mode (F), Torsional mode (T), Radial-axial mode (R) and longitudinal mode (L). The particle displacement components of the lowest order of each mode is shown in Fig. 2.5.

It is important to point out that the F, T, and R modes are all guided modes if guiding conditions are met but the longitudinal mode is also guided but leaky, which causes propagation loss for this mode. L modes are perfectly guided only if the densities and the shear wave velocities of the core and the cladding are same, and the longitudinal velocity of the core is less than that of the cladding [10].

Cladded acoustic rods consisting of core and cladding are much preferred over uncladded rods because:

- (1) the acoustic energy is guided in the core therefore the first echo from the end of the rod loses little energy and remains strong after a long propagation path.
- (2) few trailing echoes exist.
- (3) no leakage exists when they are immersed in liquids.
- (4) no cross-talk exists if cladded rods are in contact one another.

Weak guidance, which states that the velocity of the core is slightly (< a few percent) less than that of the cladding, provides low dispersion [11]. Boyd et al [12] demonstrated flexural (F_{11} mode) acoustic wave long delay lines using cladded fiber rods operated in tens of MHz. Jen provided some examples of applications using guided longitudinal waves in the cladded rods [10].

The details of the analysis of acoustic modes in weakly guiding cladded rods can be found in Refs. [10],[11]. Let V be the normalized frequency defined as

$$V = \frac{2\pi fa}{v_{L,core}(1-\eta^2)^{1/2}} \quad (4)$$

where

$$\eta = \frac{v_{L,core}}{v_{L,clad.}} \quad (5)$$

If V is less than 2.405, only the lowest longitudinal mode (L_{01}) can be guided [11]. Furthermore, under weak guidance the L_{01} mode is close to a planar longitudinal wave.

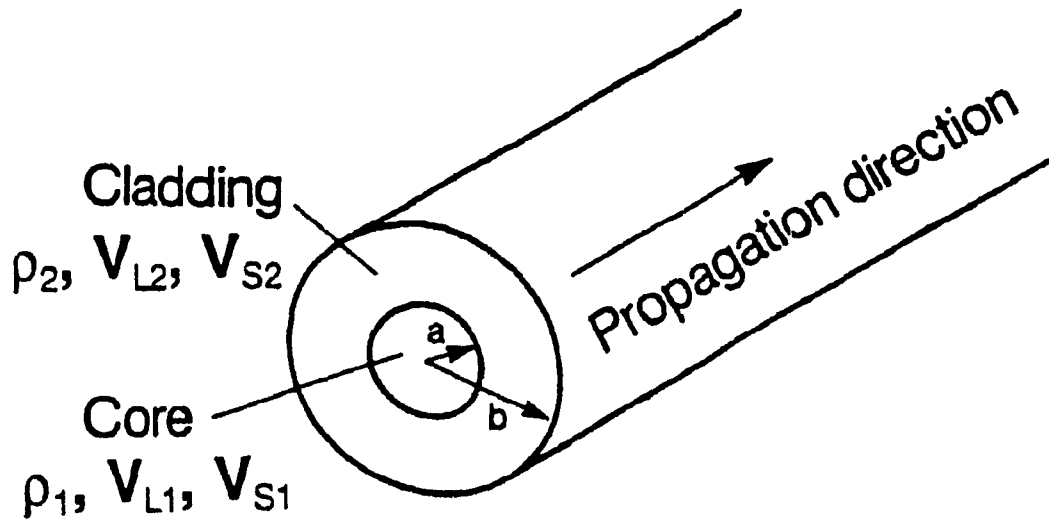


Figure 2.4 A cladded acoustic rod, consisting of a core and a cladding.

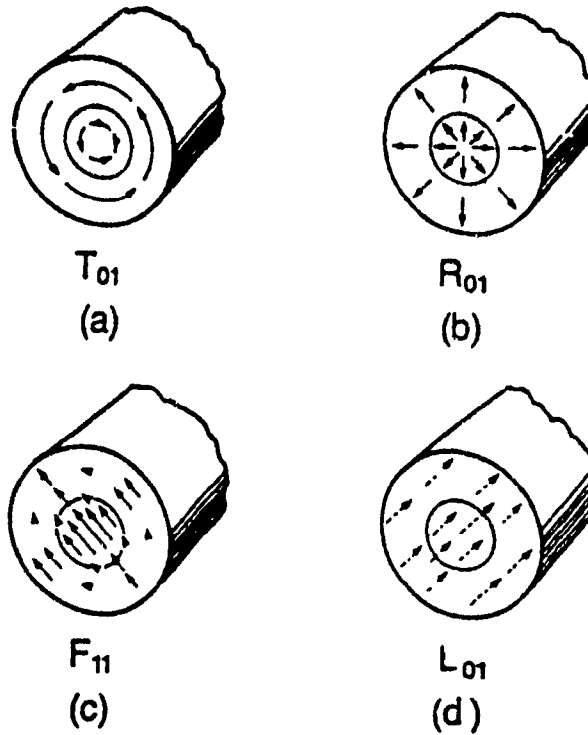


Figure 2.5 The dominant particle displacement components of the lowest order of (a) Torsional, (b) Radial-Axial, (c) Flexural and (d) Longitudinal modes.

2.3 Cladded Glass Rods With Radially Graded Acoustic Velocity Profiles

Glass rods having a graded index of refraction along the radial direction are commonly used in optical lens design. They are referred to as graded-index (GRIN) lenses [13] or SELFOC rods [14]. The parameters that define the index distribution provide valuable new degrees of freedom for designers of optical imaging systems [13]. Previously, Jen et al in their work on the acoustic characterization of doped fused silica optical fibers fabricated by the modified chemical vapor deposition method, have demonstrated that such fibers having step or graded refractive index profiles also exhibit step or graded leaky surface acoustic

velocity variations respectively [15],[16]. Here we show that glass rods having radially graded acoustic velocity profiles can be also used as long acoustic buffer rods with low spurious signals.

The techniques to fabricate such GRIN lenses or SELFOC fibers are ion exchange, chemical vapor deposition, sol-gel, etc. They are commercially available. Jen has showed an analogy between weakly guiding optical and acoustic fibers [17], and has also showed that rods having graded acoustic velocity profile in the radial direction possess similar "focussing" behavior existed as in counterpart optical GRIN lens [16]. It means that diffraction in such buffer rods exists to a lesser extent.

Since both bulk shear (S) and longitudinal (L) acoustic waves are present in an isotropic glass rod, in contrast to optical waves for which only the S wave exists, acoustic profiles of GRIN rods should be evaluated for both S and L waves. However, it appears that there has been no report about such measurement. It has been found that the leaky surface acoustic wave velocity, v_{LSAW} , and leaky surface skimming compressional acoustic wave velocity, v_{LSSCW} , could be measured using the $V(z)$ analysis of a reflection scanning acoustic microscope (SAM) [16],[18]. It is well known that transverse components play a major influence on v_{LSAW} ; therefore, we expect that the profile of S wave is close to that of v_{LSAW} . Furthermore, because the velocity of the surface skimming compressional wave in an isotropic material is nearly the same as that of the L wave, velocity profile of leaky surface skimming compressional waves, v_{LSSCW} , is expected to be close to that of L wave in the GRIN rod. For instance, for fused silica $v_S/v_{LSAW} = 1.02$ and $v_S/v_{LSSCW} = 1.014$. In our study we have measured v_{LSAW} and v_{LSSCW} profiles and found that GRIN rods also have graded v_{LSAW} and v_{LSSCW} profiles. The acoustic profiles (v_{LSAW} and/or v_{LSSCW}) for our cladded rods are also given in this chapter.

Equation (4) indicates that a higher value of V of a cladded acoustic rod means a larger number (N) of propagation modes inside the core, and also higher pulse dispersion for a broadband acoustic pulse. During nondestructive evaluation of materials we often require higher frequency operation which leads to higher value of V and N . In the counterpart optical fiber system, cladded glass fibers having a core with radially graded refractive index profile are used in order to reduce the modal dispersion [14]. We expect a similar behavior for cladded acoustic rods.

We have carried out ultrasonic pulse-echo measurements on both step and GRIN type of cladded rods and the measurements are given in the next sections. By comparing the results of the nearly the same step and GRIN rods we can say that GRIN cladded rods have less dispersion and low spurious signal. This comparison has been made by Jen [19]. Two 350mm long GeO_2 cladded glass buffer rods which consist of a core of ~ 2.4 mm radius and a cladding of 2.5mm thick were used. The variations of the index for these two rods are step and graded. The measured $v_{\text{LSAW,center}}/v_{\text{LSAW,clad}} \sim 0.93$. By comparing the echoes reflected from the end of these rods it was concluded that for multimode acoustic propagation the cladded rod with a core having graded velocity profile has less dispersion, low spurious signal and also less wave diffraction exists in GRIN rod.

2.4 Waveguide Materials

Table 2.1 lists four material candidates as buffer rods. Most of these waveguide materials can operate in the temperature range up to 1000°C . It is still difficult to find a good cladded acoustic buffer rod which can operate at molten steel temperature (1650°C). For a focussed spherical transducer since the spherical aberration is inversely proportional to the velocity ratio ($v_{\text{buffer rod}}/v_{\text{coupling liquid}}$) [20], high velocity material is preferred for high resolution applications.

At present time we have fused silica cladded rods provided by Mr. L. Bonnell and Dr. K. Abe of National Optics Institute at Ste Foy, Quebec. Mr. H. Soda and Professors A. Ohno and A. McLean at University of Toronto supplied us with metallic rods and cladded metallic rods.

In this study we have mainly used fused silica rods with different core dopant materials and different concentrations. Glass rods are of great interest because their potential supplier can be any one in the optical fiber research or production institute. The other advantages of glass over other isotropic materials are their light weight, cheap and abundant. In addition, the weak acoustic guidance conditions can be easily obtained using the existing glass fiber fabrication technologies which produce fibers with core and cladding materials made of pure or doped fused silica. In order to design a desired glass acoustic rod the fundamental knowledge of the acoustic properties of these glasses must be known. Effects of the con-

centration of some common dopants on acoustic velocities and densities have been reported in reference [21]. Metal rods are also studied. Their advantages over glass and other materials are discussed in chapter 4.

Table 2.1 Buffer Rod Material Considerations

Materials	Acoustic Att.	Thermal Shock	Machining	Other Properties
Fused Silica	Low	Medium	Difficult	Diameters can be varied easily.
Metallic Single Crystal	Medium	High	Easy	(*)
Advanced Ceramics	Low	Low	Difficult	Some have high acoustic velocities. (*)
Non-Metallic Single Crystals	Very Low	Low	Difficult	Only for very high frequencies. (*)

* In the radial direction of a cladded rod graded acoustic velocity profiles are easier to be obtained than step.

2.5 Buffer Rod Profile Measurements

2.5.1 Sample Fabrication

Five glass ultrasonic buffer rods, as listed in Table 2.2, some with a graded index and some with a step index profile were used in the experiments. They were fabricated by the National Optics Institute (NOI) using a modified chemical vapor deposition (MCVD) method [22] which is a standard technology to fabricate optical fibre preforms. So far, NOI has been the only supplier which can provide us the designed acoustic profiles. Silica rods were doped with GeO_2 , P_2O_5 , and TiO_2 to form a core and a cladding. These rods, as shown in Fig.2.6 and listed in Table 2.2 have been made to lengths of up to 400mm.

2.5.2 Acoustic Velocity Profile Measurements

Since it is very difficult to obtain the radial distribution of bulk longitudinal, v_L , and shear wave velocity, v_s , for small diameter rods, an approach which uses reflection scanning acoustic microscopy (SAM) and the $V(z)$ technique to obtain leaky surface acoustic wave (LSAW) and leaky surface-skimming compressional wave (LSSCW) velocities is used [16],[18]. Such measurements have been reported previously using a 775MHz point focus beam (PFB) SAM [15] and the accuracy was about 2%. Here, a 225MHz line focus beam (LFB) SAM [18] is used. With this microscope for optical polished fused silica plates, v_{LSAW} velocity measurements with accuracy better than 0.02% has been obtained [18]. The velocity measured was along the direction perpendicular to the LFB and parallel to the radial direction of the rod. The 775MHz PFB SAM offers better spatial resolution, but the 225MHz LFB SAM provides higher accuracy in velocity measurements due to the higher signal-to-noise ratio especially for LSSCW.

Due to the defocussing requirement of $V(z)$ measurements, the measured velocity represents an average value over the defocussed area which is about $150\mu\text{m}$ by $1000\mu\text{m}$ for the LFB SAM. All the samples, as shown in Fig.2.7, for the LFB SAM were cut to approximately a 6mm thickness and then polished; the last and the finest polishing step was with a mechanical-chemical ($0.06\mu\text{m}$) polishing. Since the LSSCW is very weakly excited, the signal-to-noise ratio for such a wave is much less than that for LSAW, hence less accuracy is available in v_{LSSCW} measurements. More studies are required in order to understand the effects of graded velocity profiles on the measurement accuracy. However, detailed descriptions for the $V(z)$ measurement of the LFB SAM is given in [18]. Because LSAW and LSSCW have predominantly shear and longitudinal wave components, respectively, their velocity profiles can be regarded as those of v_s and v_L [16].

The LSAW and LSSCW velocity profiles of the 6.1% GeO_2 doped step and 8% GeO_2 doped GRIN index rods, the 3.5% TiO_2 doped step index rod and 9.8% P_2O_5 doped step index rod are shown in Figs.2.8 to 2.11, respectively. The scan-line was also across the rod center. Since the LFB SAM only measures the average velocity over a $150\mu\text{m}$ by $1000\mu\text{m}$ area and the measurements have been taken at a distance of 0.1mm/step, the fine details appearing in the optical refractive index profiles [15],[16],[21] cannot be seen in the cor-

responding acoustic measurements. It is noted that there exists a center dip in the refractive index profile of the rods made by the MCVD method [22]. However, this dip cannot be clearly seen by our SAM method due to the relatively poor spatial resolution.

Table 2.2 *Description of the glass rods used in our experiments*

Glass Rod No.	Core Dopant	Cladding	Acoustic Profile	Length (mm)	Core Diameter (mm)	Total Diameter (mm)
1	Pyrex Glass		UNIFORM	250	----	10
2	6.1% GeO ₂	SiO ₂	STEP	182	4.8	12.1
3	8% GeO ₂ + 3.5% P ₂ O ₅	SiO ₂	GRIN	392	5	9.4
4	5.2% GeO ₂ + 3.5% P ₂ O ₅	SiO ₂	GRIN	395	5	9.9
5	3.5% TiO ₂	SiO ₂	STEP	260	2.2	8.0
6	9.8% P ₂ O ₅	SiO ₂	STEP	400	4.6	9.4

6
6



Figure 2.6 *Two long cladded buffer rods fabricated by the MCVD method at National Optics Institute.*



Figure 2.7 *Some of the samples used in the LFB SAM measurement of the acoustic velocity profiles.*

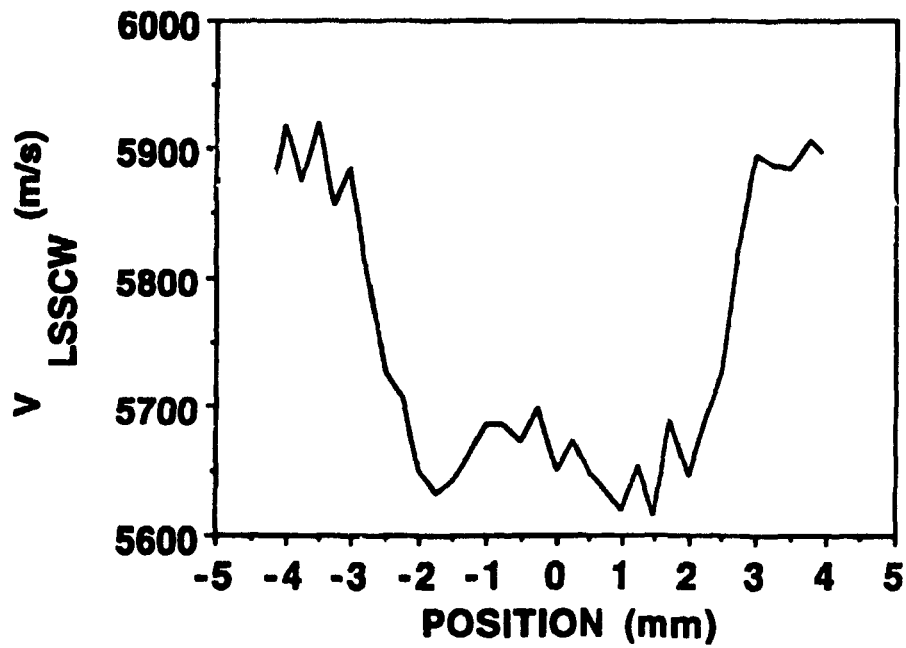
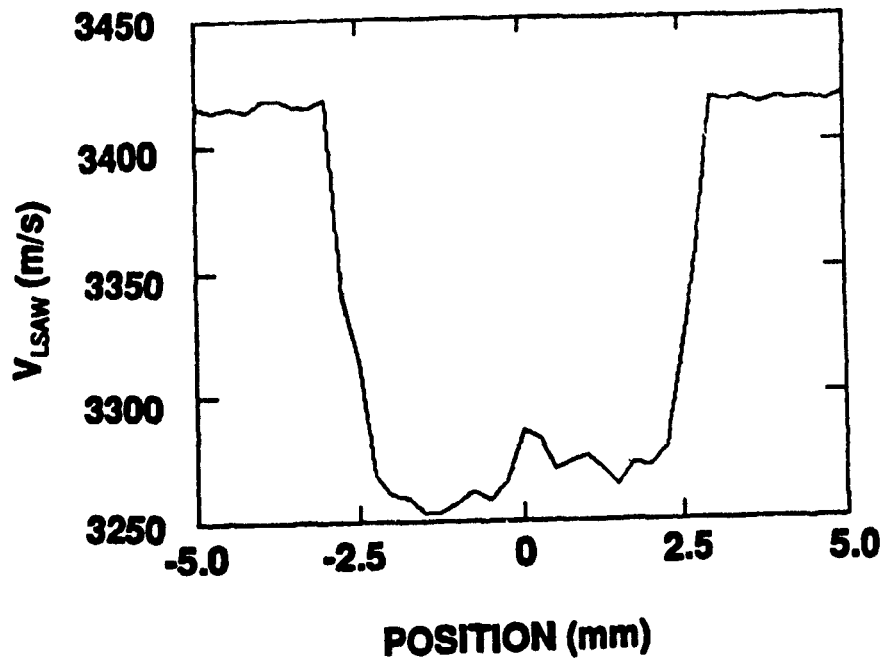


Figure 2.8 Acoustic velocity profiles of the 6.1% GeO_2 doped step index glass rod.

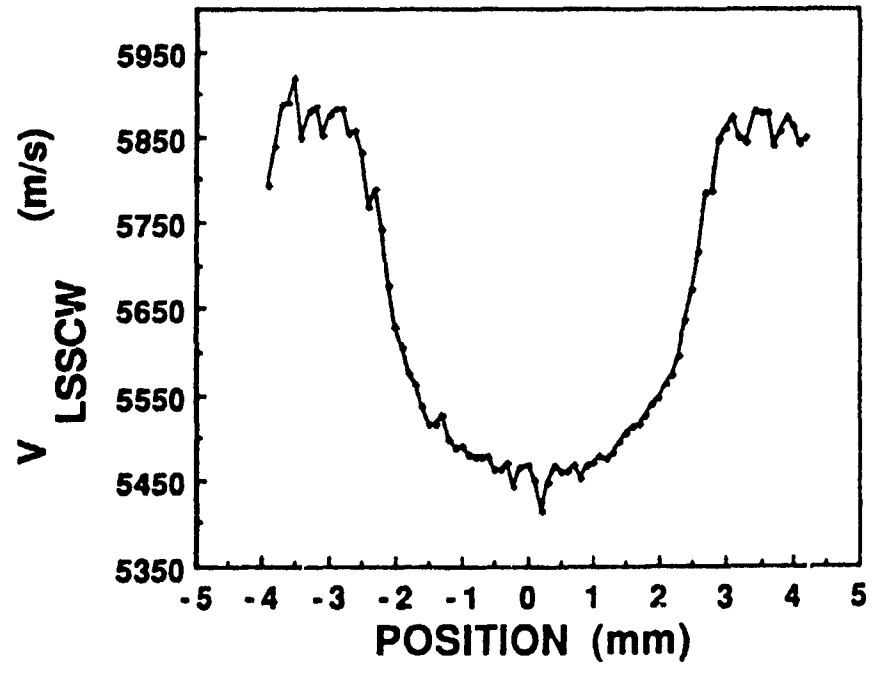
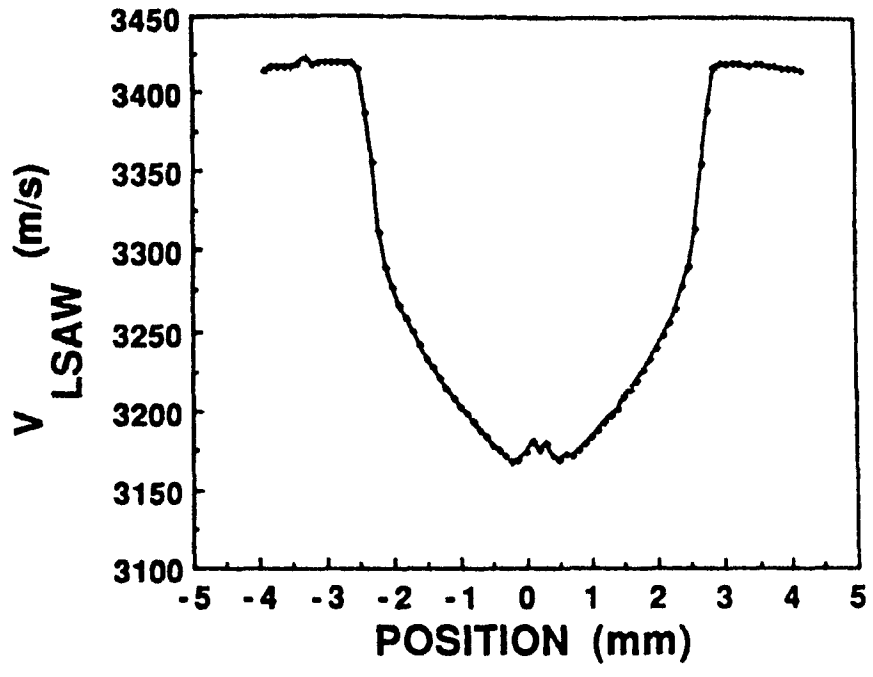


Figure 2.9 Acoustic velocity profiles of the 8% GeO_2 doped GRIN glass rod.

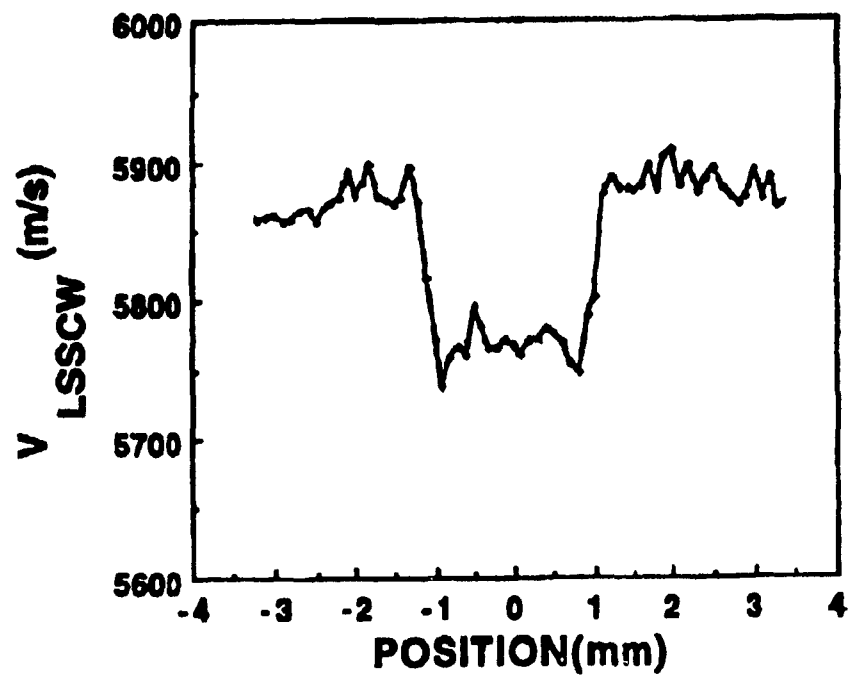
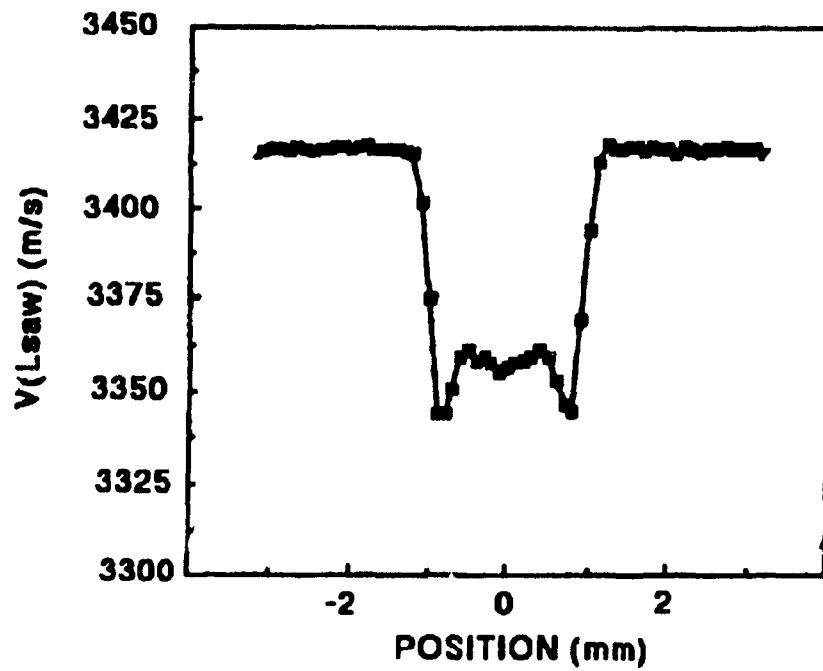


Figure 2.10 Acoustic velocity profiles of the 3.5% TiO_2 doped step index glass rod.

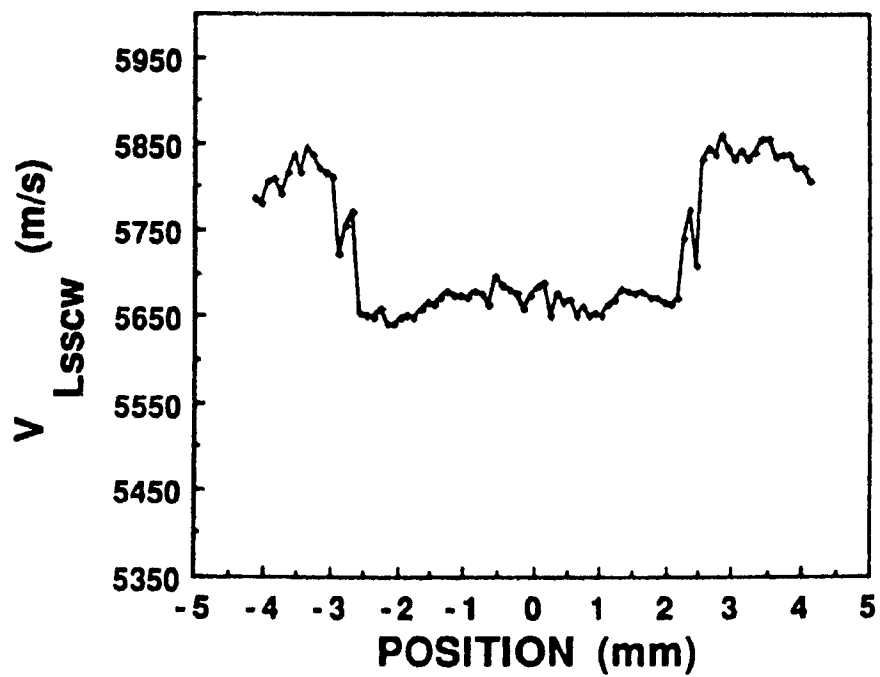
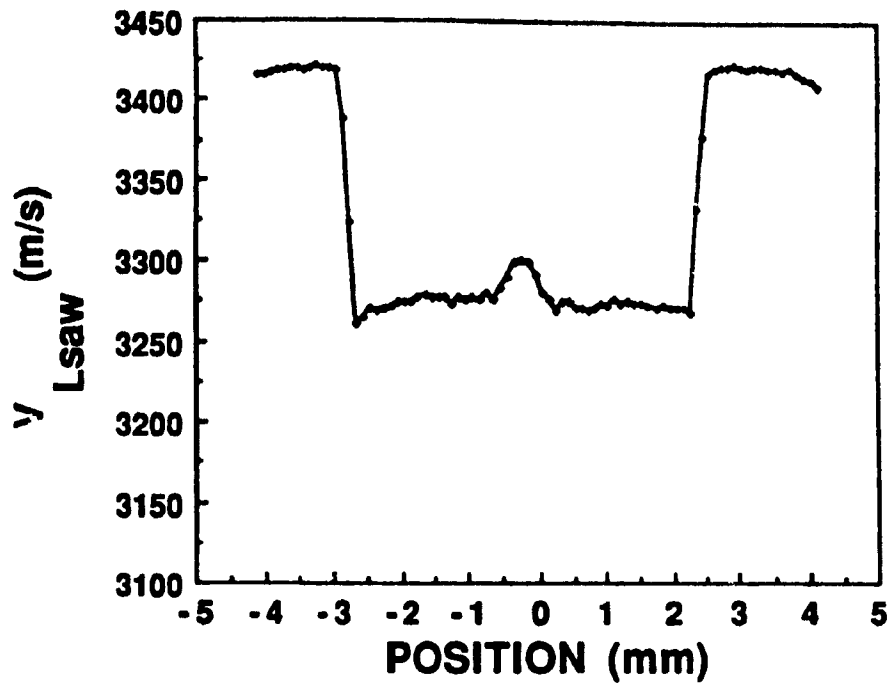


Figure 2.11 Acoustic velocity profiles of the 9.8% P_2O_5 doped step index glass rod.

2.6 Ultrasonic Pulse-Echo Measurements

2.6.1 Longitudinal Waves

Ultrasonic pulse-echo measurements were carried out on all the rods listed in Table 2.2 at 5 and 10MHz frequencies. A single transducer was used as both transmitter and receiver. We used 6.35mm diameter longitudinal transducers (5 and 10MHz). Transducer was attached to one end of the long buffer rod and the echoes reflected from the other end of rod were studied. In all the measurements commercial gel was used as the ultrasonic couplant between the transducer and the rod. The position of transducer was very important and it was adjusted so that its center is aligned with the center of the buffer rod. The condition of the end surfaces of the rods were also found to have an affect on the measurements. Both end surfaces have to be flat and smooth and they were polished by 400 grid sand paper.

The reflected echoes through a 250mm long and 10mm diameter pyrex glass rod (rod No. 1) which has a uniform acoustic velocity profile across its diameter were shown in Figs 2.2 and 2.3. From these figures we can see that there are many trailing echoes (B_0^0 , B_0^1 , B_0^2 , B_0^3 , ...) existing and they are much stronger than the desired echo i.e. B_0^0 , the first longitudinal arrival from the end of the rod. Because of the wave diffraction the acoustic energy which in ideal case should be carried by the desired echo, now is distributed among the unwanted trailing echoes, hence, even the third longitudinal arrival couldn't be observed.

The results of pulse-echo measurements for the cladded rods are shown in Figs.(2.12, 2.13) to (2.20, 2.21) at 5 and 10Mhz for rods number 2 to 6 respectively. The goal here is to show the better acoustic performance and the superiority of cladded rods over uncladded ones. At 5MHz all the rods except rod number 5 show a better performance compared to uncladded glass rod and there are little or no trailing echo existing. For example if we look at the 5MHz reflected echoes (Fig.2.16) of 395mm long and 9.9mm diameter cladded GeO_2 doped rod (rod No. 4) there exists little trailing echo what so ever. Echoes B_0^0 , B_1^0 , B_2^0 , ..., are the echoes traversing back and forth between the top and bottom surfaces of this rod. This rod is 145mm longer and a bit narrower than the pyrex glass rod, but due to high performance of this cladded rod we could see even the third echo for which the total ultrasonic path is more than 2.3 meters and still no trailing echoes exist. Figure 2.20 shows the 5MHz

reflected echoes through a 400mm long and 9.4mm diameter P_2O_5 doped cladded rod. This figure clearly indicates the superiority of this rod over uncladded one. Even the 5th and 6th echoes for which the ultrasonic total path is more than 4.5 meter could be observed and only a little spurious signals exist. Rod No. 5 does not show a superiority over pyrex glass rod at 5MHz frequency. One reason is that the core-cladding boundary of this rod is not uniform and it is also narrower compared to the other rods, hence, 5MHz acoustic waves are not well guided in these rods. However, even for this rod we can see a much better acoustic performance compared to uncladded pyrex glass rod at higher frequencies. This can be clearly seen from the experiments carried out at 10MHz.

At 10MHz the difference between the echoes obtained from uncladded and cladded rods is more clear. All the cladded rods show better acoustic performance compared to uncladded one. As it could be seen from Fig.2.3, there are many trailing echoes existing for uncladded pyrex glass rod. Figures 2.13, 2.15, ... and 2.21 show the 10MHz reflected echoes through rods number 2 to 6 respectively. All these rods perform very well acoustically. Rod 2 is a 182mm long and 12.1mm thick GeO_2 doped step index cladded rod. Figure 2.13 shows the excellent behavior of this rod for which there exist little trailing echoes or spurious signals. The B_0^0 echo is very nice and sharp showing the concentration of the acoustic energy in the core without any diffraction. The second, third and even up to the seventh echo were observed and they have nearly the same quality (the seventh echo travels more than 2.5 meter). The result for the 8% GeO_2 doped GRIN profile cladded buffer rod is shown in Fig.2.15. For this rod some trailing echoes were observed but are much weaker compared to the first longitudinal arrival, B_0^0 . The measurement for rod 4 is shown in Fig.2.17. This rod has high performance and the echoes are in ideal form. Rod 4 is narrower than rod 2 and two times longer but still performs as well or even better. The echoes for the TiO_2 doped step profile cladded rod is shown in Fig.2.19. The echoes for the 9.8% P_2O_5 doped step profile 400mm long cladded buffer rod is shown in Figs.2.21. Again the good acoustic behavior can be seen i.e. sharp signals with little trailing echoes. For the seventh echo the total ultrasonic path was 5.6 meter and still the signal was in good shape. This is a strong proof for good longitudinal wave guidance in the core. Finally, the 30MHz measurement for rod 3 is shown in Fig.2.22 and it is shown that at this frequency there is almost no trailing echo. At higher frequencies attenuation is higher but due to the better confinement of the acoustic energy in the core there are fewer spurious signals present, the signal to noise ratio could be better.

Our experimental results presented in this chapter confirm that because the acoustic energy is guided in the core, therefore: (1) the first longitudinal arrival loses a little energy and remains strong after a long propagation path, (2) only little trailing echoes exist. We also immersed them into water and brought them into contact with each other and confirmed that: (1) there was no leakage when they are immersed in liquids, (2) there is no cross-talk when they are touched one another. Hence, we conclude that the cladded rods are preferred over uncladded ones and are excellent candidates as ultrasonic buffer rods.

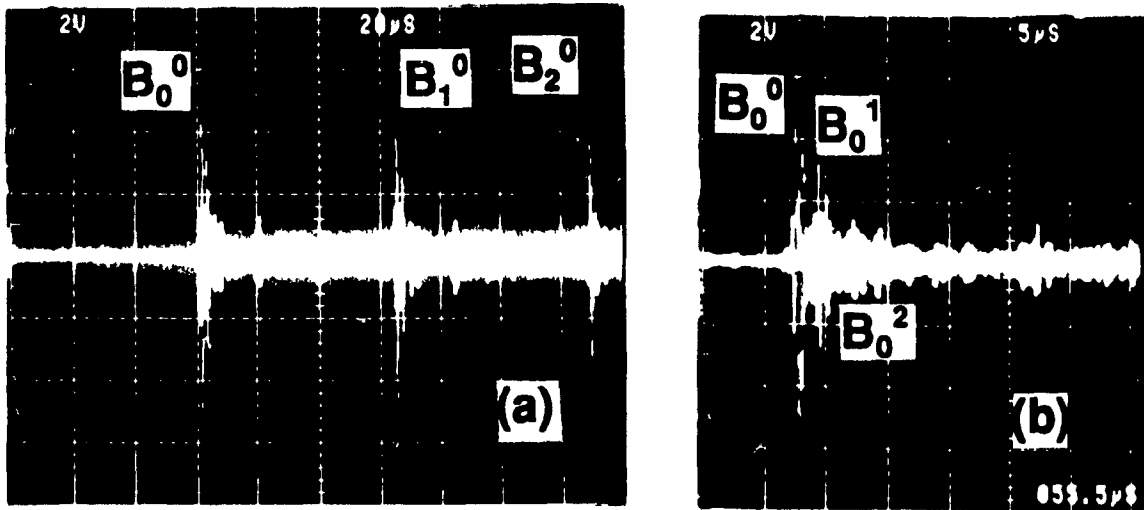


Figure 2.12 (a) The reflected 5MHz longitudinal echoes through a 182mm long cladded glass rod (No. 2). (b) The zoomed picture of (a).

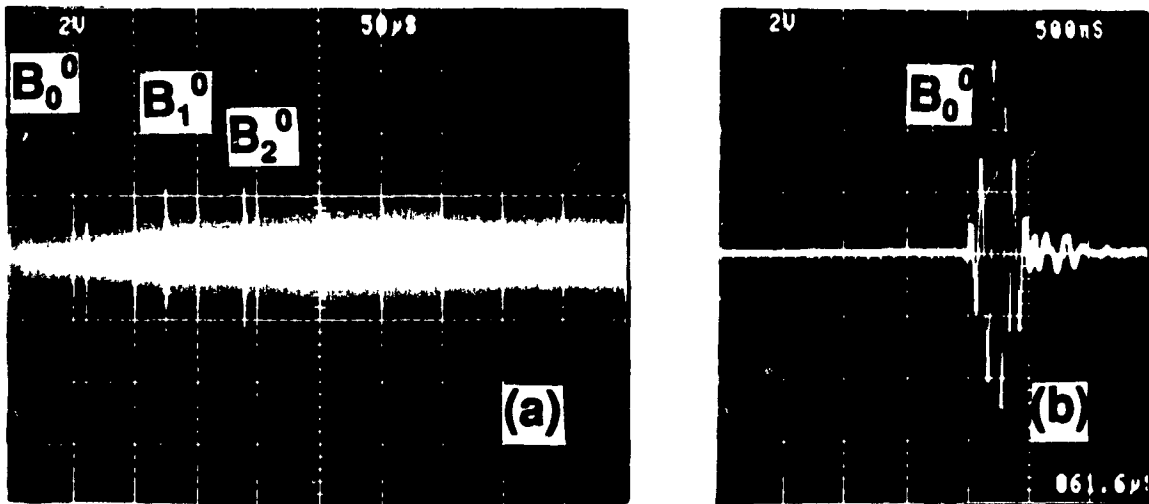


Figure 2.13 (a) The reflected 10MHz longitudinal echoes through a 182mm long cladded glass rod (No. 2). (b) The zoomed picture of (a).

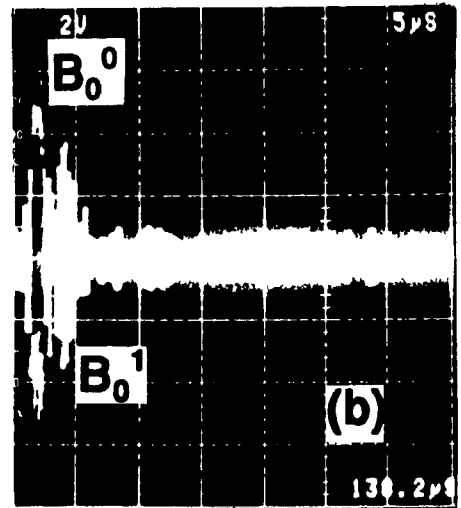
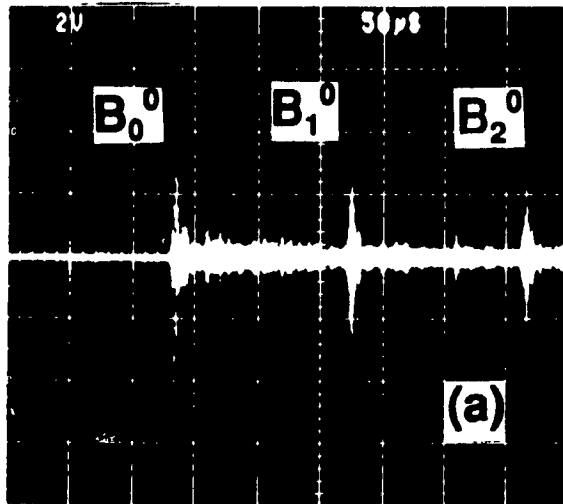


Figure 2.14 (a) The reflected 5MHz longitudinal echoes through a 392mm long cladded glass rod (No. 3). (b) The zoomed picture of (a).

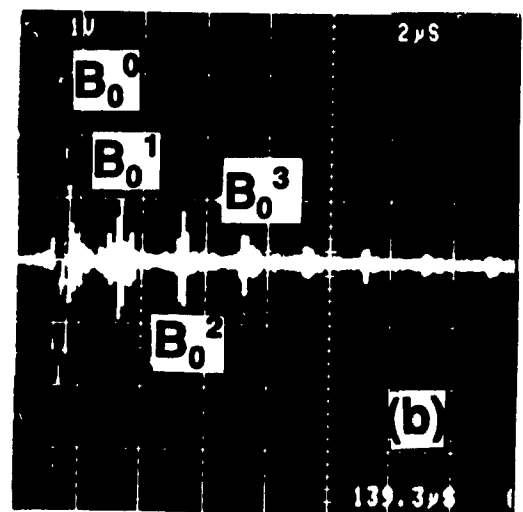
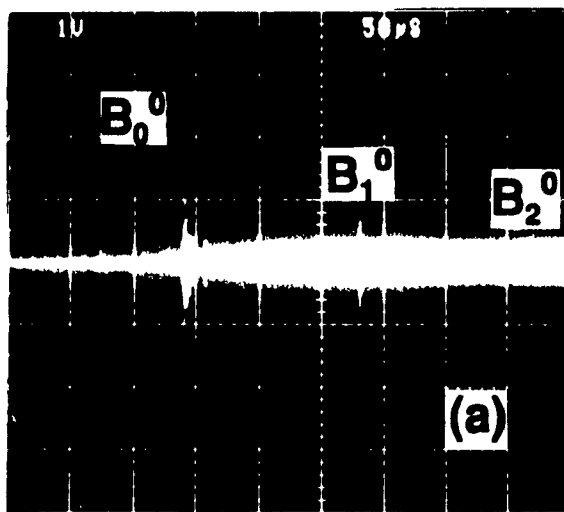


Figure 2.15 (a) The reflected 10MHz longitudinal echoes through a 392mm long cladded glass rod (No. 3). (b) The zoomed picture of (a).

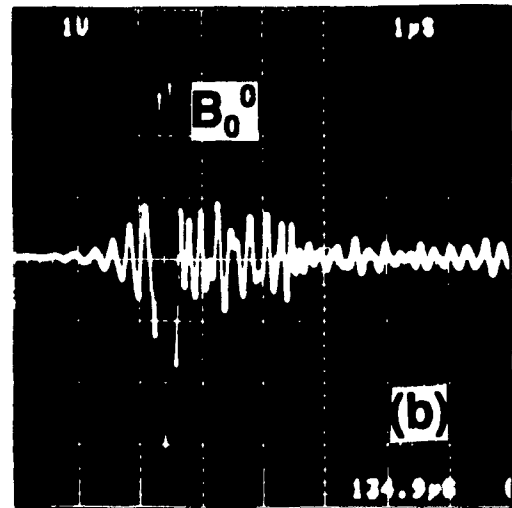
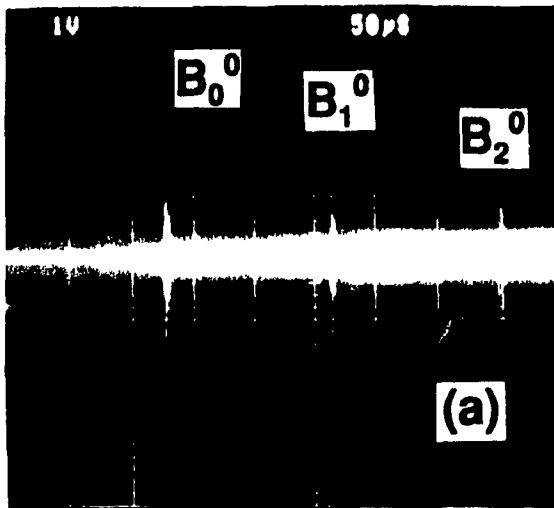


Figure 2.16 (a) The reflected 5MHz longitudinal echoes through a 395mm long cladded glass rod (No. 4). (b) The zoomed picture of (a).

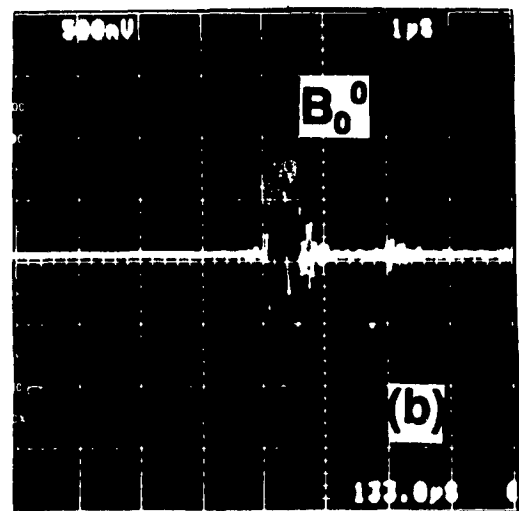
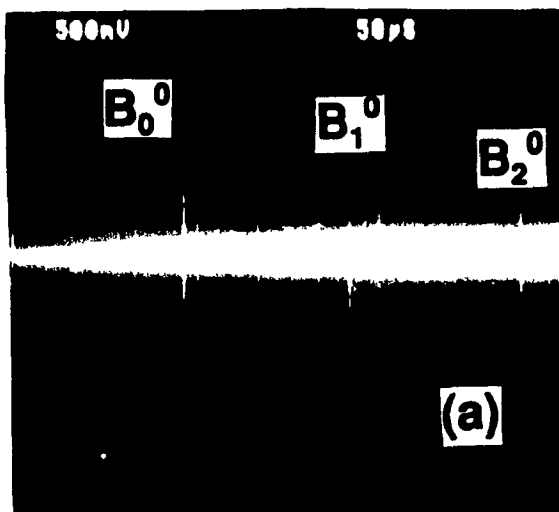


Figure 2.17 (a) The reflected 10MHz longitudinal echoes through a 395mm long cladded glass rod (No. 4). (b) The zoomed picture of (a).

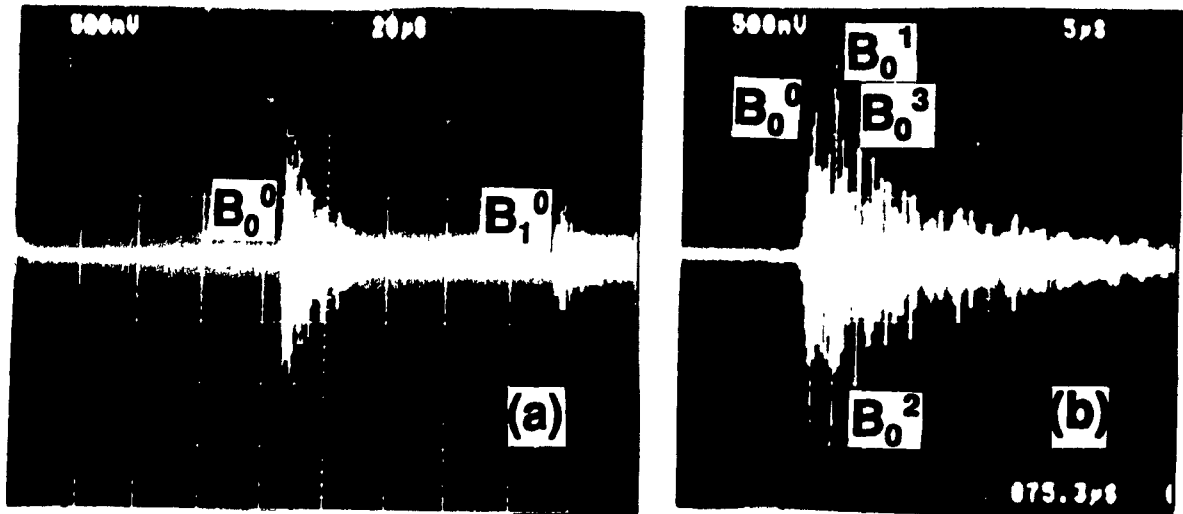


Figure 2.18 (a) The reflected 5MHz longitudinal echoes through a 260mm long cladded glass rod (No. 5). (b) The zoomed picture of (a).

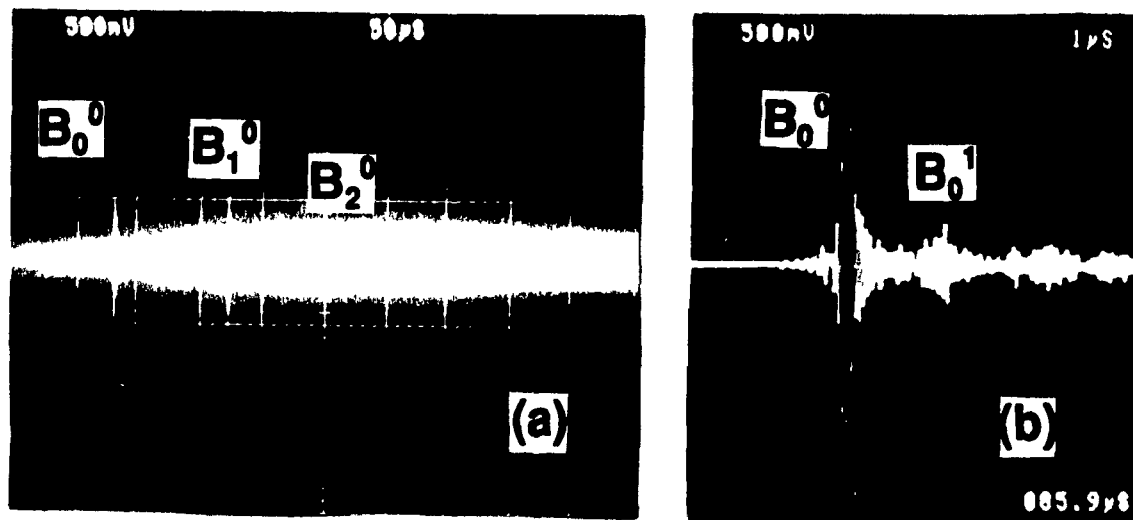


Figure 2.19 (a) The reflected 10 MHz longitudinal echoes through a 260mm long cladded glass rod (No. 5). (b) The zoomed picture of (a).

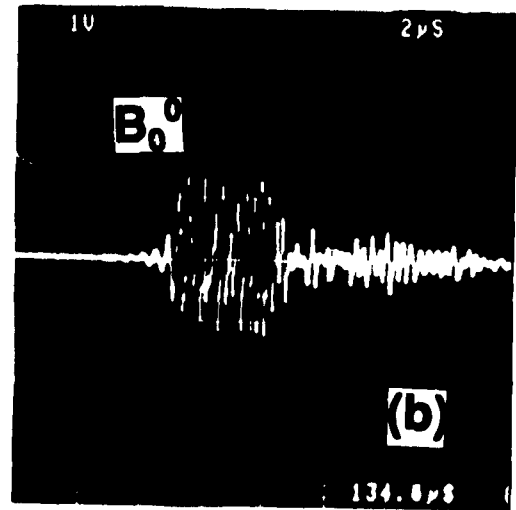
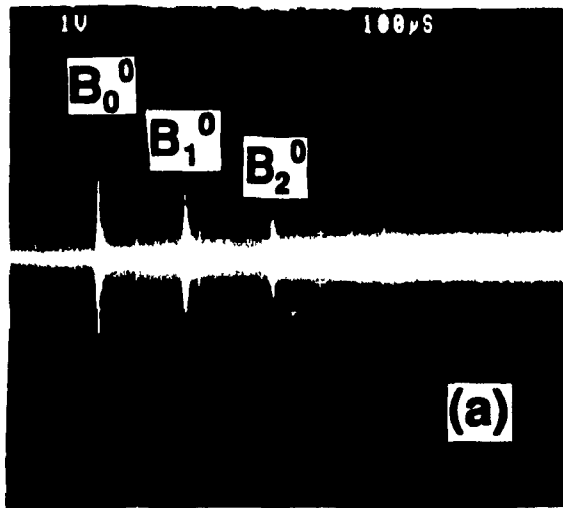


Figure 2.20 (a) The reflected 5MHz longitudinal echoes through a 400mm long cladded glass rod (No. 6). (b) The zoomed picture of (a).

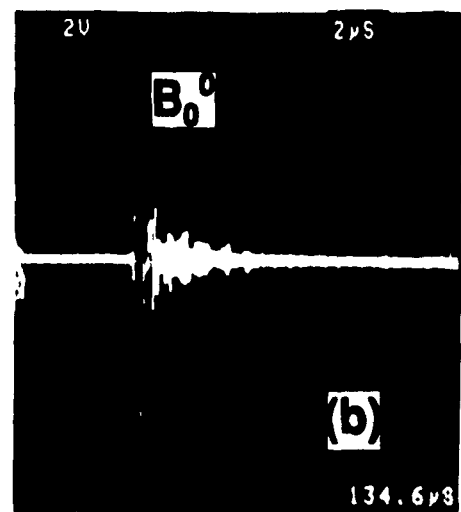
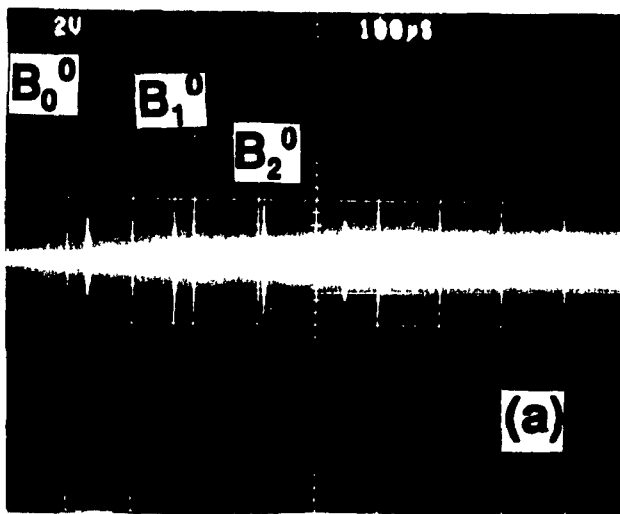


Figure 2.21 (a) The reflected 10MHz longitudinal echoes through a 400mm long cladded glass rod (No. 6). (b) The zoomed picture of (a).

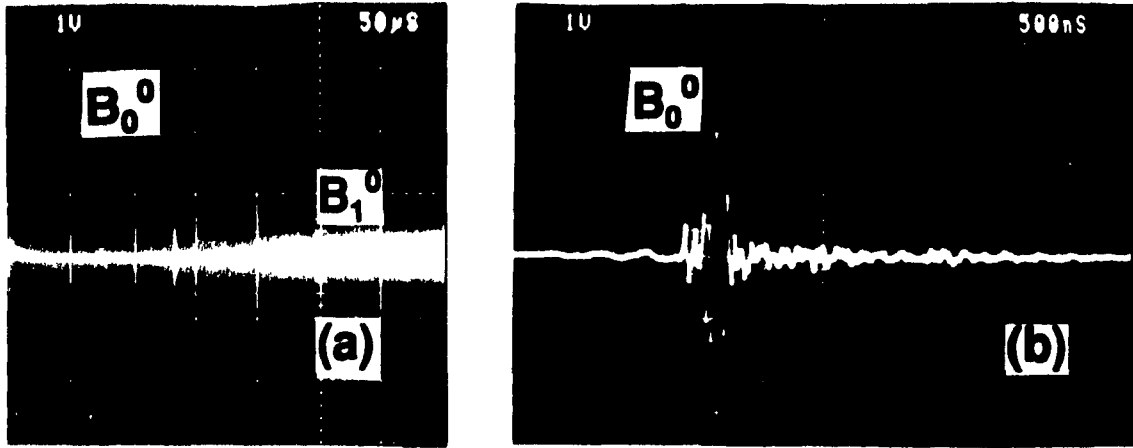


Figure 2.22 *The reflected 30MHz longitudinal echoes through a 392mm long cladded glass rod (No. 3). (b) The zoomed picture of (a).*

2.6.2 Shear Waves

Ultrasonic shear pulse-echo measurements were also carried out on all the rods listed in Table 2.2. The transducer was a 5MHz 6.35mm diameter shear transducer and a very high viscosity gel was used as ultrasonic couplant between the transducer and the end surface of the buffer rod.

Our measurement results are shown in Figs.2.23 to 2.28 for rods number 1 to 6 respectively. Although the acoustic attenuation in pyrex glass is higher than that in fused silica however, our shear pulse-echo measurements suggest that cladded rods have a higher signal strength and a narrower pulse width. For the shear waves, since the mode conversion process [6],[7], which is the source of trailing echoes for longitudinal waves, does not exist, no trailing echoes exist for either cladded or uncladded rods, so from this point of view the cladded and uncladded rods are the same.

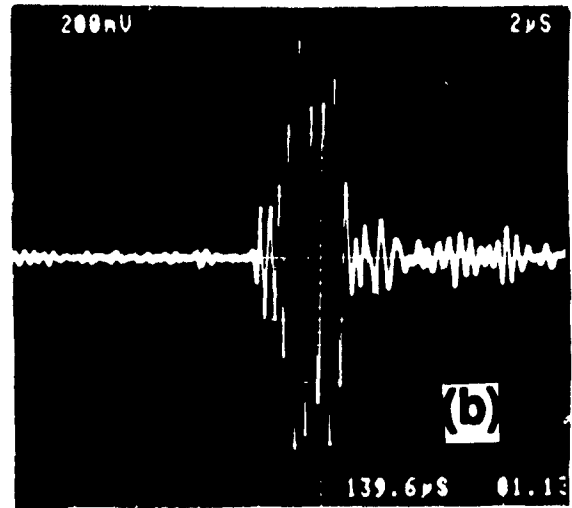


Figure 2.23 (a) The reflected 5MHz shear echoes through a 250mm long pyrex glass rod (No. 1). (b) The zoomed picture of (a).

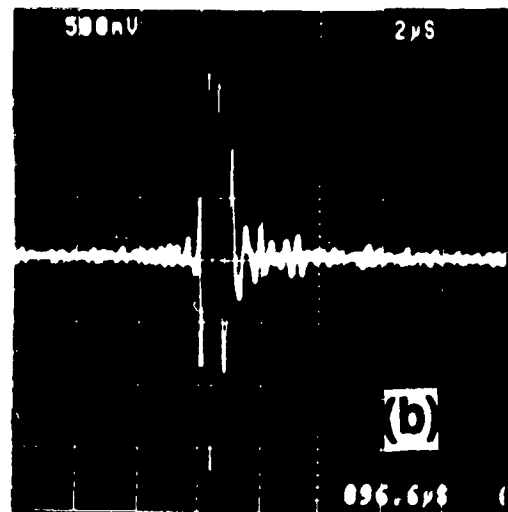
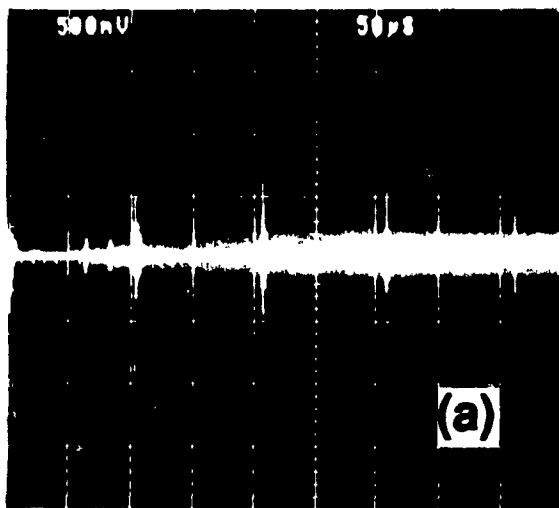


Figure 2.24 (a) The reflected 5MHz shear echoes through a 182mm long clad glass rod (No. 2). (b) The zoomed picture of (a).

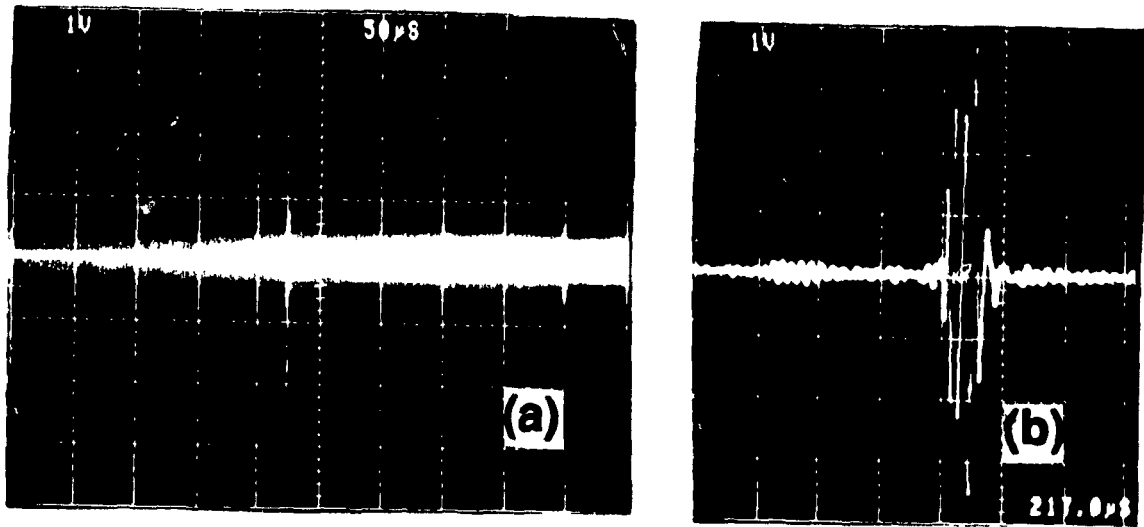


Figure 2.25 (a) The reflected 5MHz shear echoes through a 392mm long cladded glass rod (No. 3). (b) The zoomed picture of (a).

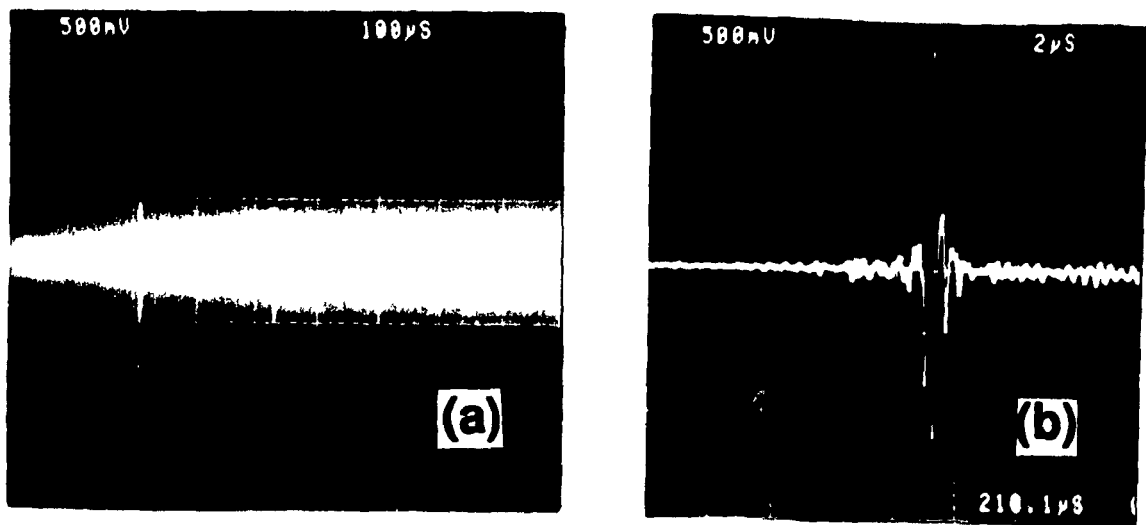


Figure 2.26 (a) The reflected 5MHz shear echoes through a 395mm long cladded glass rod (No. 4). (b) The zoomed picture of (a).

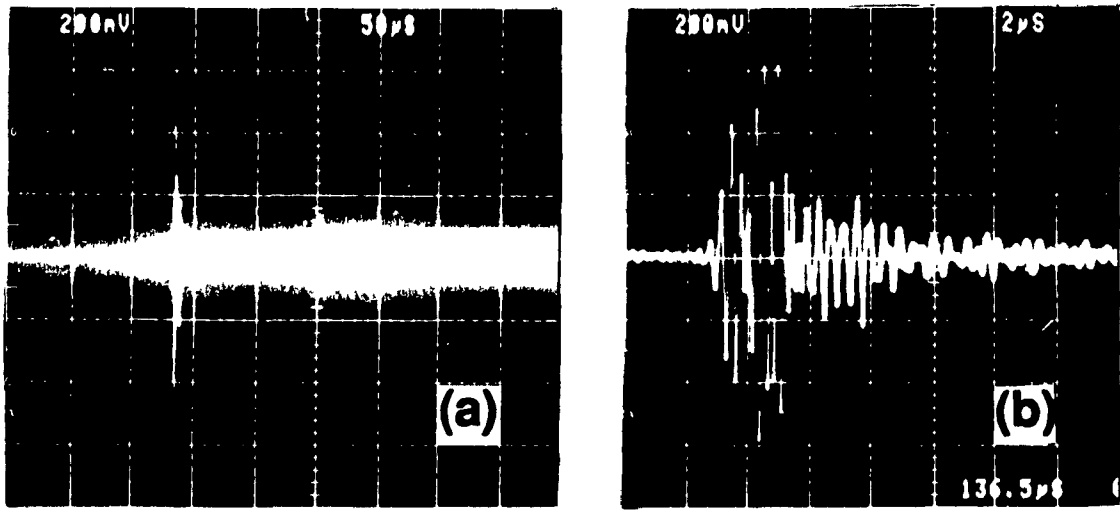


Figure 2.27 (a) The reflected 5MHz shear echoes through a 260mm long cladded glass rod (No. 5). (b) The zoomed picture of (a).

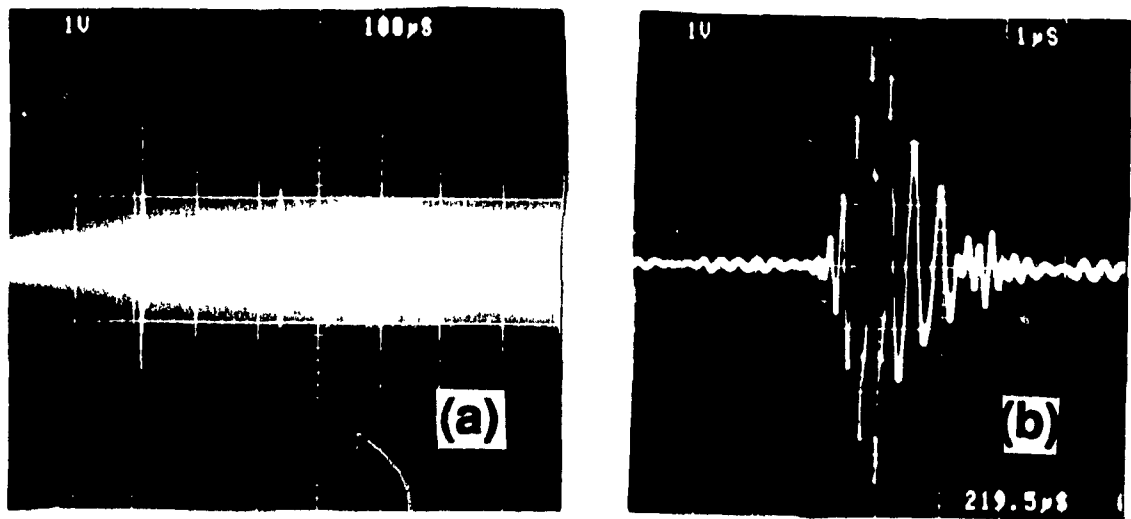


Figure 2.28 (a) The reflected 5MHz shear echoes through a 400mm long cladded glass rod (No. 6). (b) The zoomed picture of (a).

2.7 Visualizing the Acoustic Field

A visualizing system was used to visualize the acoustic beam exiting from the end of long buffer rod. Due to the consideration of the acoustic attenuation in long rods the operating frequency was chosen to be 10MHz. The aim was to observe the acoustic guiding effect due to the presence of the cladding. The details of the guiding effect in such long rods can be found in [19].

2.7.1 Methods of Visualizing an Acoustic Field

Much work has been done dealing with visualization techniques for over a century. Two main approaches of visualizing an acoustic field are the Schlieren method and the photoelastic methods which have been reviewed in [23].

The Schlieren method depends on detecting the deviation of light caused by the refractive index perturbations induced by ultrasonic waves. The photoelastic method, on the other hand reveals the stresses in an ultrasonic wave using crossed polaroids to detect the stress induced birefringence of the medium. Since we are interested in the intensity distribution of the acoustic field, we have decided to use the Schlieren technique.

The basic arrangement of the Schlieren system is shown in Fig.2.29. A parallel beam of light traverses an acoustic field. At zero acoustic intensity light will be focussed by the lens at a single point blocked by a spatial filter at the Fourier plane, and there will be a dark screen at the image plane. However, a continuous wave ultrasound will act as a phase diffraction grating and will form a series of diffraction orders. By filtering out the 0th order, we can reveal the diffracted order and the intensity of the acoustic field will appear as a bright image in a dark field. However, the individual wave fronts will not be resolved. It is noted that a collimated acoustic beam will appear as a diffracted spot at the Fourier plane, while a focussing acoustic beam will appear as an arc around the 0th order.

2.7.2 Experimental Setup

We installed an experimental set-up as shown in Fig.2.29. Figures 2.30a, 2.30b and 2.30c are photographs of the experimental system. The optical probe beam was expanded to a diameter of 50mm. The focal length of the focussing lens was 75cm. In the beginning of the experiment we found out that due to the cylindrical shape of the rod and fine structures of the index profile which scatters the probe beam, it was very difficult to observe the acoustic beam propagating inside the rod. Therefore, acoustic waves exiting out of the rod into a water bath were used to evaluate the necessary information instead. The advantage of water is its uniformity, transparence, high photoelastic coefficient and reasonably low acoustic attenuation. The disadvantage is the acoustic reflection and refraction present at the rod-water interface. Furthermore, because liquid does not support shear acoustic waves, only experiments involving longitudinal acoustic waves are presented.

In order to evaluate the performance of the experimental system, a non-focussed ultrasonic transducer directly contacting a bath of water was used initially. We observed a uniform light beam at the Fourier plane and a uniform acoustic field at the image plane. At the image plane a two dimensional CCD camera connected to a video recorder as shown in Fig.2.29 was used as the image recorder. We then tried a focussing ultrasonic transducer also directly contacting the water bath and an arc light beam at the Fourier plane along with a focussing acoustic field at the image plane was observed.

The first rod tested was a 290mm 8.6% GeO_2 doped step index rod and at 10MHz the field was basically collimated and concentrated in the core as shown in Fig.2.31. Then we tried a 392mm 8% GeO_2 doped GRIN rod. At 10MHz, the field shown in Fig.2.32 was slightly narrower than the previous sample. These figures indicate that at 10MHz, the acoustic waves are guided in the core and that the cladding has an effect. In both these samples, the signal exiting from the rods was quite strong. The dark area at near the center region of the core is due to the effect of the center dip of the velocity profile [24]. A further observation of the center dip is given in section 2.8.

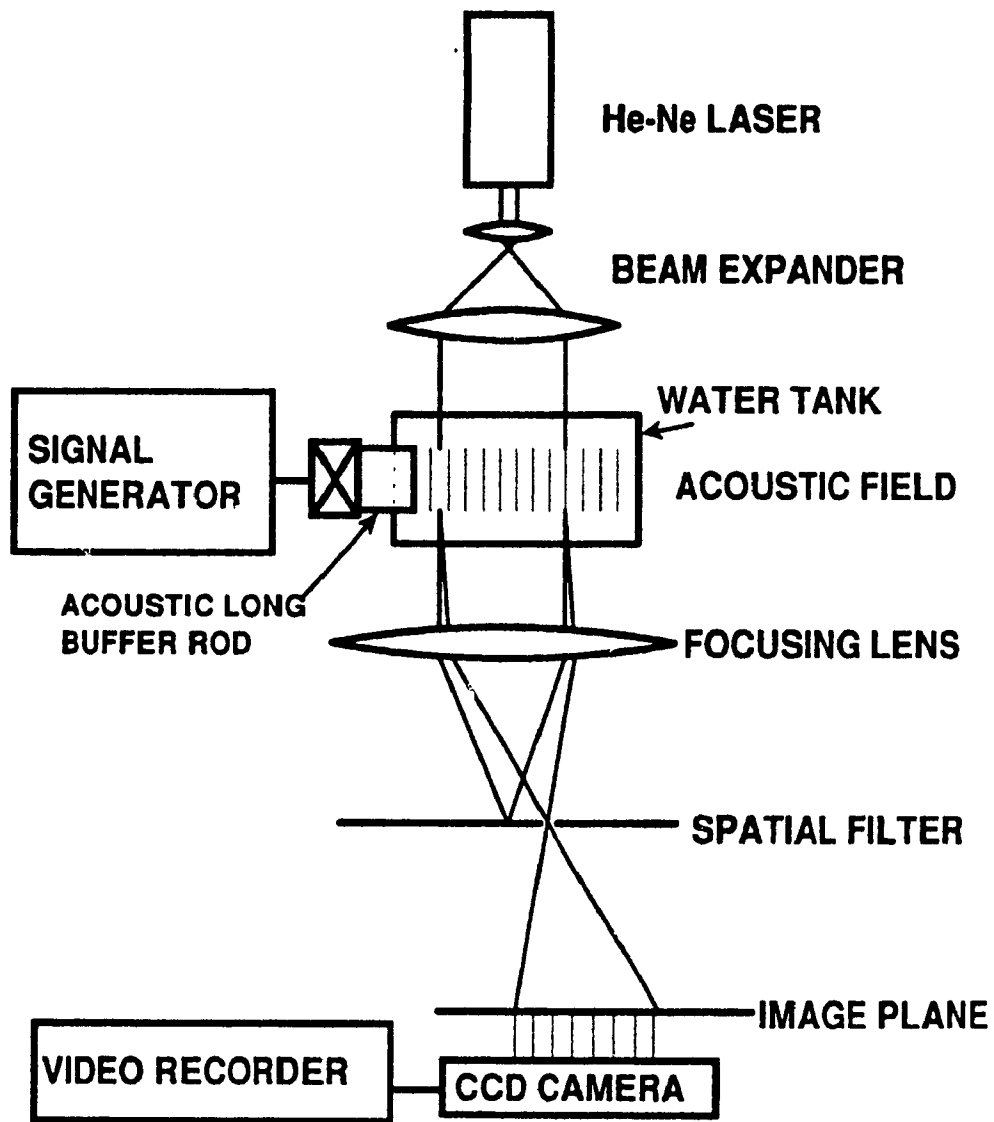


Figure 2.29 Schematic of a Schlieren visualization system.

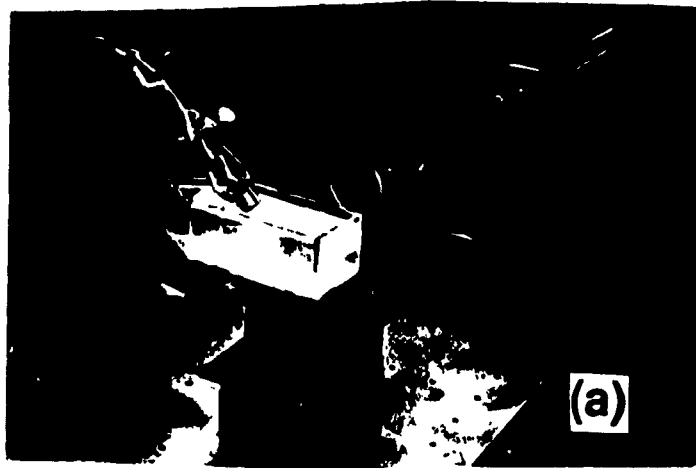


Figure 2.30 Photographs of the experimental set-up for the visualization of ultrasound, (a) He-Ne laser and transducer, (b) ultrasonic frequency generator, CCD camera and monitor (c) A complete view



Figure 2.31 *Image of acoustic waves coming out of a 290mm long 8.6% GeO₂ doped step index rod. Arrow indicates the rod-water interface.*

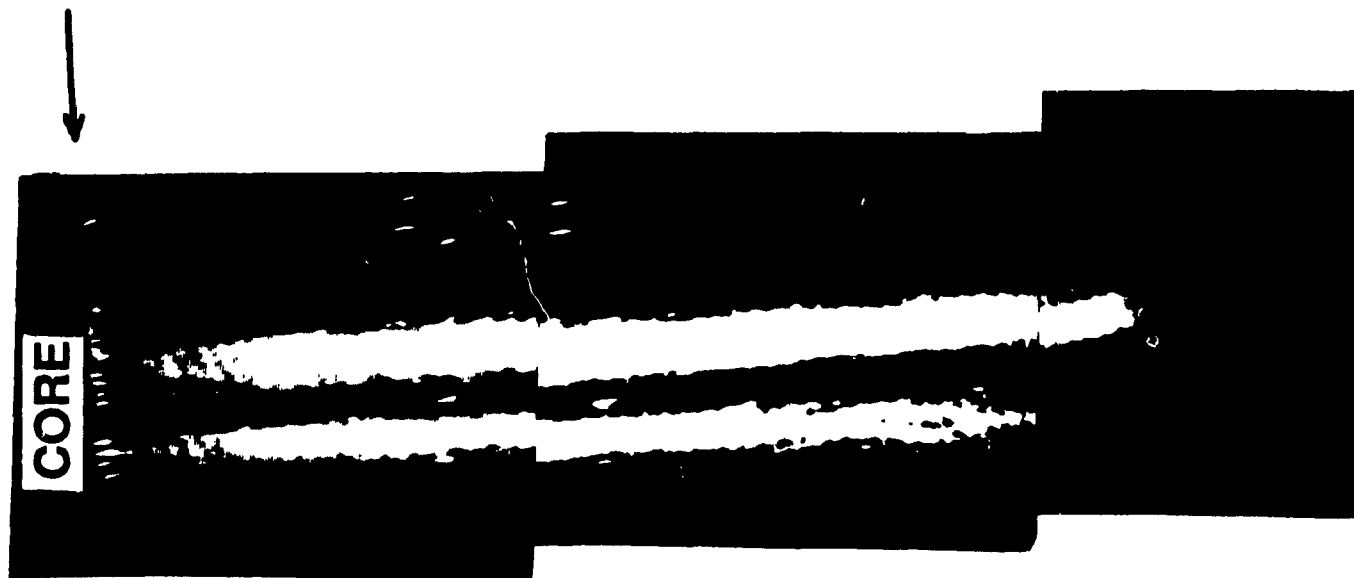


Figure 2.32 *Image of acoustic waves coming out of a 392mm long 8% GeO₂ doped GRIN rod. Arrow indicates the rod-water interface*

2.8 The Effect of the Center Dip on the Acoustic Performance of the Cladded Rods.

As it was discussed earlier the rods made by MCVD method have a center dip. Because of low spatial resolution of the acoustic microscopy, this center dip cannot be seen in the acoustic profile. Again, the presence of such center dip has been proved by Jen et al [24]. Because of the abrupt index change at the rod center, the acoustic energy is not really concentrated at the very center of the core. The acoustic performance of the rod is affected by this fact. To show this effect we performed simple shear pulse echo measurement on two cladded rods one with center dip and the other one without center dip.

Figure 2.33 shows the first shear arrival through a 65mm long GeO_2 doped GRIN index profile at 5 and 10MHz. This rod is made by MCVD method and has a center dip. In Fig.2.34 we see the first shear arrival through a 66mm long GeO_2 doped GRIN index profile at 5 and 10MHz. The only difference between the latter and the former one is that the latter rod has been made with a Vapor Axial Deposition, VAD [25], method and has no center dip. The VAD method can be used to fabricate cladded rods with long lengths and large diameters. These figures indicate the difference. We got much sharper and nicer acoustic signals from the second rod which has no center dip. This shows that the rod with no center dip has better energy confinement in the core than the one with a center dip. Therefore, we conclude that for buffer rod applications, cladded rods without the center dip should have a better performance than those with a center index dip.

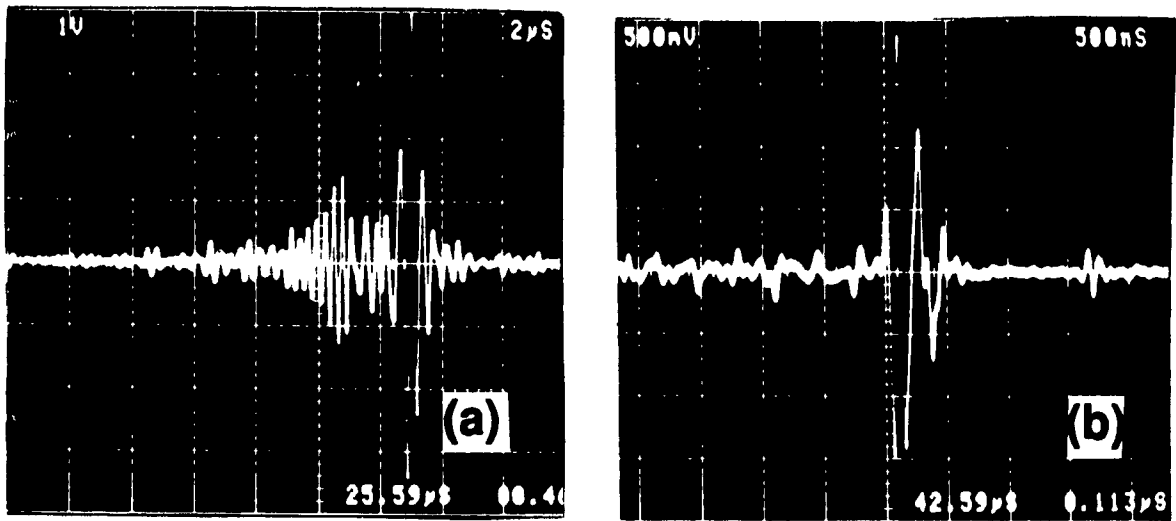


Figure 2.33 The first reflected shear echo from the end of a 65mm long cladded rod with a center index dip, (a) at 5MHz and (b) at 10MHz.

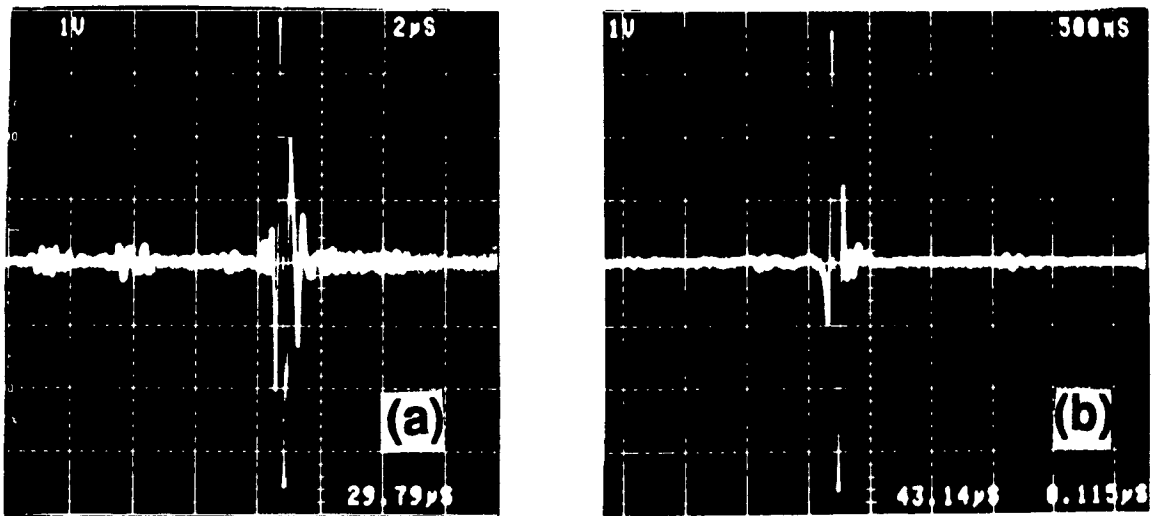


Figure 2.34 The first reflected shear echo from the end of a 66mm long cladded rod without a center index dip, (a) at 5MHz and (b) at 10MHz.

2.9 Spherical Concave Lens

2.9.1 The Lens Fabrication Process

We have also fabricated a spherical concave lens 9.5mm in diameter at the end of the buffer rod. The spherical concave lens was made by gradually polishing out the glass from the end surface of the rod using a 9.5mm (3/8") diameter spherical ball bearing. The setup for making the lens is shown in Fig.2.35. A motor is used to rotate the glass rod around its axis and a ball bearing is brought into contact with the center of rod end surface. The ball bearing is pushed by a small spring force. The ball bearing and the end surface of the glass rod are coated by diamond paste. The coating has to be continuously checked more paste added periodically. We started with 45 micron paste and when the desired spherical shape is formed we do the fine polishing down to 6 micron in three steps (15, 9 and 6 micron). It is to be noted that the lens fabrication process is slow and takes more than a day to make a good lens.

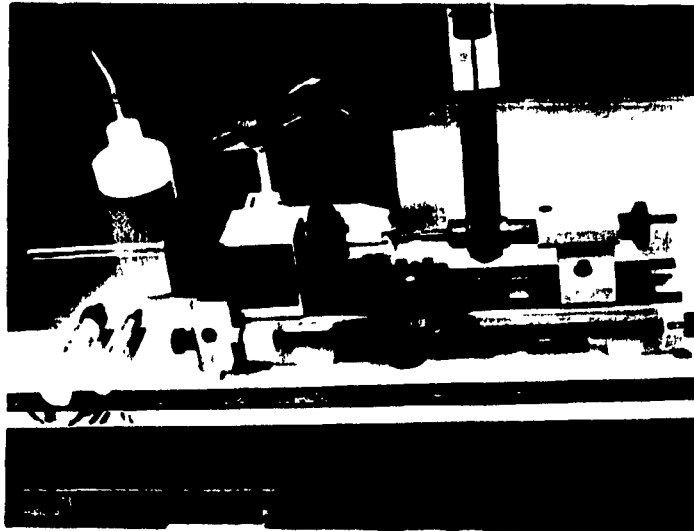


Figure 2.35 *The setup for spherical concave lens fabrication at the end of glass rods.*

2.9.2 Acoustic Measurements

Figure 2.36 shows the schematic for the setup of focussing measurements and Fig.2.37 shows the photograph of the experimental setup. In this setup the sample can be moved vertically and horizontally. The buffer rod was fixed and the sample was displaced along the rod axis direction. The "Linear Voltage Displacement Transducer" (LVDT) is used to monitor the displacement of the sample and its output is a dc voltage which varies linearly with the displacement of the sample. The LVDT output is connected to the X channel of the oscilloscope. The detector detects the peak value of the acoustic signal and sends it to the Y channel. When the sample is displaced along the rod axis direction, the amplitude variation versus the distance is obtained as shown in Fig.2.38. Figures 2.39a and 2.39b show the first, S_0^f , and the second, S_1^f , echoes from the sample surface at focal point, at 10MHz. From these figures we can clearly see the nice focussing behavior.

One lens fabricated at the end of a rod was used to scan a microscope calibration grid which has spacing of 500um. The grid was located on a flat surface and the whole surface was displaced horizontally using a step motor together with a controller, as shown in Fig.2.40. The vertical distance of the flat surface and the end surface of the rod is so adjusted that the flat surface is located at focal point. Again, the dc output voltage of the LVDT which shows the horizontal distance is connected to the X-channel of scope and the peak value of the reflected echo after it is converted to a dc voltage by the detector is connected to the Y-channel. As the grid moves under the focal point the amplitude variation of the reflected echo versus the horizontal distance is obtained as shown in Fig.2.41. Figure 2.41 demonstrates that the focussed rods can be used to image or scan the sample surface.

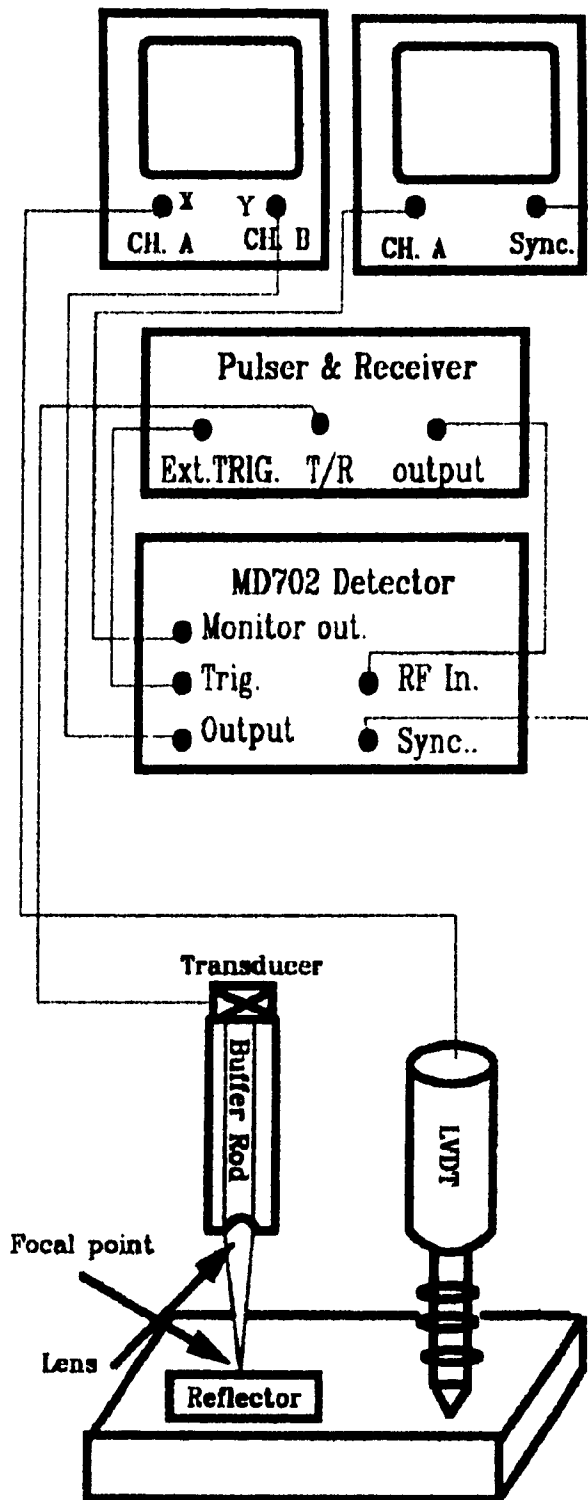


Figure 2.36 Schematic for the focussing measurement setup.

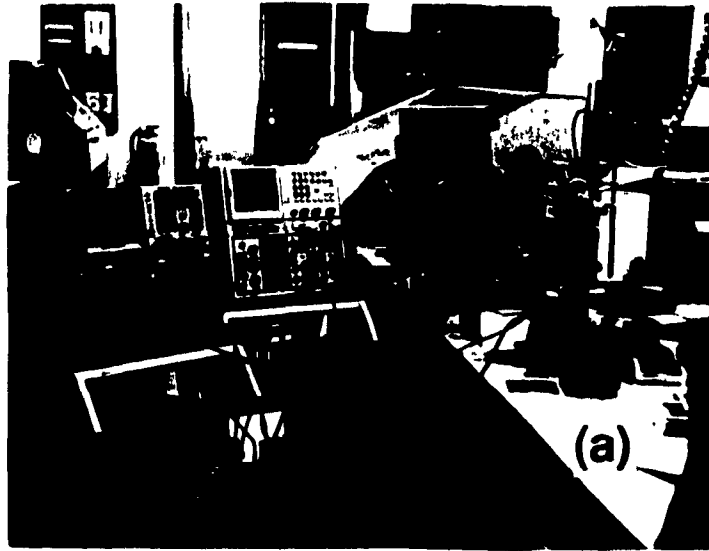


Figure 2.37 (a) Photograph of the experimental setup for focussing measurement. (b) Shows the pulser, detector and receiver units, from left to right respectively.

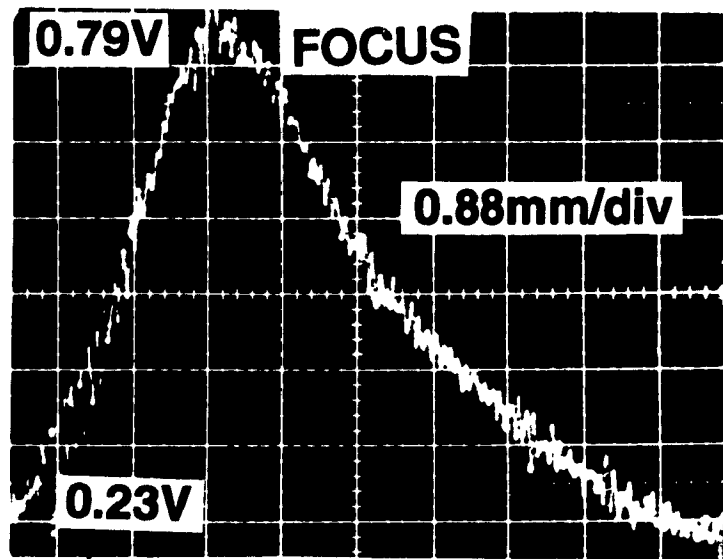


Figure 2.38 *The axial amplitude variation for the received signal near the focal point.*

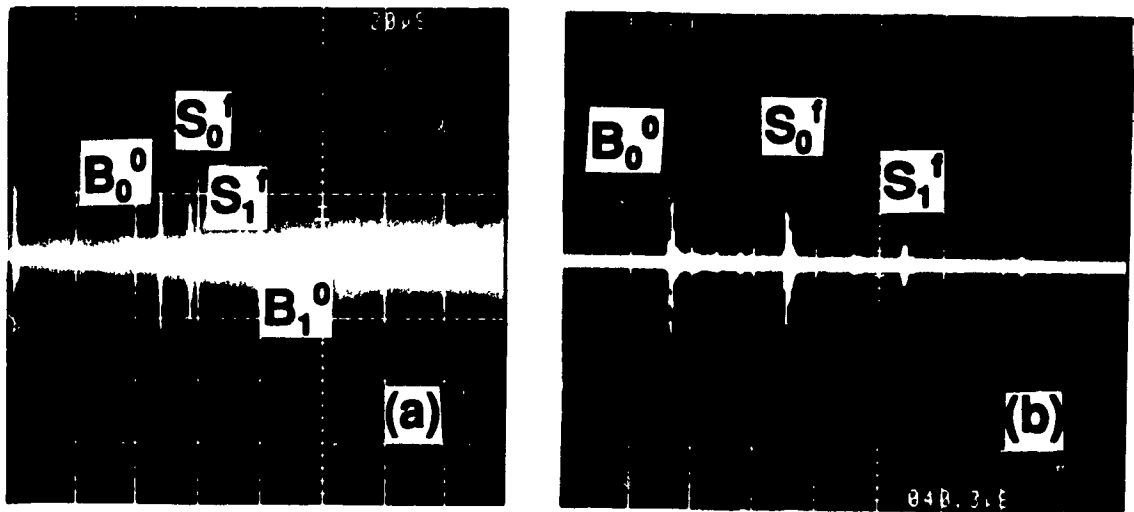


Figure 2.39 (a) *The received echoes when a flat sample is located at the focal point. (b) is the higher magnification near B_0^0 .*

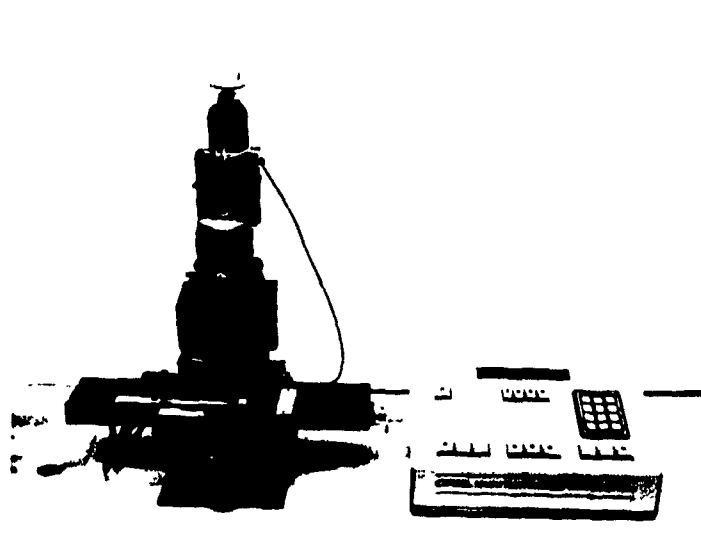


Figure 2.40 *Setup for acoustic scanning of a grid.*

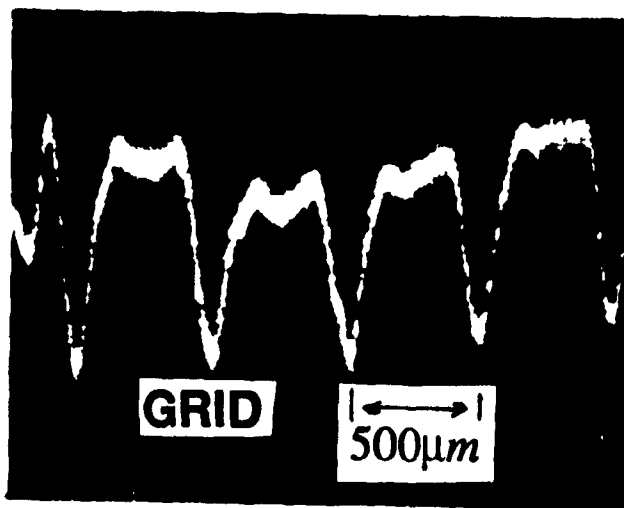


Figure 2.41 *A line scan of a grid scanned at the focus of a long buffer rod with a spherical concave lens at its end surface.*

CHAPTER 3: Tapered Rods

In the previous chapters the cladded acoustic buffer rods were discussed thoroughly and many advantages were counted for them. For high frequency acoustic imaging ($>20\text{Mhz}$) the diameter of the rod can be made small enough. High spatial resolution ultrasonic measurements may also be performed because the acoustic energy is concentrated in the small core. Small diameter is needed for many applications where tiny features are dealt with. For example, in some medical applications we need thin and bendable buffer rods to monitor certain properties inside of the human body, like blood vessels. However, small rod diameter makes the process of bonding the ultrasonic transducer to the endface of the rod inconvenient and time consuming. In this chapter we report a unique probe to overcome such bonding difficulty. A cladded silica rod of a large diameter is tapered gradually to a rod of a small diameter. The characterization and ultrasonic measurements of such tapered acoustic buffer rods are presented. Also, at the end of this chapter we will show a novel acoustic lens fabricated at the very small end of these tapered rods, using optical techniques.

3.1 Characterization of Tapered Rods

Figure 3.1 shows a few tapered silica rods used in the experiments. At first, they were made in a uniform diameter by a modified chemical vapor deposition method [22]. Then the taper was formed by heating and drawing the rod. Along the tapered rod the ratio of the core over the total rod diameter remains constant. In order to obtain the desired guidance condition, the acoustic velocity profile of a cladded rod must be measured.

The measured LSAW and LSSCW velocity profiles across the rod are shown in Figs.3.2a and 3.2b, respectively. The ratio of the velocity difference between the core and the cladding over the velocity of the core is near 2%. For good acoustic guidance, the velocity of the core is required to be less than that of the cladding. For the tapered rod sample used in the acoustic profile measurement the core diameter at the thick end is 7mm and the total diameter is 16mm. Figures 3.3a and 3.3b indicate that this cladded buffer rod can be used as a good ultrasonic waveguide for frequencies above 20MHz. It is noted that the attenuation and the pulse dispersion set the high frequency operation limit and the dimension including the core diameter and the cladding thickness sets the low frequency limit. At the same frequency, a smaller velocity difference between the core and the cladding of a cladded rod requires a thicker cladding [10],[11].

3.1.1 Ultrasonic Measurements

Figure 3.3a shows the 30MHz reflected echoes through a 225mm long tapered rod in air. The thicker end of this tapered rod has a total diameter of 16mm and a 7mm diameter core, and the thin end has a total diameter of 1.5mm and a 0.66mm diameter core. This geometry offers the convenience to bond a transducer of a larger diameter to the thicker end of the cladded rod. In this case a 30MHz 4mm diameter longitudinal transducer and a commercial gel couplant was used. The echo B_0^0 , is the first longitudinal arrival from the end of the buffer rod. Echoes B_T 's come from the tapered section having a sharper diameter reduction which causes an acoustic impedance mismatch along the axial direction of the rod. Signals B_H represent the higher order acoustic propagation modes whose acoustic energies are concentrated in the cladding region. When this probe tip is immersed in the water, B_H is reduced as shown in Fig.3.3b due to the energy leakage into the surrounding water. We put a flat thick reflector 3.3mm in front of the probe in the water, the reflected

echoes S_0^0 , S_1^0 are shown in Fig.3.3c. It is noted that the echoes B_1^0 and S_0^1 indicated in Fig.3.3c have travelled a distance of nearly 900mm. Figures 3.3a to 3.3c have demonstrated the good performance of this tapered probe at 30MHz. If the operating frequency is very low (i.e. long acoustic wavelength), the acoustic wave energy is no longer sharply concentrated in the core, the cladded rod will behave as an "uncladded" rod. Figure 3.4 shows the reflected signals obtained with a 5MHz transducer for the same tapered rod used in Figs.3.3a to 3.3c. From many similar measurements we find that for this particular cladded rod, reflected signals with good SNR can be obtained when the frequency is between 20 to 35MHz.

A nearly spherical concave lens was also fabricated at the thin end of the tapered rod. Figure 3.5 shows a scanning electron micrograph of one concave surface at the thin end of one tapered buffer rod shown in Fig.3.1 (Scanning Electron Microscopy -SEM- has been used quite a few times in this work and its working principals are briefly discussed at the end of this chapter.). Figure 3.6 shows the shape of the concave surface. It is measured by an optical interferometer mechanically scanned along two perpendicular directions of the same concave surface as Fig.3.5. In this Fig.3.6 the solid line shows a very nice concave surface and the dashed line also indicates the concave surface but a bit diverted at the very right edge. That is because of the uneven polishing of this particular end surface. When the sample used in Fig.3.3c is displaced along the rod axis direction in front of the thin end of the tapered rod having a spherical concave surface as shown in Fig.3.5, the amplitude variation shown in Fig.3.7 of the first echo, S_0^0 , clearly indicates the focussing behavior. In Fig.3.7, the circles are measured data and the solid line is the fitted curve by the third order polynomial regression.

3.1.2 Scanning Electron Microscopy measurement

Because of very small dimension and low contrast difference between core and cladding it was very difficult to see the fabricated lens under optical microscope and to judge about its performance. Hence, Scanning electronic microscopy (SEM) measurements was introduced to see the end face of buffer rod or cross section of the buffer rods. SEM is also used in the next chapter to see the cross section and the surface morphology of the cladded metal rods.

In a SEM the image of a sample is formed on the cathode ray tube (CRT) synchronized with an electron beam probe as it scans the sample surface. The electron beam probe stimulates secondary electrons, backscattered electrons and X-ray photons from the scanned surface. A detector mounted above the sample picks up the secondary electrons or the backscattered electrons and converts them into a real time image of the sample.

In order to obtain a clear images it is important that the contaminants be removed because they deteriorate the quality of the imaging. The samples should also be thoroughly degreased so as to avoid hydrocarbon contamination [26], otherwise the cracking of the hydrocarbon will create a dark spot on the image. Moreover, coating and polishing the sample also play important roles in obtaining a good image. Coating provides a thin conducting layer of Au or Au/Pd alloy on the top of the sample to carry the scanning electrons to the ground and helps to increase the emission of secondary electrons. The thickness of the coating is critical. If it is too thick it will obscure the surface details but if it is too thin then it cannot provide a continuous conductive layer to ground the electrons properly, which will charge up on the sample surface, resulting in repelling and deflecting further incoming electrons, and therefore distorting the surface image. The thickness of our coatings was about 100-200Å of Au/Pd material.

The details of the acoustic lens fabricated at the thin end of tapered rod surface can be clearly seen from the SEM photograph shown in Fig.3.5. From this figure we can see that the surface of the lens is smooth.

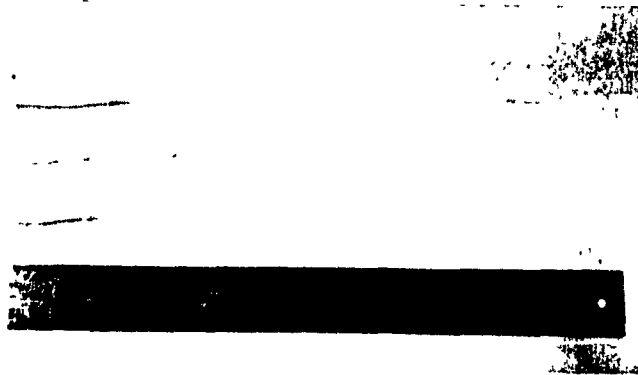


Figure 3.1 *Tapered acoustic buffer rods.*

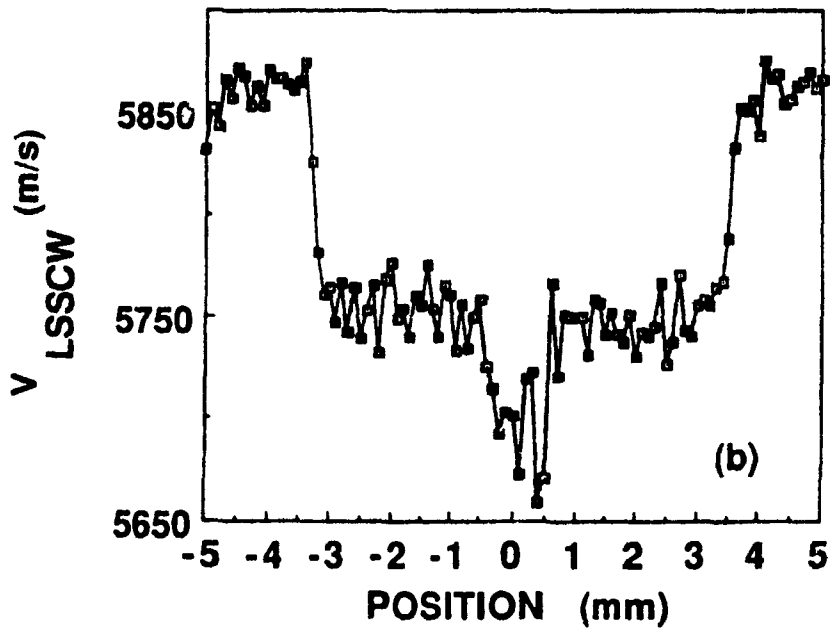
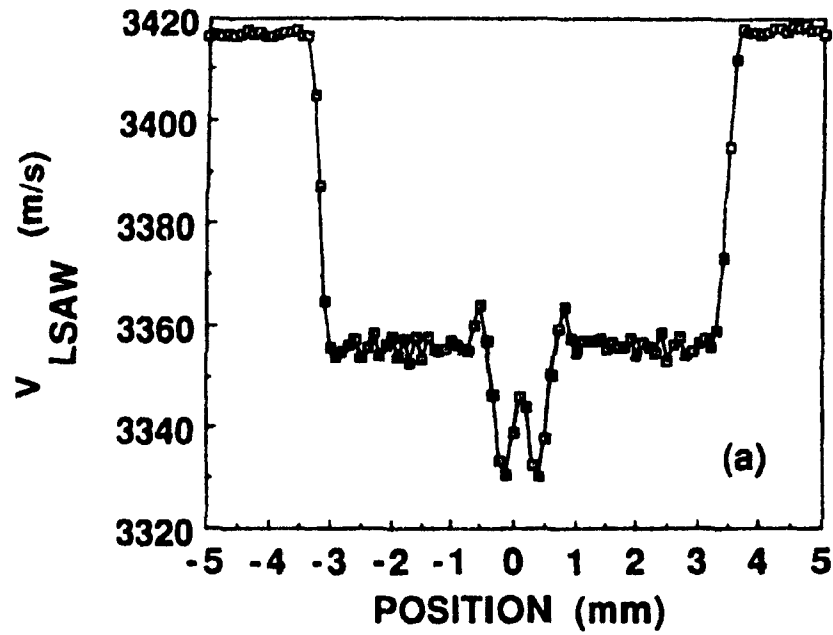


Figure 3.2 The measured (a) V_{LSAW} and (b) V_{LSSCW} profiles for the clad rods shown in Fig. 3.1.

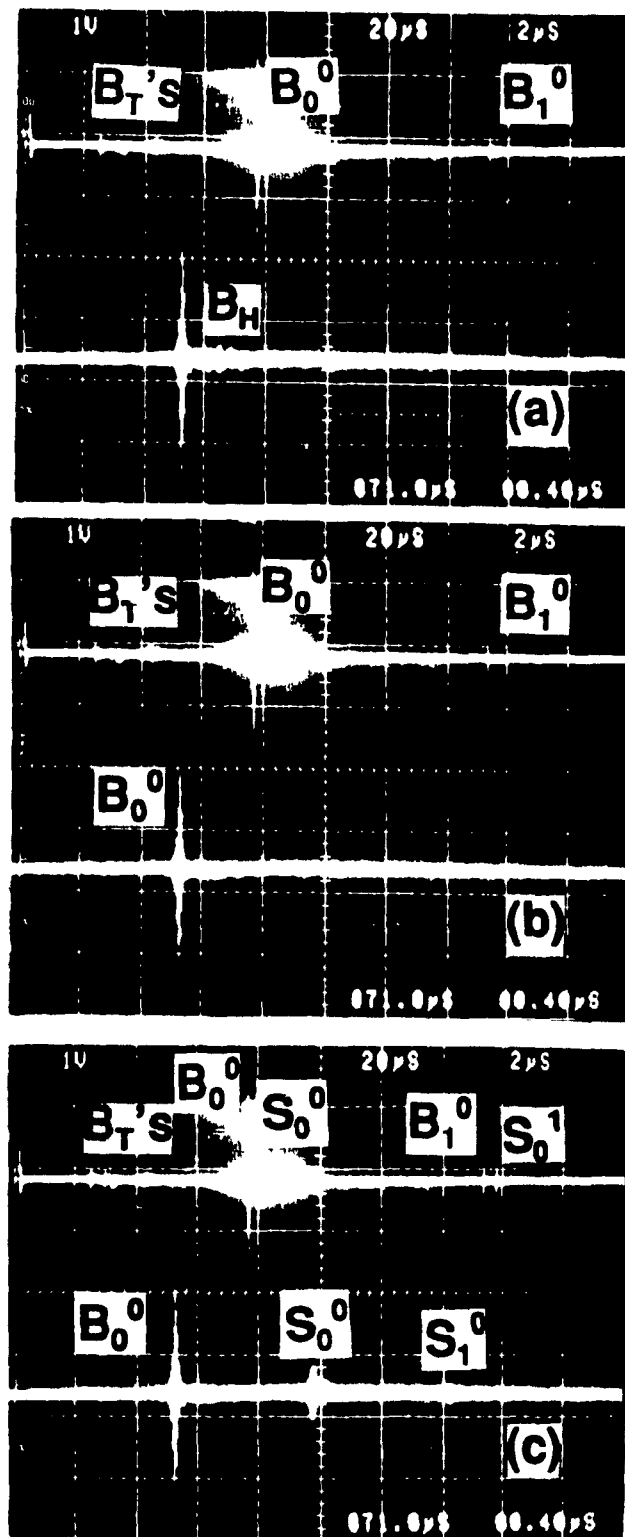


Figure 3.3 The reflected 30MHz longitudinal echoes through a 225mm long tapered rod. (a) in air, (b) in water without a reflector (c) in water with a reflector. The lower trace is a zoomed picture near B_0^0 .

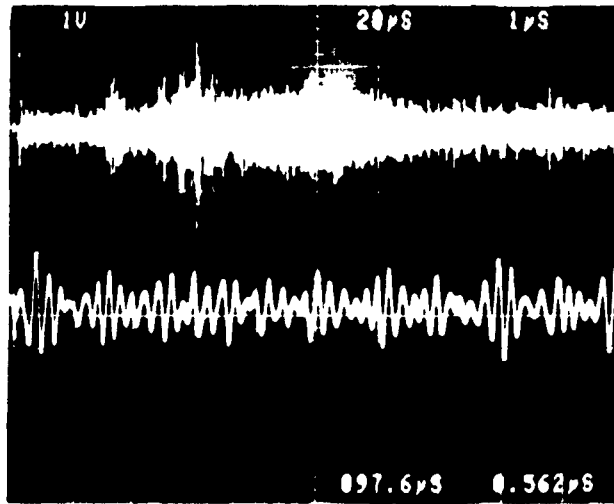


Figure 3.4 *The reflected 5MHz longitudinal echoes through a 225mm long tapered rod in air. The lower trace is a zoomed picture.*



Figure 3.5 *A scanning electron micrograph of a concave surface fabricated at the thin end of the tapered rod.*

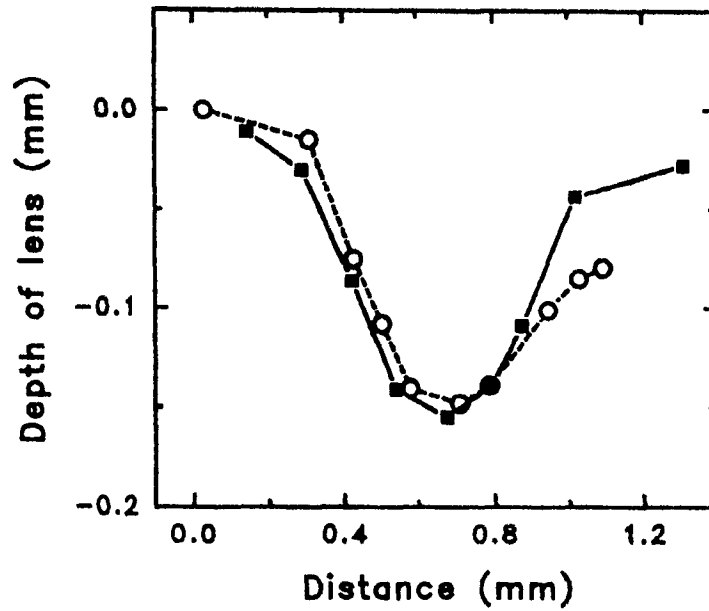


Figure 3.6 *The measured surface profile of the lens fabricated at the thin end of the tapered rod in two perpendicular directions.*

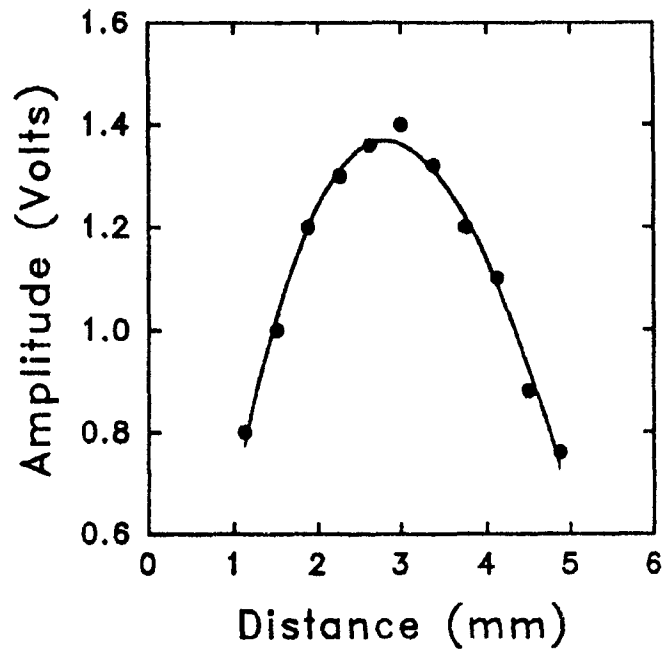


Figure 3.7 *The axial amplitude variation for the received signal near the focus.*

CHAPTER 4: Metallic Long Acoustic Buffer Rods

In the previous chapters we have demonstrated that cladded silica acoustic rods consisting of a core and a cladding are very good candidates for acoustic buffer rods and have superior performances over uncladded rods when used as long acoustic buffer rods. But they have disadvantages, they are very fragile and not easily machinable. These limitations may hurdle their industrial applications. Thus it is of interest to search for buffer rods made of other materials which do not have the disadvantages of glass. A good candidate is a cladded metallic rod. In this chapter the fabrication and acoustic characterization of metallic cladded buffer rods consisting of a tin/lead alloy core and a pure tin cladding are presented. We also discovered that metallic rods fabricated by Ohno Continuous Casting (OCC) method [27],[28] have much better acoustic performance over conventional metallic rods. The comparison is given in this chapter. The obvious advantages of metal over glass materials are machinability and bendability. At the end of this chapter we also show the unfocussed and focussed ultrasonic measurements using such a cladded rod.

4.1 Experimental Aspects

Metallic rods of aluminum and tin made by the conventional casting method and a novel method, namely OCC process [27],[28] were used for the experiments. The ultrasonic pulse echo measurements were carried out at 5 and 10MHz frequencies. In all the experiments gel was used as ultrasonic couplant and the ultrasonic transducers were 5 and 10MHz 6.35mm diameter broadband transducers.

Figure 4.1 shows the 5MHz reflected echoes through a 290mm long and 13mm diameter aluminum rod. This rod was cast by a conventional method and the velocity profile is uniform across the whole rod diameter. The echo B_0^0 , is the first longitudinal arrival. Echoes B_0^1 , B_0^2 , are the trailing echoes which result from the wave diffraction and finite diameter of rod as mentioned previously. Figure 4.2 shows the 5MHz reflected echoes through a 285mm long and 12.5mm diameter pure aluminum rod. This rod was cast by the OCC method and its velocity profile is also considered to be uniform across the whole rod diameter. Comparing Figs.4.1 and 4.2 we can see that the first longitudinal arrival, B_0^0 is weaker than unwanted trailing echoes in Fig.4.1 but it is stronger in Fig.4.2. This means that the second rod which will be referred to as the OCC rod has better acoustic performance over the first rod which will be referred to as the conventional rod. The same experiment was carried out at 10MHz frequency and a similar result was obtained. Figure 4.3 shows the 10MHz reflected echoes through the conventional aluminum rod and Fig.4.4 shows the same reflected echoes through the OCC aluminum rod. Here the difference is much clearer and it can be easily seen that for the case of OCC aluminum rod the unwanted spurious signals or trailing echoes are much less strong than those of conventional aluminum rod. Hence the OCC aluminum rod is preferred over the conventional aluminum rod as an ultrasonic long buffer rod.

We performed the same measurements described above on tin rods. Figure 4.5 shows the 5MHz reflected echoes through a 73mm long pure conventional tin rod of 10.3mm diameter (from Johnson Matthey, Brampton, Ont.) with a uniform velocity profile across the whole rod diameter. In Fig.4.6 we see the same echoes for a 98mm long pure OCC tin rod of 10.6mm diameter. These two figures indicate that there are fewer and weaker unwanted trailing echoes present for the OCC tin rod than those for conventional tin rod. Therefore we can say that this OCC tin rod has a better acoustic performance over conventional tin rod. This conclusion is supported by an identical experiment performed at

10MHz frequency. Figure 4.7 shows the 10MHz reflected echoes for our conventional tin rod. The same echoes for the OCC tin rod are shown in Fig.4.8. Echoes B_1^0 and B_2^0 are the second and the third longitudinal arrivals respectively. Figure 4.8 shows that at 10MHz there are no trailing echoes present for the OCC pure tin rod.

These experiments demonstrate that OCC metallic rods have better acoustic performance than conventional metallic rods. This is mainly because, the Ohno Continuous Casting (OCC) process which is different from conventional methods enables the crack-free production of a very fine structure metallic rod with a smooth surface. With this method it is also very easy to produce a very long length metallic rod with uniform structure along the whole rod. OCC method is further discussed in the next section.

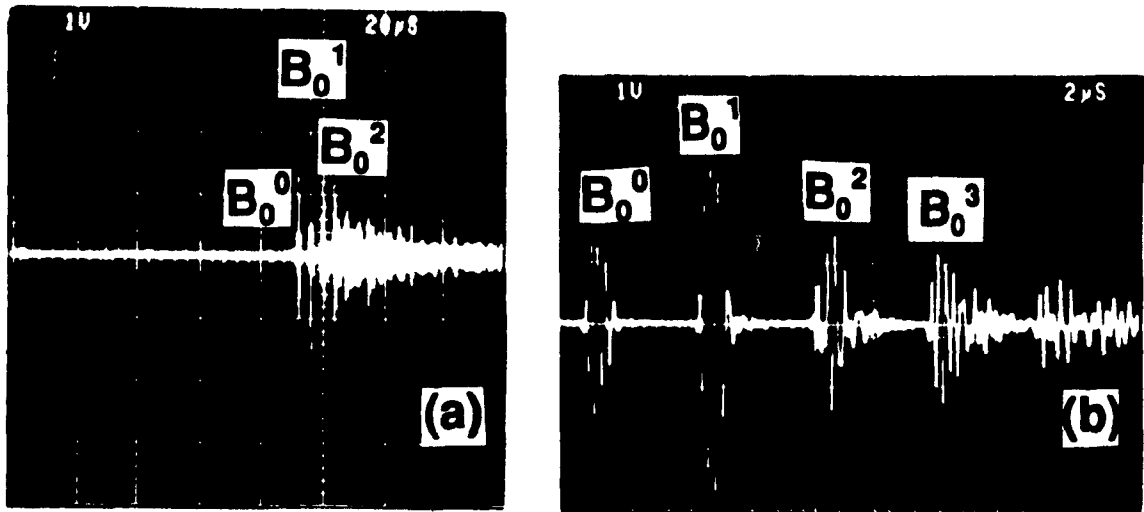


Figure 4.1 (a) The reflected 5MHz longitudinal echoes through the 290mm long conventional aluminum rod. (b) A higher magnification picture near B_0^0 .

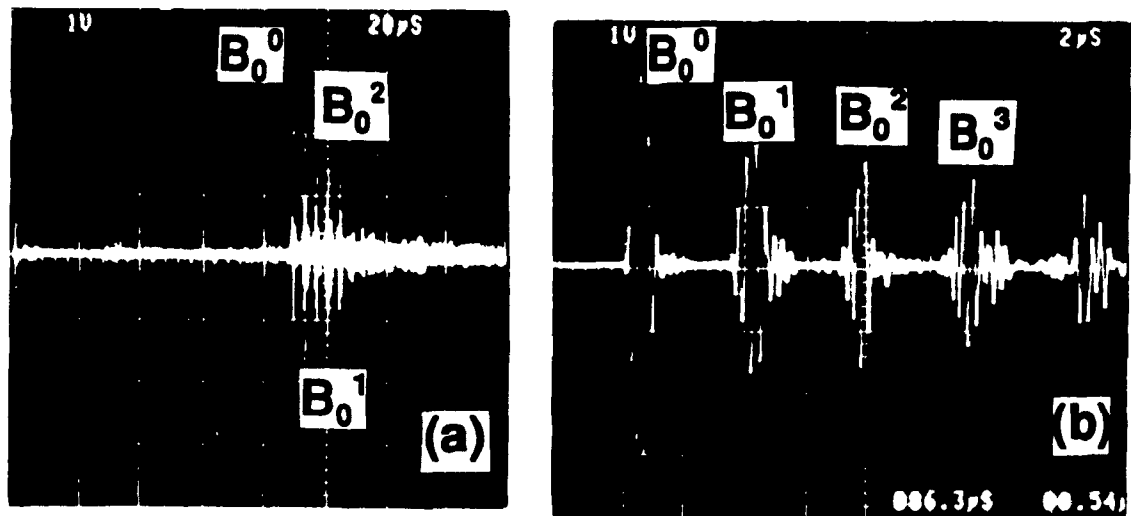


Figure 4.2 (a) The reflected 5MHz longitudinal echoes through the 285mm long OCC aluminum rod. (b) A higher magnification picture near B_0^0 .

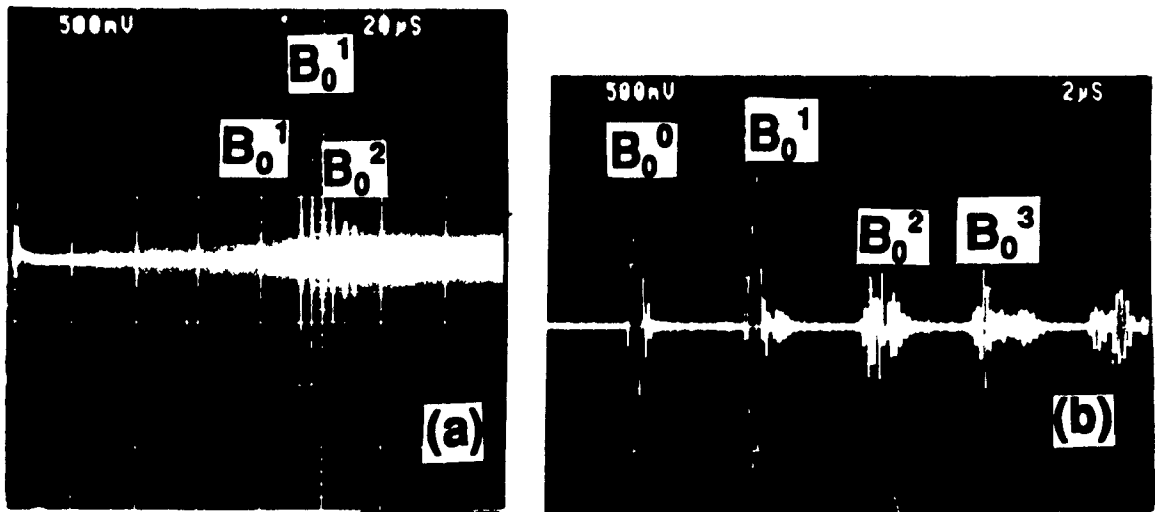


Figure 4.3 (a) The reflected 10MHz longitudinal echoes through the 290mm long conventional aluminum rod. (b) A higher magnification picture near B_0^0 .

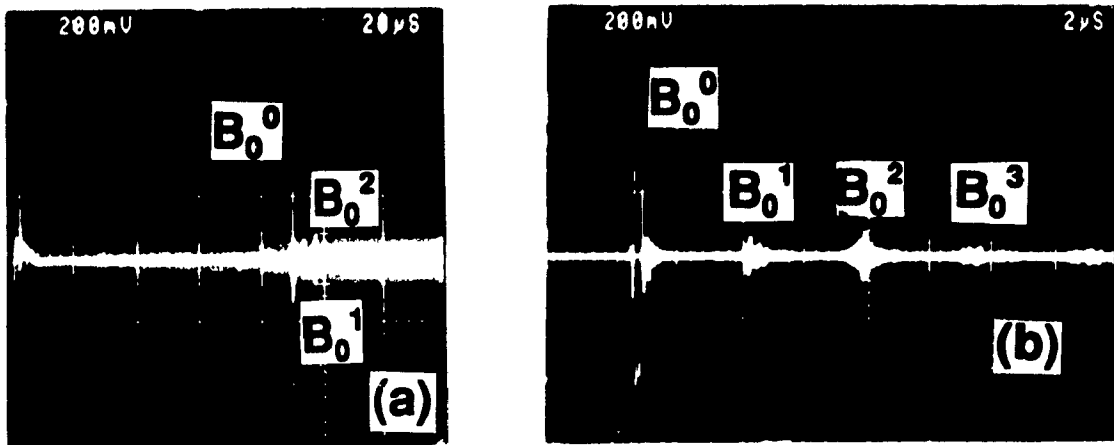


Figure 4.4 (a) The reflected 10MHz longitudinal echoes through the 290mm long OCC aluminum rod. (b) A higher magnification picture near B_0^0 .

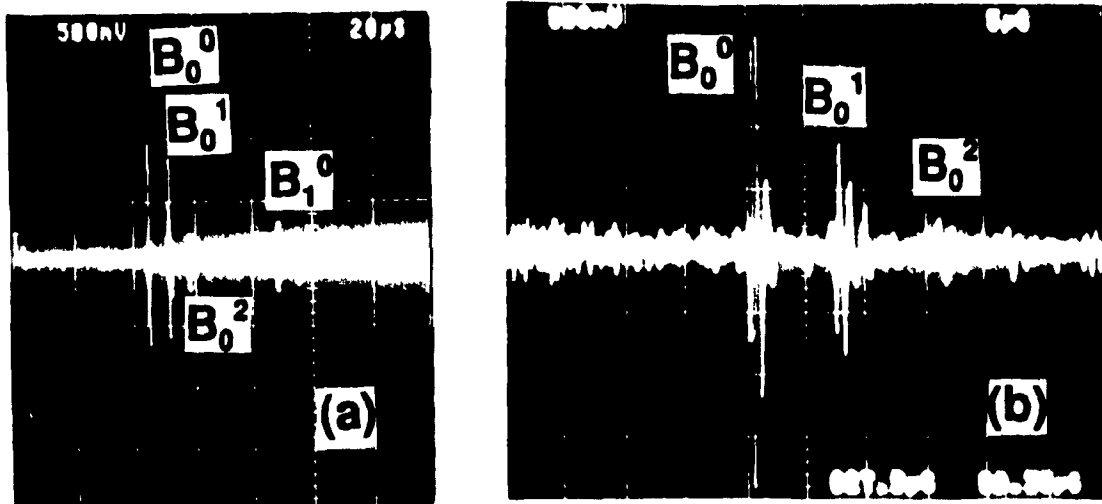


Figure 4.5 (a) The reflected 5MHz longitudinal echoes through the 73mm long conventional tin rod. (b) A higher magnification picture near B_0^0 .

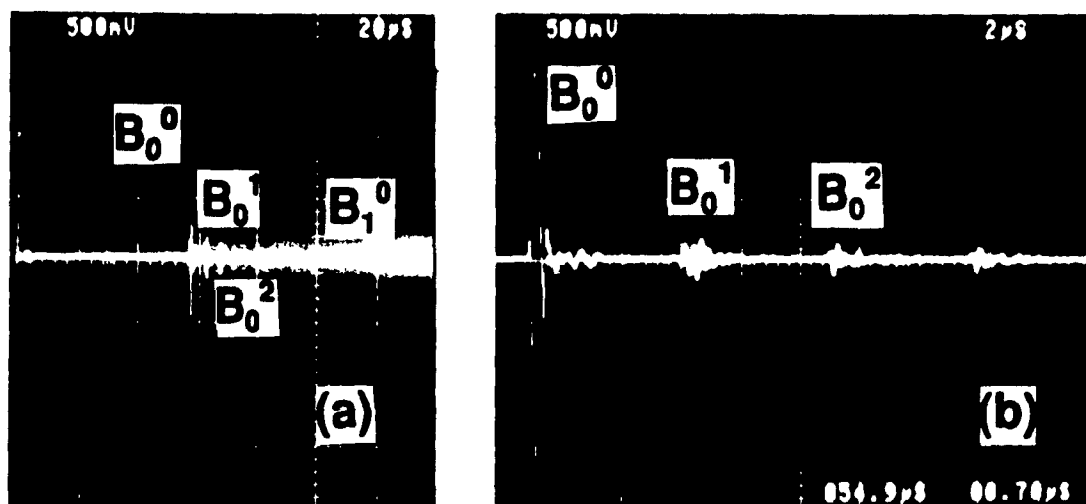


Figure 4.6 (a) The reflected 5MHz longitudinal echoes through the 98mm long OCC tin rod. (b) A higher magnification picture near B_0^0 .

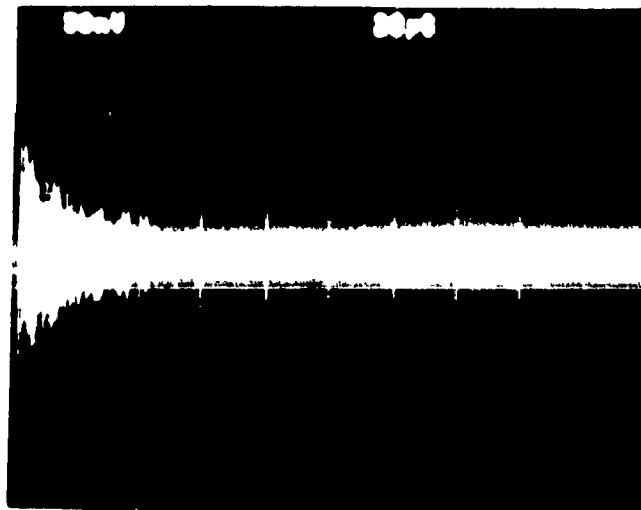


Figure 4.7 *The reflected 10MHz longitudinal echoes through the 73mm long conventional tin rod.*

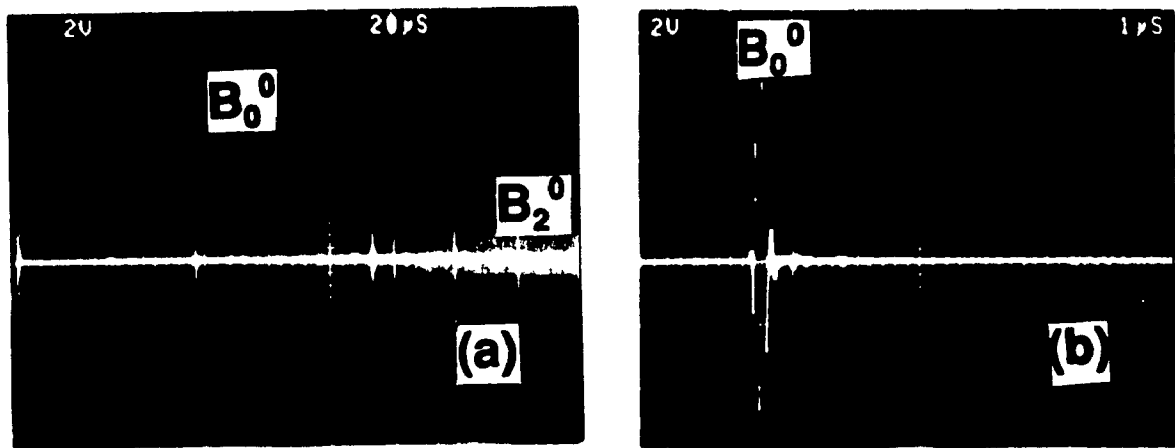


Figure 4.8 (a) *The reflected 10MHz longitudinal echoes through the 98mm long OCC tin rod. (b) A higher magnification picture near B_0^0 .*

4.1.1 OCC Method

The Ohno Continuous casting (OCC) Process was invented by Professor A. Ohno of the Chiba Institute of Technology (CIT) in Japan several years ago. Features of this process include the ability to produce single crystals, unidirectional columnar grains, very clean cast surfaces free from witness marks and good internal structures free from segregation and shrinkage cavities [27],[28]. In Japan the process has been implemented in regular production for the near-net shape casting of copper rods and wires for the audio and video industry.

The key factor which distinguishes the OCC process from conventional continuous casting techniques is the delivery of molten metal into a heated mold, the temperature of which is held just above the solidification temperature of the metal to be cast. In conventional systems, the mold is water-cooled, thus crystals nucleate on the mold surface and grow towards the inner portion of the casting and the direction of crystal growth is perpendicular to the casting direction. In the OCC process, due to the external heat applied to the mold, there is no nucleation on the mold surface and heat is only extracted through the strand being cast. As a result crystal growth occurs parallel to the casting direction. This gives rise to the change in solidification morphology which significantly influences metallurgical and mechanical properties of the solidified materials.

4.2 Cladded Metallic Buffer Rod

As we discussed earlier, in order to reduce the spurious trailing signal the common method is to increase the diameter, or shorten the length of the rod, or roughen the rod periphery or taper the rod [7], but these approaches will not increase the signal strength of B_0^0 and S_0^0 in Fig.3.3. However, we have demonstrated that acoustic rods consisting of core and cladding are much preferred over uncladded rods. Again, it should be that the guidance of acoustic waves in a clad rod requires that the velocity in the core be less than that in the cladding [10]-[12]. We applied the same concept to our metallic rods and obtained clad metallic rod with excellent acoustic performance at frequencies from 2 to 10MHz.

Very recently the OCC process has been extended to produce a clad metallic rod consisting of a 61.9% tin - 38.1% lead alloy core and a pure tin cladding as shown in Fig.4.9. The core diameter is 4.8mm and the cladding thickness is 2.6mm. This buffer rod was cast at a speed of 24mm per minute and the mold temperature was 242°C. The detailed description of the casting process is given in [29]. The optical and scanning electron microscope images of the core-cladding interface are given in Figs.4.10a and 4.10b respectively. Figures 4.10a and 4.10b clearly show that a diffused boundary exists between the core and the cladding. This boundary ensures that the buffer rod has a very good signal strength and signal to noise (spurious signals) ratio (SNR) as shown in Figs.4.11 to 4.14.

Figure 4.11a shows the reflected echoes through an 80mm long clad metallic tin rod (Fig.4.9) using a broadband 1MHz 6.35mm diameter longitudinal ultrasonic transducer and a commercial gel couplant between the transducer and the buffer rod. Figure 4.11b is a magnification of Fig.4.11a near B_0^0 . We performed similar measurements at frequencies of 2, 5 and 10MHz and obtained very good results. The reflected echoes are shown in Figs.4.11 to 4.14 at 1, 2, 5 and 10MHz respectively. The SNR for B_0^0 in Figs.4.12 to 4.14 is better than 30 dB. We have also used a Schlieren visualization system and confirmed that the acoustic energy is indeed concentrated in the core. Figure 4.15 shows the acoustic energy exiting from the end of the buffer rod into a water pool. The acoustic frequency was 5MHz.

We have used two other casting speeds, 6mm and 12mm per minute, to fabricate such buffer rods and found that the buffer rod shown in Fig.4.9 performed the best acoustically. Microstructures and interface conditions are the main reasons for the difference in performance. Furthermore, Jen [9] in 1987 has reported on a clad metallic rod consisting of a pure copper core and a pure aluminum cladding. A copper rod inside an aluminum tube, whose inner diameter was slightly larger than the copper rod diameter, went through several dies of smaller diameters to achieve the clad rod geometry. The signal strength and the ultrasonic SNR obtained for such 'extruded' clad buffer rods [9] were much poorer than those presented in Figs.4.11 to 4.14. We believe that the main difference is due to the interface condition.

In order to verify a designed guidance condition, the acoustic velocity profile of the clad metallic rod must be measured. As we discussed before, the acoustic guidance in a clad rod requires that the phase velocity of the core is less than that of the cladding. We have again used a 225MHz line focus beam (LFB) scanning acoustic microscope (SAM) [18] to measure the leaky surface skimming compressional wave (LSSCW) velocity profile

across the metallic rod as shown in Fig.4.16. The velocity profiles shown in Fig.4.16 were measured by two orthogonal scans in the radial direction and across the rod center. The LSSCW velocity of the core is indeed smaller than that of the cladding. The propagation direction of the LSSCW wave is perpendicular to the LFB and parallel to the radial direction of the rod. The velocity discrepancy of the two scans mainly comes from the acoustic anisotropy and the roughness of the soft sample surface. The ratio of the velocity difference, Δv , between the core and the cladding over the velocity of the cladding is near 15%. Again, SSCW has predominantly longitudinal wave components, respectively, their velocity profiles can be regarded as those of the longitudinal wave velocity, v_l . It is noted that only the longitudinal acoustic wave is of interest here. Due to the difficulty in achieving good surface polishing of such a soft metallic alloy the measurement accuracy is estimated to be around 80 m/s.

Figures 4.11 to 4.14 and other measurements indicated that this clad metallic buffer rod can be used for ultrasonic frequencies between 2 to 10MHz. The attenuation and the pulse dispersion set the high frequency operation limit and the dimension including the core diameter and the cladding thickness sets the low frequency limit. At the same frequency, a smaller Δv between the core and the cladding of a clad rod requires a thicker cladding.

If a liquid couplant and a thick sample are used as shown in Fig.4.17a, the first echo from the end of the buffer rod, B_0^0 , and the echoes (S_0, S_1, S_2, \dots) traversing back and forth between the rod endface and the sample surface are shown in Fig.4.17b. A 10MHz transducer was used in this experiment. The result of this experiment supports the conclusion that this clad metallic rod is an excellent acoustic buffer rod.

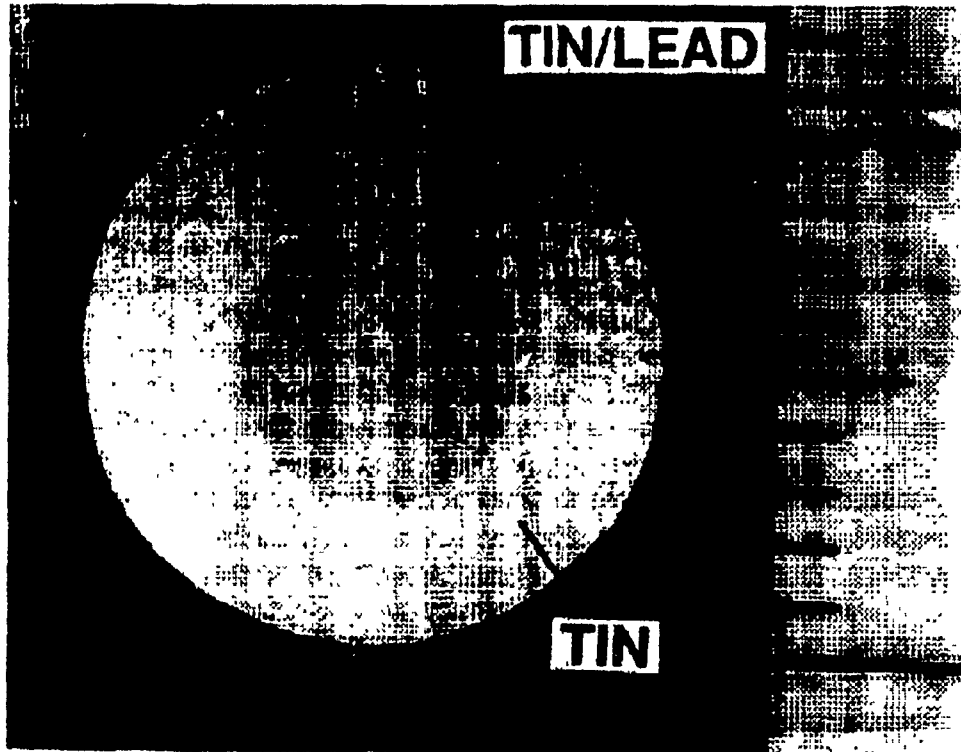


Figure 4.9 *A cross section view of a cladded metallic buffer rod.*

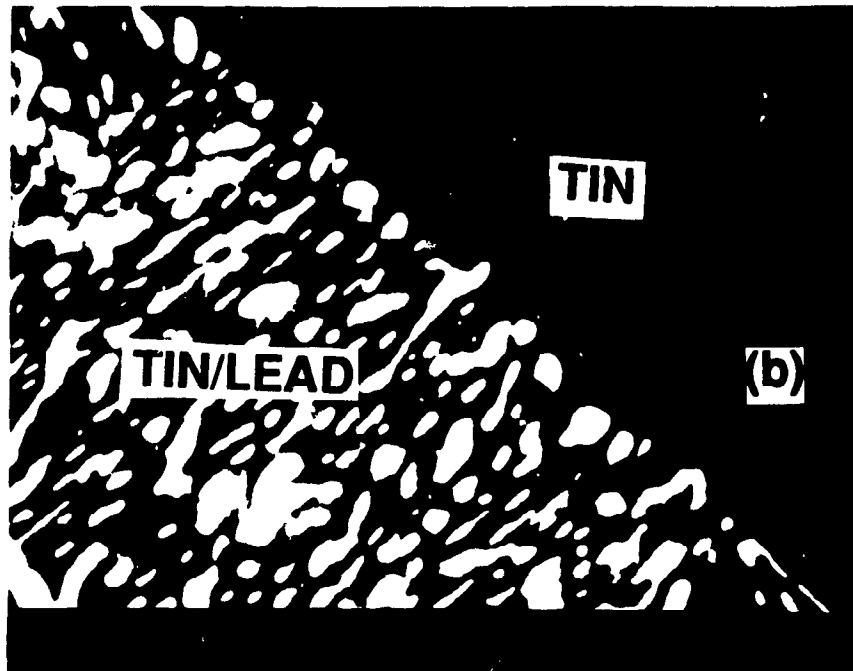
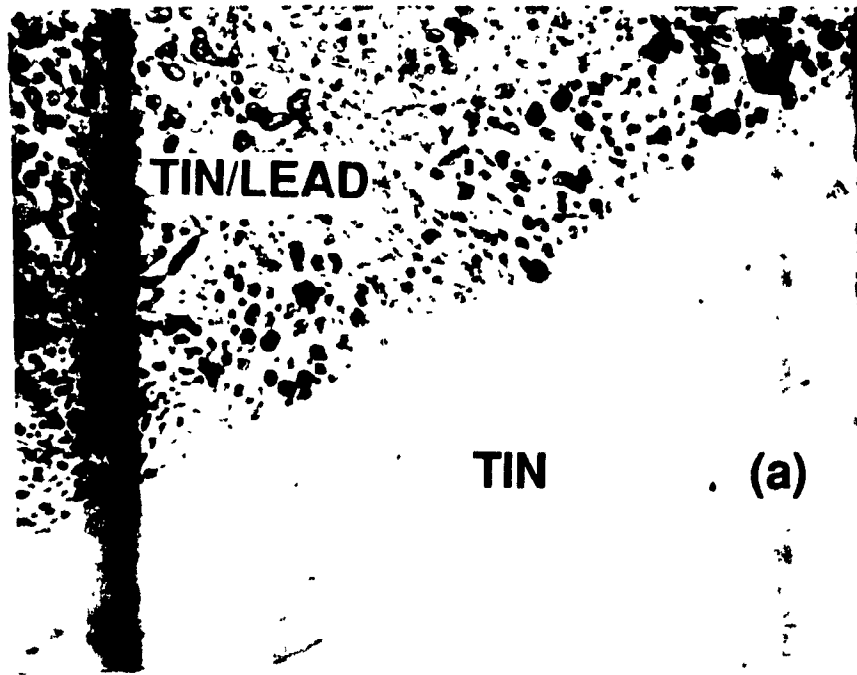


Figure 4.10 (a) An optical and (b) an SEM image of the tin/lead alloy core - tin cladding interface.

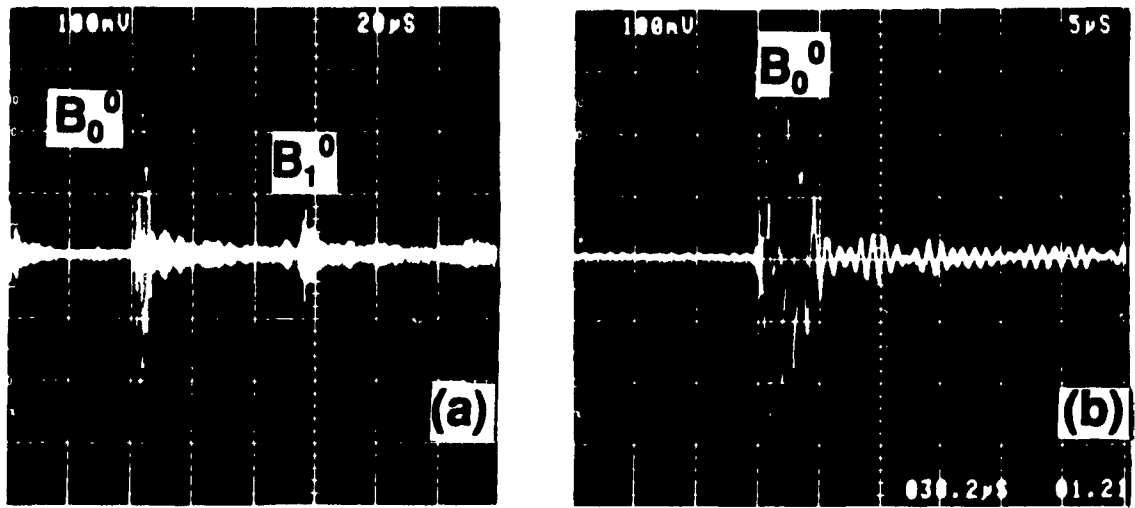


Figure 4.11 (a) The reflected 1MHz longitudinal echoes through the 80mm long cladded metallic rod shown in Fig.4.9. (b) is a higher magnification near B_0^0 .

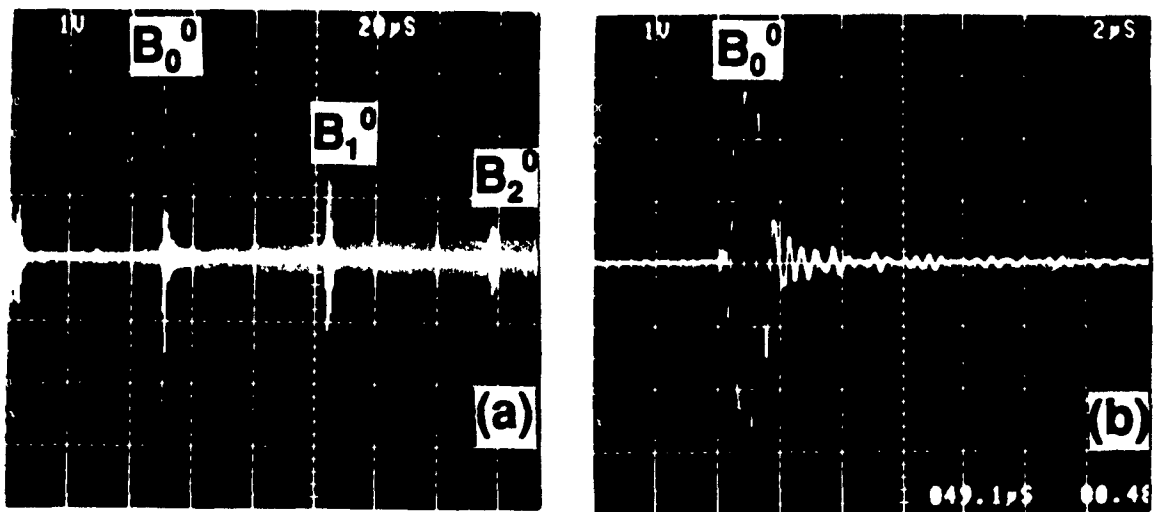


Figure 4.12 (a) The reflected 2MHz longitudinal echoes through the 80mm long cladded metallic rod shown in Fig.4.9. (b) is a higher magnification near B_0^0 .

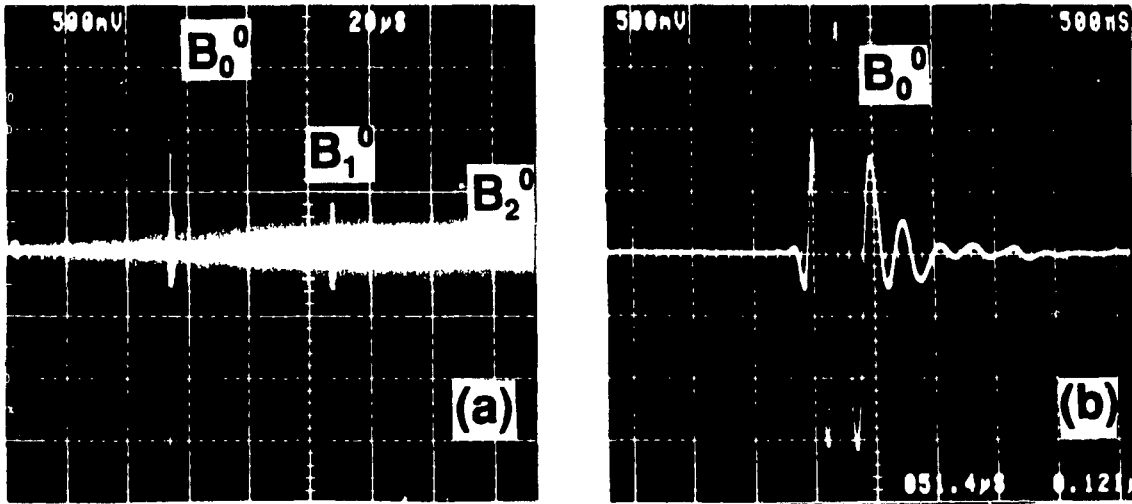


Figure 4.13 (a) The reflected 5MHz longitudinal echoes through the 80mm long cladded metallic rod shown in Fig.4.9. (b) is a higher magnification near B_0^0 .

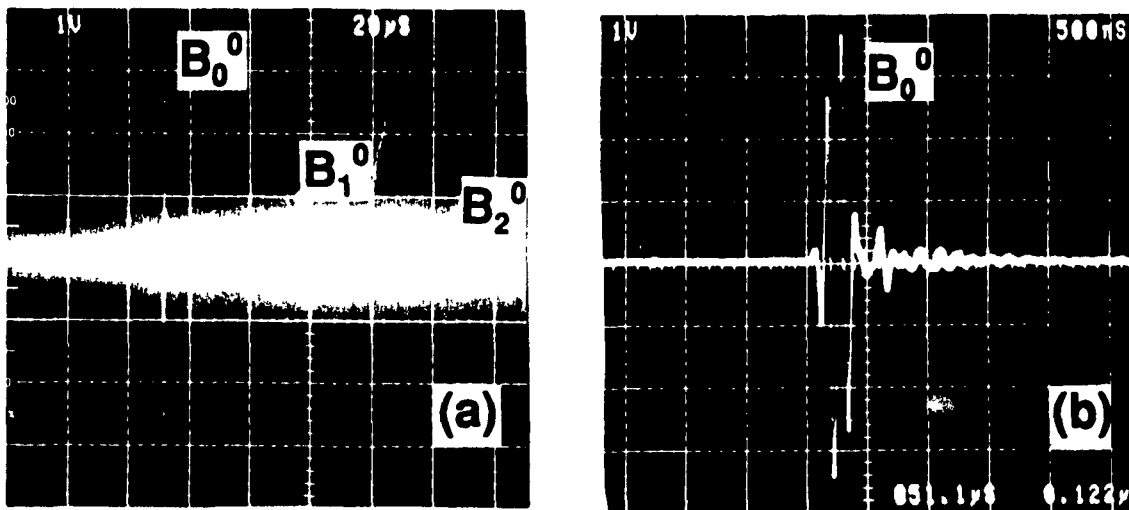


Figure 4.14 (a) The reflected 10MHz longitudinal echoes through the 80mm long cladded metallic rod shown in Fig.4.9. (b) is a higher magnification near B_0^0 .

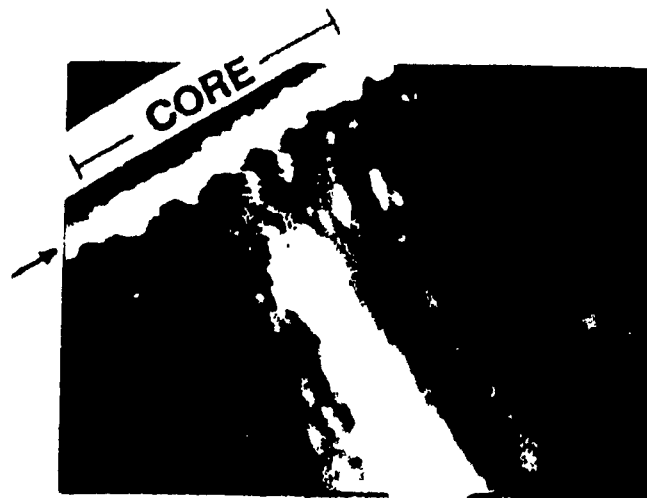


Figure 4.15 Image of an acoustic beam from the 80mm long cladded buffer rod shown in Fig.4.9. Arrow indicates the rod-water interface.

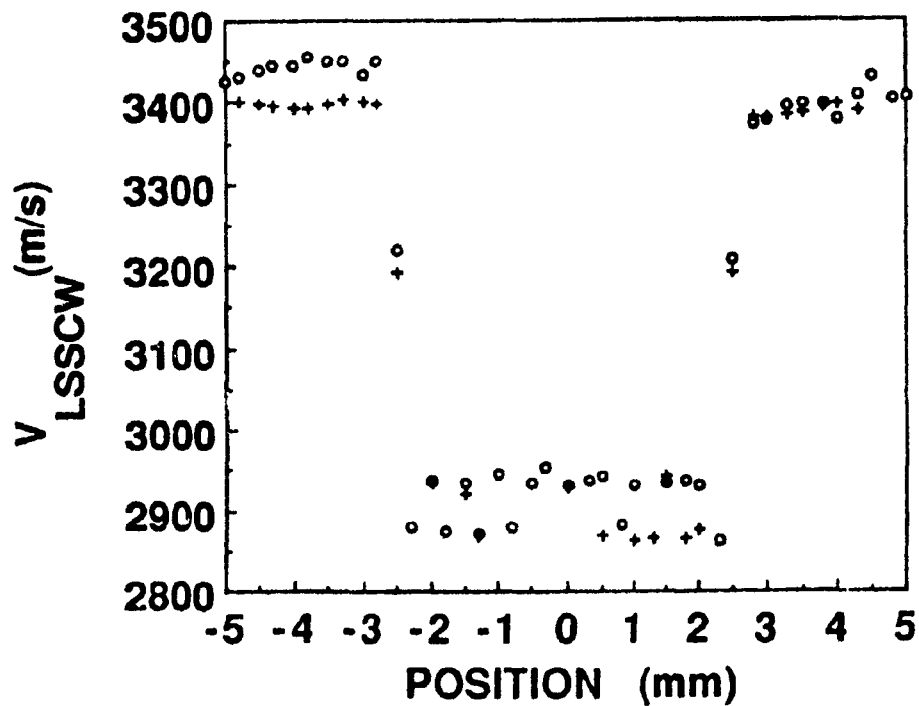


Figure 4.16 The measured V_{LSSCW} profiles for two orthogonal scans across the center of the cladded metallic rod shown in Fig.4.9.

Transducer



Buffer Rod

(a)

LIQUID
COUPLANT

Reflector

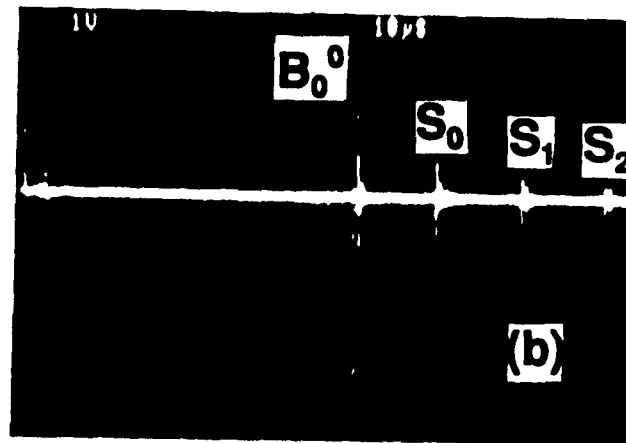


Figure 4.17 (a) A 10MHz longitudinal ultrasonic pulse-echo measurement with the cladded buffer rod shown in Fig.4.9, a liquid couplant and a sample. (b) A typical measurement result of (a) near B_0^0 .

4.2.1 Spherical Concave Lens

A spherical concave lens was fabricated with ease at the end of tin clad rod. At the end of chapter two we discussed the lens fabrication at the end of glass rods and we saw that it takes more than a day to fabricate a spherical concave lens. But for our metallic rods it takes just a few minutes to make a reasonably good performance lens. Machinability of the metal allowed us to use a round drill of 9.5mm diameter to drill out a semi sphere and to make a lens at the end of our tin clad metallic rod. Then, the concave surface of the lens was roughly polished by gently hammering a ball bearing of the same size on the lens. Then fine polishing was done down to 1 micron by coating the lens surface with diamond paste and rolling the ball bearing on that. The different lens fabrication processes show the advantage of machinability and the flexibility and the facility of the metallic rods.

The same setup as in chapter two was used for the focussing measurement. The amplitude variation versus the distance is shown in Figures 4.18 and 4.19 for 5 and 10MHz respectively. Figures 4.20 and 4.21 show the first, S_0^f , and the second, S_1^f , echoes from the sample surface at focal point, at 5 and 10MHz respectively. From these figures we can clearly see the nice focussing behavior.

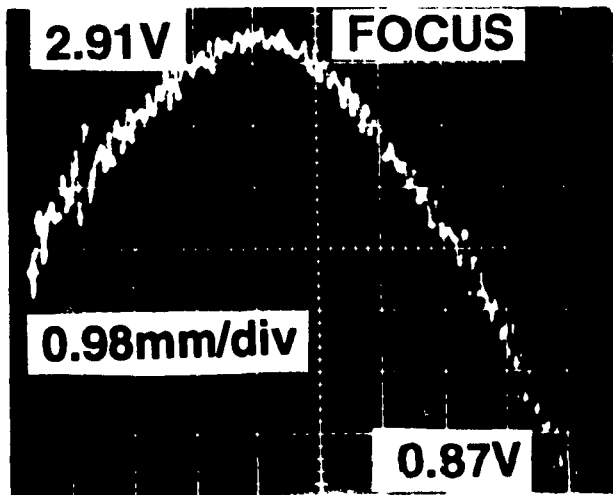
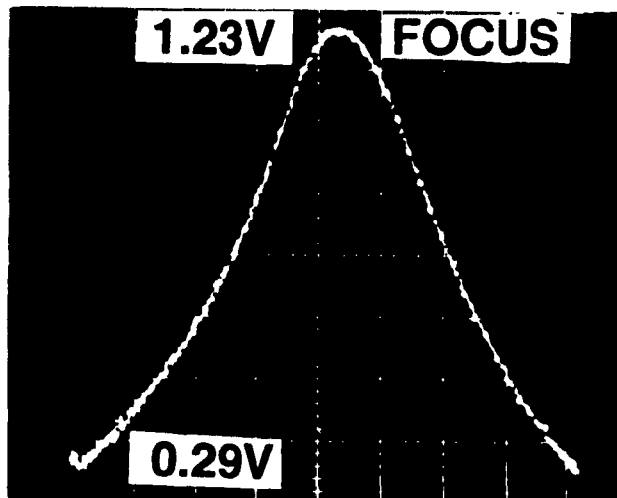


Figure 4.18 *The axial amplitude variation for the received signal near the focal point, at 5MHz*



1.34mm/div

Figure 4.19 *The axial amplitude variation for the received signal near the focal point, at 10MHz.*

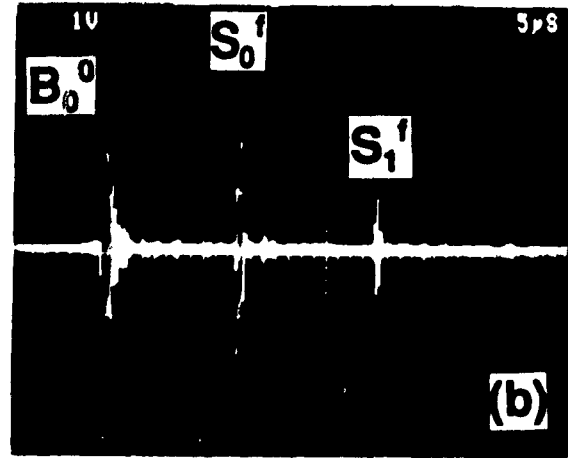
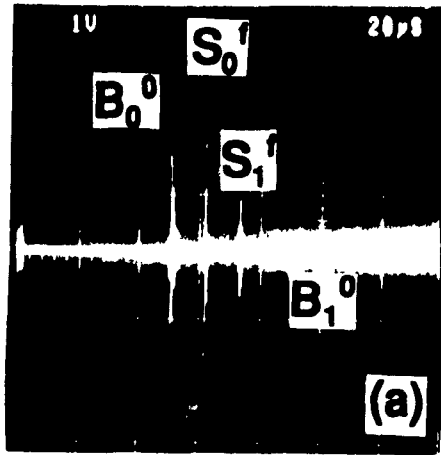


Figure 4.20 The received 5MHz longitudinal echoes when a flat sample is located at the focal point. (b) is the higher magnification near B_0^0 .

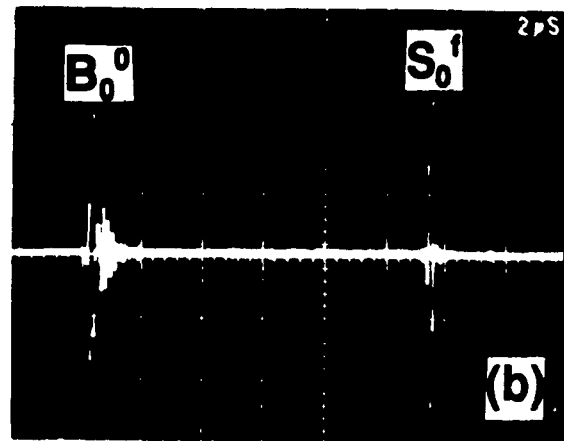
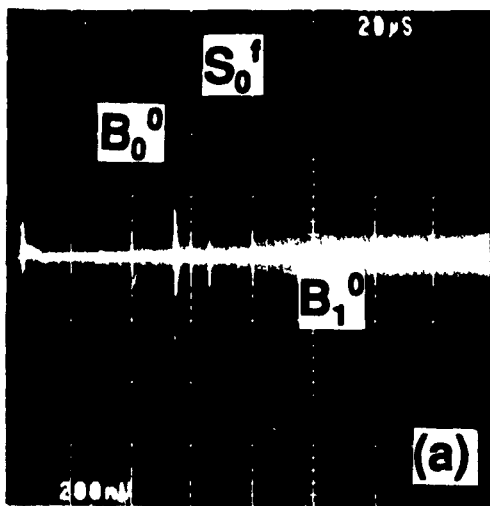


Figure 4.21 The received 10MHz longitudinal echoes when a flat sample is located at the focal point. (b) is the higher magnification near B_0^0 .

CHAPTER 5: Application of Long Cladded Acoustic Buffer Rods at Elevated Temperatures

5.1 Introduction

Ultrasonic techniques have become of great importance in the metallurgical industry in recent years. The use of ultrasonic waves to inspect molten metals is known but not widely applied to industry yet. In metal processing, quality is associated with the entrainment of non-metallic material within the liquid metal. In the case of aluminum, the entrained material can be oxide films together with hard carbide inclusions which are derived from the original smelting process. Aluminum also picks up hydrogen which can, on solidification, diffuse to entrained oxide particles, and during the finishing stages, result in blisters on the sheet material. The hard particles may be associated with the oxide films, are detrimental in the forming of thin-walled cans. These particles scratch or deform the draw dies and rejections from such a defect are usually costly. The steel industry also has similar problems. There are many sources from which particles can be introduced into liquid metal. Liquid steel can absorb oxygen from atmosphere during transfer operations, leading to the formation of oxide products which may remain within the melt. In addition, other reaction products such as

nitrides and sulphides, may be present. Particle sizes can vary from less than 1 micron to 150 microns, however, above this size natural floating forces tend to separate the non-metallics to the surface [30].

The various techniques which are currently used for evaluating metal quality are based on the extraction of a metal sample followed by analysis in the laboratory. Although this approach is often capable of providing the desired information regarding inclusion content, it also requires considerable sample preparation and analysis time to discover possible liquid metal processing problems which can no longer be corrected. Beyond the inability of the laboratory techniques to provide feedback control of the casting process, they are also not sufficiently rapid to prevent the rolling and treatment of poor quality metallic products. Clearly, while many of the existing sampling and analysis techniques are capable of determining product quality, a more direct method could be highly beneficial.

Ideally, the evaluation of the cleanliness of metallic products would be conducted on large samples which could be rapidly analyzed with little or no sample preparation. This can only be achieved by analyzing the metal when it is still in the liquid state. When successfully implemented in industry, this type of on-line monitor could potentially provide information regarding liquid metal processing problems and also prevent further processing of unsatisfactory slabs, billets, ingots and castings.

Ultrasonics techniques have been reported as practical on-line methods to monitor the liquid metal properties [2],[3],[31]-[35]. For example, it is known that molten aluminum can be inspected with ultrasonic waves of relatively high frequencies (1-10MHz). The most practical means of inspection is the pulse-echo method wherein an ultrasonic wave pulse is transmitted into the molten aluminum and the pulse reflections or echoes are detected and measured. Melt quality can be characterized in terms of the number and amplitude of the echoes reflected from discontinuities such as insoluble melt constituents, attenuations in pulse amplitude, pulse velocity through the melt, and shifts in the ultrasonic wave frequency.

To transmit or receive ultrasonic waves to or from an aluminum melt, it is common to use a piezoelectric transducer. A transducer can conventionally be coupled to the melt using a buffer rod. The buffer rod serves to isolate the transducer from high melt temperatures, which will usually run in the range of about 675°C to 825°C and to introduce a time

delay between a transmitted pulse and echoes from inclusions located near where the pulse first enters the melt. The buffer rod is usually in the form of a bar or rod, one end of which will be immersed in the melt and the other probe end is coupled to the transducer.

So far, encouraging results have been obtained by using ultrasonic pulse-echo techniques, however, poor ultrasonic signal to noise ratios (SNR) were obtained due to the lack of proper ultrasonic probes. The ultrasonic buffer rods reported so far used uncladded rods and suffered the drawbacks of uncladded rods i.e., the presence of spurious signals and the weakened signal strength due to the wave diffraction in such rods. As we discussed in previous chapters our cladded buffer rods do not have these drawbacks, and could be much superior for ultrasonic inspection of molten aluminum or other metals provided that the melt temperature doesn't go beyond which the rod cannot resist in.

In this chapter the performance of ultrasonic pulse-echo measurements on molten aluminum is presented. Different aspects and difficulties of these experiments are also discussed. But before we use our probes at high melting temperature of aluminum ($650^{\circ}\text{C} - 800^{\circ}\text{C}$) we examined our probes by doing some experiments at elevated temperatures up to 270°C on Dow Corning 200 fluid.

5.2 Ultrasonic Pulse-Echo Measurement at Elevated Temperatures.

As ultrasonic transducers cannot be exposed to high temperatures, we may need a long buffer rod. Figure 5.1 shows a setup of a typical pulse-echo measurement, but performed at medium temperatures. A high viscosity (1000 cs) liquid (Dow Corning 200 Fluid) is heated in a glass container and the temperature is monitored by a digital thermometer. The buffer rod is a 144mm long cladded rod consisting of a 4.7mm diameter core and 2mm thick cladding. The $v_{LSSCW,core}/v_{LSSCW,clad} = 0.96$. It is immersed into fluid from one end and from the other end is coupled to a 10MHz transducer and commercial gel is used as ultrasonic couplant.

Figures 5.2 to 5.4 show pulse-echo reflection measurements at 160°C , 240°C and 270°C respectively. The echo B_0^0 is the first longitudinal arrival from the end of rod and the echoes S_0, S_1, S_2, \dots etc. are the echoes traversing the Dow Corning Fluid at temperatures

mentioned above of about 2mm thick back and forth between one end surface of the buffer rod and the top surface of the container which acted as an ultrasonic reflector. In these figures the echo B_0^0 has been saturated by the receiver amplifier.

Because of the high performance long buffer rod if one is interested, can study the change in the ultrasonic velocity, attenuation and hence, viscosity of such fluid versus temperature. Figure 5.5a, b and c show the pulse-echo measurement at 50°C , 100°C and 150°C , respectively. From this figure we can see that as temperature increases the time delay between B_0^0 and S_0 increases or the acoustic velocity decreases and the signal gets more attenuated. It is noted that in this measurement we just varied the temperature and the distance between the end of rod and reflector was not changed. In this figure all the signals were 30 dB attenuated.



Figure 5.1 *Setup for Ultrasonic pulse-echo measurement for high viscosity Dow Corning 200 Fluid.*

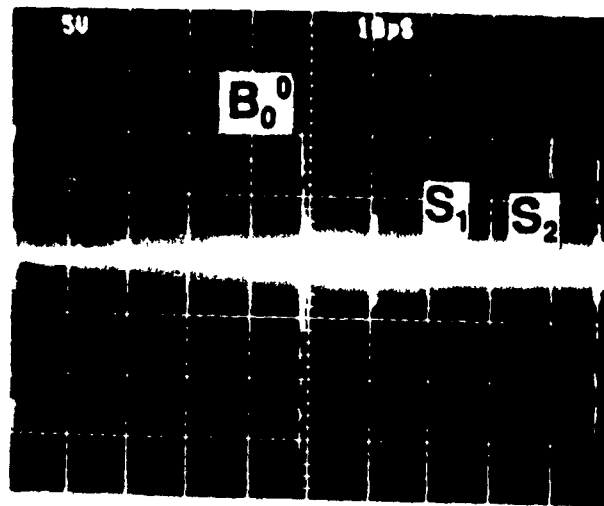


Figure 5.2 An ultrasonic pulse-echo reflection measurement performed on hot liquid sample (Dow Corning 200 Fluid). The temperature was 160°C.

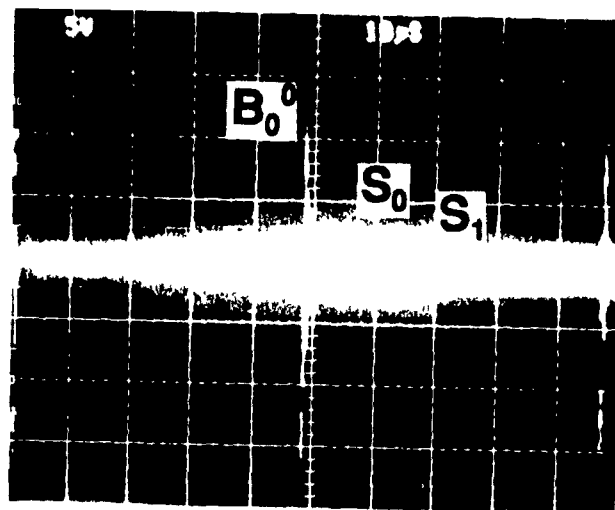


Figure 5.3 An ultrasonic pulse-echo reflection measurement performed on hot liquid sample (Dow Corning 200 Fluid). The temperature was 240°C.

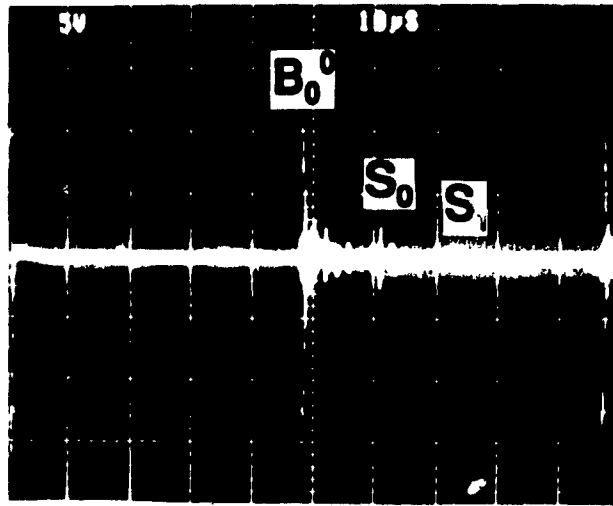


Figure 5.4 *An ultrasonic pulse-echo reflection measurement performed on hot liquid sample (Dow Corning 200 Fluid). The temperature was 270°C.*

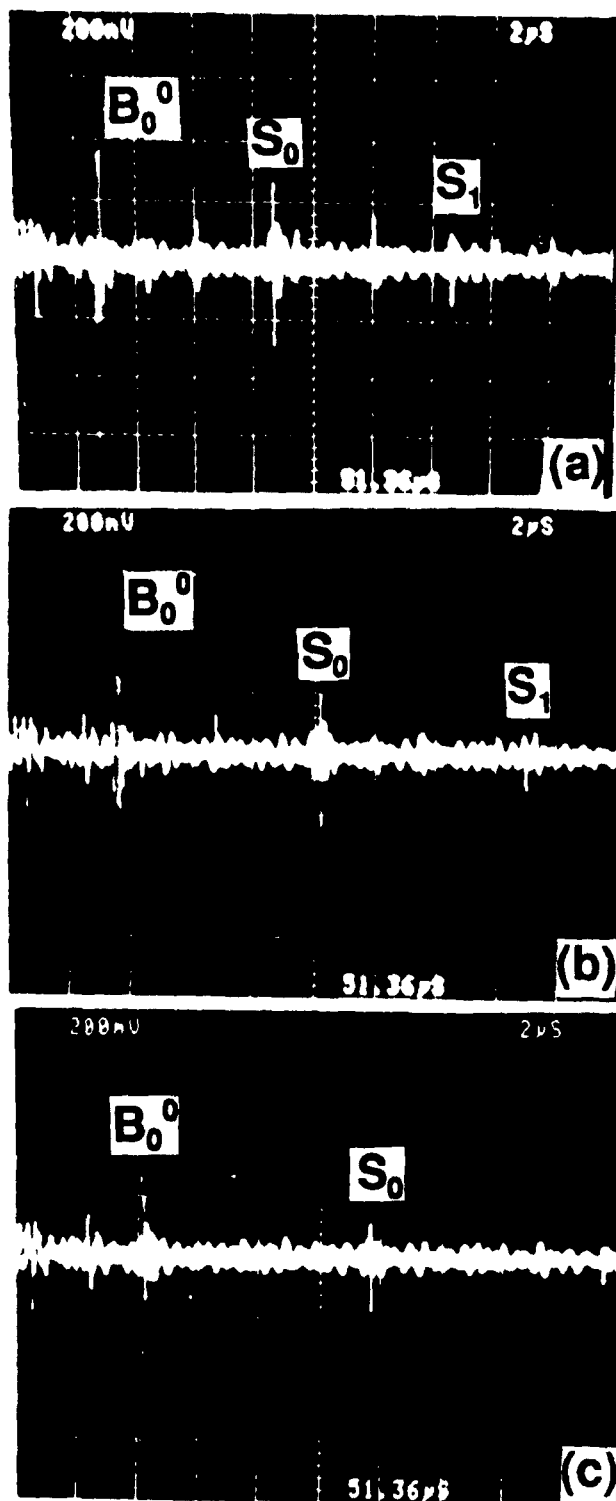


Figure 5.5 An ultrasonic pulse-echo reflection measurement performed on hot liquid sample (Dow Corning 200 Fluid). The temperature was (a) 50°C, (b) 100°C and (c) 150°C.

5.3 Ultrasonic Pulse-Echo Measurement Performed on Molten Aluminum

Aluminum was heated in a small furnace up to 800°C . The furnace is composed of a ceramic container around which is surrounded by three heating coils which are connected in series and are formed into a helix shape (as shown in Fig.5.6). We used a variable output transformer to control the heating. Before the measurement we examined our probes to see if they can tolerate that temperature. The cladded silica rods were immersed into molten aluminum and taken out rapidly after a few seconds and we found that they were resistant to thermal shock. Although the core and cladding are made of different dopants which may induce internal stresses, there were no cracks observed. After our rods passed this step successfully we performed the experiment at high temperature of 700°C to 800°C .

At first the we could not observe any echo reflected from the reflector which was an adjustable moving steel plate located in the melt. After performing similar experiments we found out that there were two main reasons (a) corrosion and (b) poor wetting, of which the second one played the key role.

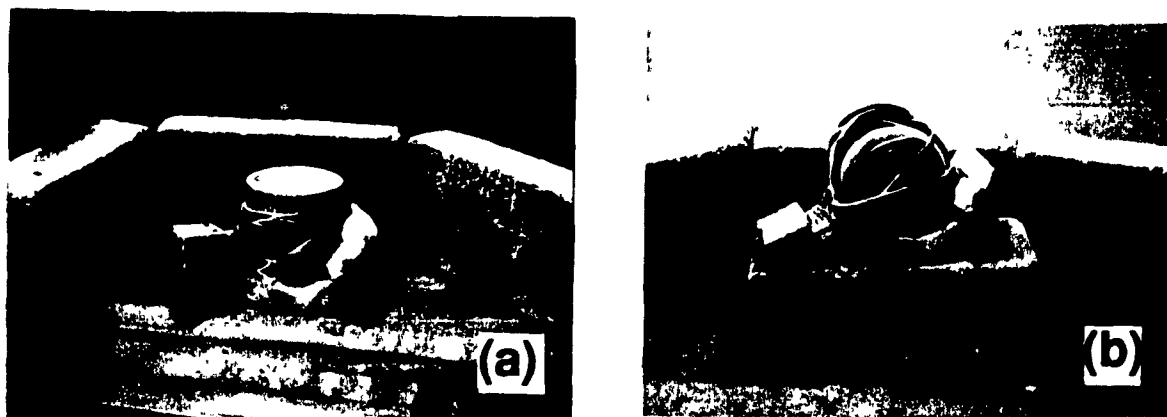


Figure 5.6 A small furnace for melting Aluminum. (a) The side view and (b) the bottom view of the furnace.

5.3.1 Corrosion

The corrosion problem is that hot aluminum melt attacks the working-tip of the glass buffer rod (the end that is immersed into the melt) and consumes it. This leads to a deformation of the working-tip. When ultrasonic plane waves hit this deformed surface some reflect in different directions and some divert. Even if some can manage to pass this deformed surface without changing direction, after they are reflected back by the reflector they will face the same problem at the melt rod interface. However this is not an immediate problem and it happens after repeated use of rod in the melt or if we leave the rod in the melt for a long time, more than several minutes.

One solution to this problem is to coat the working-tip with a protective layer as shown in Fig.5.7. We plasma sprayed thin layers of nickle-5%aluminum alloy and zirconia on a few rods. Although this approach could solve the corrosion problem by a great degree but it couldn't solve our main problem. The coating layer may introduce another problem though. Because of poor adhesion between certain coatings and the rod it was slightly pealed off when immersed into the melt and created a very small gap between the end surface of the rod and the melt. This gap significantly reduces the ultrasonic energy coupled into the melt. However, we believe that the adhesion can be improved by choosing the proper material, thickness and the conditions of plasma spraying.

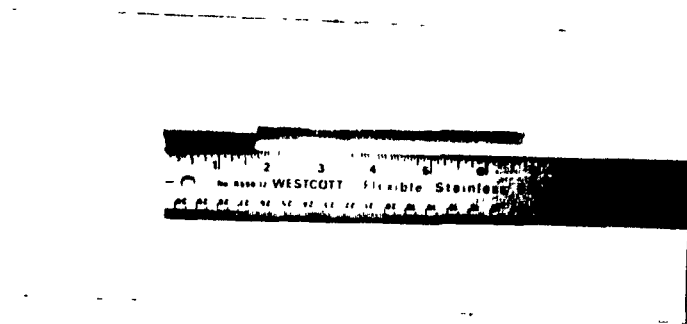


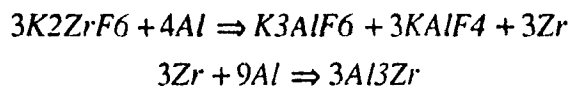
Figure 5.7 A cladded buffer rod whose working-tip is plasma sprayed by zirconia.

5.3.2 Wetting

At initial experiments not only we could not observe any echo reflected from reflector but also we did not see any change in the energy of the first echo reflected from the end of buffer rod. Because of relatively good acoustic impedance matching between our buffer rods and molten aluminum we were expecting a sudden change in the amplitude or energy of the first echo from the end of rod, showing that a large amount of energy is transferred into the melt. Since, no acoustic energy was transferring into the melt we realized that the glass clad buffer rods were not wetted by the molten aluminum.

Glass is usually poorly wetted by liquid aluminum at temperatures lower than 1000°C. The poor wettability of glass by liquid aluminum and light alloys at low temperatures is thought to be related to a thin layer of alumina which always coats the liquid [36] and acts as a barrier. Therefore, removing this thin layer (i.e. by a chemical reaction taking place near the glass surface and resulting in the formation of new species able to dissolve or vaporize the alumina layer) should improve the wetting of the glass rod thus allowing its impregnation by liquid aluminum alloys. To improve the poor wettability we used the treatment explained in [36].

The working-tip of rod was coated by a thin layer of K_2ZrF_6 (Hexafluorozirconate-potassium). K_2ZrF_6 was dissolved in boiling water and then we immersed the tip of rod into solvent. As the solvent was being cooled down we rotated and pulled the rod out of the solvent, in this way a thin layer of K_2ZrF_6 was deposited on the rod. K_2ZrF_6 is preferred over other fluoride salts because of its high solubility ($25g/100cm^3$ water at $100^\circ C$). The thickness of K_2ZrF_6 coating layer is very important and the surface concentration of $12mg\ cm^{-2}$ was thought to be the best [36]. Reactions taking place at high temperatures between pure aluminum and K_2ZrF_6 can be represented by the following equations,



From the above formulas, several mechanisms can be suggested to try to explain why a pretreatment with an aqueous solution of K_2ZrF_6 improves the wettability of glass by liquid aluminum: (1) the alumina thin layer coating the liquid metal is dissolved by the fluorides

which are released by the reaction occurring between K_2ZrF_6 and liquid aluminum allowing a direct contact between the liquid and the end surface of the buffer rod; (2) the kinetics of thermal decomposition of K_2ZrF_6 is increased at high temperatures leading to the formation of several fluoride species, according to the formulas showed in [36], thus dislocating the oxide layer and allowing wetting of the end surface of the rod by liquid aluminum; (3) the rod surface is cleaned and/or activated by these fluorides; (4) the gas phase involved in the wetting phenomenon is advantageously modified by the gaseous fluoride species formed from K_2ZrF_6 ; (5) the heat of the reactions that take place is high enough to increase the temperature locally giving rise to a better wetting. Although these five mechanisms can be expected to contribute to some extent to the wettability improvement, (1) is believed to be predominant [36].

After improving the wetting by the treatment just explained above we managed to perform pulse-echo measurement in molten aluminum at a temperature of about $750^\circ C$. Figures 5.8 and 5.9 show the echoes without and with reflector, respectively. The echo B_0^0 is the first arrival from the buffer rod and the melt interface and the echo S_0 in Fig.5.10 is the reflected echo from reflector which is placed in the molten aluminum. This was our first successful result and we believe that this result can be improved by at least 30 dB by enhancing the experiment conditions, trying to obtain the right thickness of K_2ZrF_6 coating, using the proper reflector, proper alignment of the transducer, buffer rod and reflector, cleaning the melt surface by removing the extra alumina layer and, if possible, performing the experiment in vacuum or in an oxygen free environment to avoid forming of alumina layer. However this result is encouraging and shows the potential of our cladded buffer rod. As it can be seen from Figs.5.8 and 5.9 there are exist few trailing echoes.

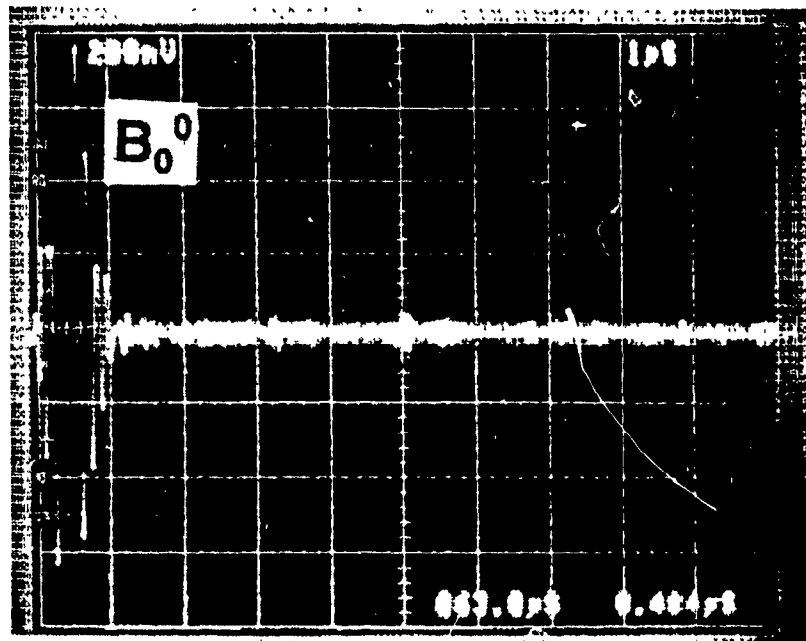


Figure 5.8 *The 10MHz pulse-echo measurement performed at 750°C on molten aluminum without a reflector.*

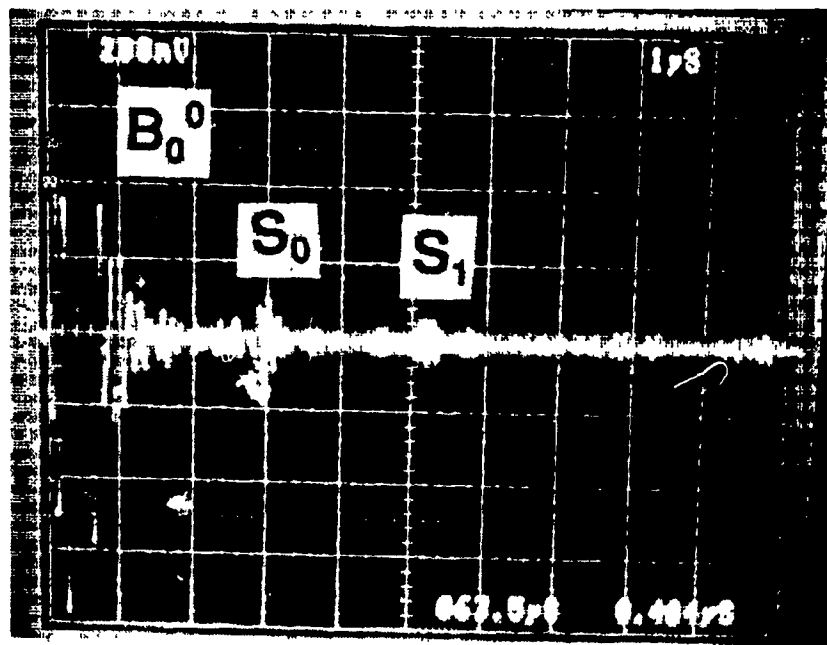


Figure 5.9 *The 10MHz pulse-echo measurement performed at 750°C on molten aluminum with a reflector.*

5.4 Discussion

An acoustic buffer rods which is designed for use at elevated temperatures should have the following properties;

- (a) Good guidance of acoustic waves.
- (b) Low acoustic attenuation over the range of working temperatures at the frequencies used.
- (c) Good resistance to thermal and mechanical shocks.
- (d) Low thermal conductivity.

The acoustic impedance, i.e. the product of density and the acoustic velocity of the buffer rod, should be of the same order as of the molten metal. In addition, to evaluate the properties of the molten metals It should have a good corrosion resistance to attack by molten metal. It appears that no probe has been found which would fulfill all of these requirements. However, our cladded buffer rod could meet most of these requirements. And so, it could be a good candidate as an acoustic probe proper for use at elevated temperatures.

CHAPTER 6: Conclusions

In this thesis we have introduced long silica cladded buffer rods consisting of a core and a cladding. Both longitudinal and shear ultrasonic pulse-echo measurements were carried out on these rods at 5 and/or 10MHz frequencies. A 225MHz line-focus beam scanning acoustic microscope has been used to measure the leaky surface acoustic wave and leaky surface skimming compressional wave velocity profiles to characterize these rods. It has been demonstrated that we can design, fabricate and verify the performance of long acoustic cladded buffer rods having different dopants, concentrations and profiles. At present the length of the silica cladded buffer rods made by the modified chemical vapor deposition (MCVD) method can be up meters. However, in this thesis the longest rod for the measurements was 400mm.

Improved performance of cladded rods over uncladded rods was demonstrated. It was shown that due to the guiding of acoustic energy in the core of the cladded rods there exist no or much fewer spurious signals and unwanted trailing echoes for the cladded rods compared to uncladded ones. Signal strength was also improved because of energy confinement in the core. The Schlieren visualization system has been used to show the acoustic guiding effect due to the presence of the cladding. Acoustic lenses were also fabricated at the end surface of cladded rods and the focussing behavior has been shown. The effect of

center dip on the acoustic performance of the cladded rod has been studied. It was shown that cladded rods without the center index dip have a better performance over those with a center dip.

Tapered silica cladded rods have also been presented. They have a very small size at one end making them proper for use at tiny openings. The large diameter at the other end facilitates the bonding of the ultrasonic transducer. A small acoustic lens was also fabricated at the small end of the tapered rod.

Metallic acoustic buffer rods were designed, fabricated and investigated. They have the advantages of machinability and bendability over glass rods. Two kind of metallic rods (one cast by a conventional method and the other one cast by the Ohno Continuous Casting, OCC, method) have been considered and discussed. Ultrasonic pulse-echo measurements performed on these rods at 5 and 10MHz frequencies indicated that the OCC rods perform better acoustically than conventional rods. The nice features of the Ohno Continuous Casting method have been briefly discussed. A cladded metallic rod consisting of a tin-lead alloy core and a pure tin cladding were produced using the OCC process. Longitudinal ultrasonic pulse-echo measurements have been performed at 1, 2, 5 and 10MHz. The results indicated that the cladded metallic rod is an excellent acoustic probe.

The application of our cladded rods at elevated temperatures was studied. Using cladded silica rods as an acoustic buffer rod, the ultrasonic pulse-echo measurements have been performed at medium temperatures on a Dow Corning liquid and at high temperatures (up to 750°C) on molten aluminum. It was demonstrated that these rods are resistant to thermal shocks and proper for use at elevated temperatures. Two major difficulties have been encountered concerning the molten aluminum experiments: one, corrosion of glass at high temperature by liquid aluminum and another, poor wettability of glass by molten aluminum. A solution has been suggested to eliminate the corrosion problem, but more effort must be made in future work. The wettability has been improved by a K_2ZrF_6 treatment and several mechanisms have been proposed to explain why a pretreatment with an aqueous solution of K_2ZrF_6 improves the wettability of glass by liquid aluminum. The reflected echoes from a steel plate reflector which was placed in the melt have been observed. We believe that with a proper coating the result of this first successful experiment can be improved by at least 30 dB. The measurements showed that cladded buffer rods are excellent candidates as acoustic probes at elevated temperatures.

REFERENCES

- [1] H.J. McSkimin, "Measurement of ultrasonic wave velocities and elastic moduli for small solid specimens at high temperatures", *J. Acoust. Soc. Am.*, Vol.31, pp.287-295, 1959.
- [2] S. Dawson, D.I. Walker, N.D.G. Mountford, I.D. Sommerville and A. McLean, "The application of ultrasonics to steel ladle metallurgy", *Proc. Int'l Symp. On Ladle Steelmaking and Furnaces*, Metallurgical Soc. of CIMM, pp.80-91, 1988.
- [3] N.D.G. Mountford, S. Dawson, I.D. Sommerville and A. McLean, "Acoustic sensors for process control in the year 2000", *Metallurgical Processes for the year 2000 and Beyond* (H.Y. Sohn and E.S. Geskin eds), The Minerals, Metals and Materials Society, pp.745-760, 1988.
- [4] L.C. Lynnworth, *Ultrasonic Measurements for Process Control*. New York: Academic Press, 1989.
- [5] L. Piche, F. Massines, G. Lessard and A. Hamel, "Ultrasonic characterization of polymers as function of temperature, pressure and frequency", *Proc. IEEE Ultrasonics Symp.*, pp.1125-1130, 1987.
- [6] M. Redwood, *Mechanical Waveguides*, Pergamon, N.Y. 1960, Chap.9, pp.191-207.
- [7] C.K. Jen, L. Piche and J.F. Bussiere, "Long isotropic buffer rods", *J. Acoust. Soc. Am.*, Vol.88, pp.23-25, 1990.
- [8] C.K. Jen, Ph. de Heering, P. Sutcliffe and J.F. Bussiere, "Ultrasonic monitoring of the molten zone of single crystal germanium", *Material Evaluation*, Vol. 49, pp.701-707, 1991.
- [9] C.K. Jen, "Acoustic fibers", *Proc. IEEE Ultrasonics Symp.*, pp.443-454, 1987.
- [10] C.K. Jen, A. Safaai-Jazi and G.W. Farnell, "Leaky modes in weakly guiding fiber acoustic wave guides", *IEEE Trans. on Ultrason., Ferroelectrics and Freq. Control*, Vol.UFFC-33, pp.634-643, 1986.
- [11] A. Safaai-Jazi, C.K. Jen and G.W. Farnell, "Analysis of weakly guiding fiber acoustic waveguides", *IEEE Trans. Ultrason., Ferroelectrics and Freq. Control*, Vol.UFFC-33, pp.59-68, 1986.
- [12] G.D. Boyd, L.A. Coldren and R.N. Thurston, "Acoustic clad fiber delay lines", *IEEE Trans. Sonics. Ultrason.*, Vol.SU-24, pp.246-255, 1977.
- [13] E.W. Marchand, *Gradient Index Optics*, Academic Press, New York, 1978.

- [14] T. Uchida, M. Furukawa, I. Kitano, K. Koizumi and H. Matsumura, "Optical characteristics of a high-focusing fiber guide and its application", IEEE J. Quantum. Elect., Vol. QE-6, pp.606-612, 1970.
- [15] C.K. Jen, C. Neron, J.F. Bussiere, L. Li, R. Lowe and J. Kushibiki, "Characterization of clad glass fibers using acoustic microscopy", Appl. Phys. Lett., Vol.55, pp.2485-2487, 1989.
- [16] C.K. Jen, Z. Wang, A. Nicolle, C. Neron, E.L. Adler and J. Kushibiki, "Acoustic graded index lens", To appear in Appl. Phys. Lett. Vol. 59, Sept. 1991.
- [17] C.K. Jen, "Similarity and differences between fiber acoustic modes and fiber optics", Proc. IEEE Ultrasonics Symp., pp.1128-1133, 1985.
- [18] J. Kushibiki and N. Chubachi, "Material characterization by line focus beam acoustic microscope", IEEE Trans. Sonics and Ultrason., Vol. SU-32, pp.189-212, 1985.
- [19] C.K. Jen, C. Neron, E.L. Adler, G.W. Farnell, J. Kushibiki and K. Abe, "Long acoustic imaging probes", Proc. IEEE Ultrasonics Symp., 90CH2938-9, pp.875-880, 1990.
- [20] R.A. Lemons and C.F. Quate, "Acoustic Microscopy", in Physical Acoustics, Vol.14, W.P. Mason and R.N. Thurston, Eds., New York, Academic, 1979.
- [21] C.K. Jen, C. Neron, A. Shang, L. Bonnell, K. Abe, J. Kushibiki and C. Sarvanos, "Acoustic characterization of optical fiber glasses" To appear in SPIE, Proc. Vol. 1590, Sept. 1991.
- [22] W.G. French, R.E. Jager, J.B. Macchesney, S.R. Nagel, K. Nassau and A.D. Pearson, "Fiber preform preparation", in *Optical Fiber Telecommunications*. S.E. Miller and A.G. Chynoweth eds, New York: Academic Press, 1979, pp. 233-261.
- [23] T. Sharpe, *Research Techniques in Nondestructive Testing*. New York: Academic Press, Vol. II, pp.317-321, 1973.
- [24] C.K. Jen, Z. Wang, A. Nicolle, J.F. Bussiere, E.L. Adler and K. Abe, "Acoustic waveguiding rods of graded velocity profiles", submitted to Ultrasonic Journal, July 1991.
- [25] H. Takahashi and I. Sugimoto, "Preparation of germanate glass by vapor-phase axial deposition", J. Am. Ceram. Soc., c66-c67, 1983.
- [26] J.I. Goldstein, " *Practical scanning electronics microscopy*", Academic Press, 1975.
- [27] A. Ohno, "Continuous casting of single crystal ingots by the O.C.C. Process", J. Metals, Vol.38, pp.14-16, 1986.
- [28] A. Ohno and H. Soda, "Development and application of OCC technology", Proc. F. Weinberg Int'l Symp. on Solidification Process, J.E. Lait and I.V. Samarasekera eds., Pergamon Press, New York, pp.215-228, 1990.
- [29] H. Soda, A. Ichinose, G. Motoyasu, A. Ohno and A. McLean, "A new fabrication method and its process variables for cored materials", to be published.

[30] B. Hoh, H. Jacubi, H. Wiemer and K. Wunnenberg, "Improvement of cleanliness in continuous casting", Proc. 4th Int'l conf. on Continuous Casting, Brussels, pp.211-222, May 1988.

[31] T.L. Mansfield, "*Ultrasonic technology for measuring molten aluminum quality*", Material Evaluation, Vol.41, pp.743-747, 1983.

[32] J. Krautkramer and H. Krautkramer, "*Ultrasonic Testing of Materials*", 3rd Ed., Springer-Verlag, 1983.

[33] C.E. Eckert, "Apparatus and method for ultrasonic detection of inclusions in molten metals", U.S. Patent No. 4563895, Jan. 1986.

[34] R.L. Parker, J.R. Manning and N.C. Peterson, "Application of pulse-echo ultrasonic to locate the solid/liquid interface during solidification and melting of steel and other metals", Appl. Phys., Vol.58, pp.4150-4164, 1985.

[35] S. Dawson, N.D.G. Mountford, I.D. Sommerville and A. McLean, "A new method for the evaluation of liquid steel cleanliness", Proc. 9th PTD conference, pp.17-32, 1990.

[36] J.P. Rocher, J.M. Quenisset, R. Naslain, "Wetting improvement of carbon or silicon carbide by aluminum alloys based on a K_2ZrF_6 surface treatment: application to composite material casting", J. Materials Science, Vol.24, pp.2697-2703, 1989.